Order Number 9014922

Direct numerical simulations of chemically reacting turbulent flows

Leonard, Andy David, Ph.D.

Iowa State University, 1989

U·M·I
300 N. Zeeb Rd.
Ann Arbor, MI 48106

Direct numerical simulations of chemically reacting turbulent flows

by

Andy David Leonard

A Dissertation Submitted to the
Graduate Faculty in Partial Fulfillment of the
Requirements for the Degree of
DOCTOR OF PHILOSOPHY
Major: Chemical Engineering

Approved:
Signature was redacted for privacy.
In Charge of Major Work
Signature was redacted for privacy.
For the Major Department
Signature was redacted for privacy.
For the Graduate College

Iowa State University
Ames, Iowa
1989

TABLE OF CONTENTS

LIST OF FIGURES

LIST OF TABLES

INTRODUCTION

A description of turbulence must include the concepts of irregularity or unpredictability, an unsteady nature, and an increased ability to mix mass, momentum, and energy compared to laminar flows. The distinction between laminar and turbulent flows was made more than a century ago (Reynolds, 1883). And yet years of turbulence research have not resulted in a comprehensive theory. despite the fact that the equations that govern turbulent flows are known. The problem is intractable because turbulent motion is complex. with a wide range of time and length scales. Analytic solutions of the governing equations are possible for some simple cases with laminar flows, but flows of interest in engineering applications are almost always turbulent. On the other hand, the complete, detailed flow field does not usually need to be known. It is often sufficient to know the means and variances of the quantities of interest. Turbulence is therefore studied primarily with statistical methods. The governing equations can be averaged, but a finite set of equations cannot be formed without resorting to some manner of approximation because of stochastic nonlinearities. This closure problem is well known in turbulence research, and various closure methods have been developed and are well established (but not always satisfactory) for the hydrodynamics problem.

In reacting turbulent flows, the presence of chemical reactions adds an additional

level of complexity to the already difficult problem of turbulence. Chemical reactions introduce new time scales to the problem. Reaction kinetics are not always known, but those that are known are often complex, with multiple steps and many intermediate species. Furthermore, highly exothermic reactions can influence the velocity field by causing large variations in density and other physical quantities. Closure methods for reacting flows are quite primitive, when compared with the models used in nonreacting flows. Many closure theories for turbulence are based on near-Gaussian behavior. Concentration variables, however, are bounded and cannot be represented as well as velocity components by Gaussian random variables. The most promising statistical treatment of reacting turbulent flows evaluates the joint pdf of reactant concentrations and velocity components from a dynamical equation that is derived from the partial differential equations that govern the local instantaneous velocity and concentration values. This approach is less traditional than those used for nonreacting flows, so little of the experience gained in the study of predicting nonreacting flows can be directly applied to systems that include chemical reactions. Advances made in the use of pdf methods for reacting flows may, however, be of benefit to the treatment of more general turbulence problems.

Direct numerical simulations are used in the present study to address some of the problems that are faced in modeling turbulent reacting flows, by providing data that are difficult, if not impossible, to obtain experimentally. This work will examine, in two separate parts, models of the rate of dissipation of concentration fluctuations in reactive flows (including joint pdf solutions) and models of the mean reaction rate in moment closures. In addition, in a third part of the dissertation, the influence of

local kinematical quantities on the local, instantaneous reaction rate are examined. Only the case of second-order irreversible reaction between two unmixed reactants will be dealt with here.

PART I.

SCALAR DISSIPATION AND MIXING IN TURBULENT REACTING FLOWS

CHAPTER 1. INTRODUCTION

Chemical reactions are often treated as an extension of the problem of turbulent mixing of passive scalars such as temperature or concentration of a tracer species. In statistical treatments, additional terms in the equations for the moments of reactant species concentrations arise and must be handled with some modeling technique. The influence of chemical reactions on models for mixing is rarely explicitly included. One method that is claimed to treat reacting turbulent flows without modeling the reaction is the probability density function (pdf) approach. Some of the terms that do need to be modeled in this method arise from the terms in the governing equations that result from molecular diffusion. The unknown terms in the pdf equation involve concentration gradients, which are affected by chemical reactions. The length or time scales used in the pdf models, on the other hand, are not usually assumed to be functions of reaction rate. In most studies, tests of pdf models are made by comparing either the pdf's or the concentration moments predicted by the pdf methods with the results of laboratory experiments or numerical simulations. The modeling assumptions themselves have not been tested by comparing the contribution of the unknown terms with any measurements.

In this paper, direct numerical simulations (DNS's) of a simple chemical reaction in decaying homogeneous turbulent flows have been used to calculate some quantities

that require modeling in the statistical methods, in particular those quantities that derive from the diffusive terms in the dynamical equations. The effect of reaction rate on length scales of the concentration of reactant species has been shown. Probabilistic models for mixing, which do not need modeling assumptions for the rate of change of the concentration of a species due to chemical reaction, have been reviewed and tested for both reactive and nonreacting flows. The tests of these methods included both comparisons of the concentration pdf's and of the moments predicted by the model with DNS data and comparison of the instantaneous rate of change of the pdf for the models and the DNS data.

CHAPTER 2. BACKGROUND

The equations governing the conservation of mass, momentum and energy are coupled nonlinear differential equations. Statistical methods must be used to treat general problems involving turbulent flows, but a closed set of equations for the various statistical quantities cannot be developed without invoking some kind of model or statistical hypothesis. This is the well known closure problem of turbulence. In this chapter some closure theories that deal with the diffusive or mixing terms in the dynamical equations are reviewed. First, we review a few models to predict the scalar dissipation rate that are appropriate for moment methods. Next, we describe models used for the mixing terms in the pdf equations. Finally, we discuss experimental studies that are appropriate for this work.

Theory

The governing equations for the conservation of mass and momentum can be expressed (see Bird et al., 1960) as

$$\frac{\partial \rho}{\partial t} + \nabla \cdot (\rho \mathbf{u}) = 0, \tag{2.1}$$

$$\rho \frac{\partial \mathbf{u}}{\partial t} + \rho \mathbf{u} \cdot \nabla \mathbf{u} = \nabla \cdot \tau - \nabla p + \rho \mathbf{g}, \tag{2.2}$$

and

$$\rho\frac{\partial\phi_\alpha}{\partial t} + \rho\mathbf{u}\cdot\nabla\phi_\alpha = -\nabla\cdot\mathbf{j}_\alpha + \rho S_\alpha, \tag{2.3}$$

for each species $\alpha = 1, 2, \ldots, N$ in a system containing N species.

These equations must be accompanied by constitutive equations to relate the viscous stress tensor τ and diffusive fluxes $\mathbf{j}_\alpha$ to the velocity $\mathbf{u}$ and species concentrations ϕ_α and by an equation of state to relate the pressure p and density ρ. The source term S_α is a function of the species concentrations. At low Mach numbers, the enthalpy equation has the same form as the set of species concentrations equations (Equation 2.3) and can be included with them. These equations are the starting point for the statistical theories of turbulence discussed here.

Scalar dissipation

The statistical theory of turbulent mixing of inert scalars originated with Corrsin (1951a,b) as an extension of the application of turbulence theory for hydrodynamics to the treatment of the decay of temperature fluctuations in isotropic turbulence. The scalars are expressed as the sum of a mean component, which is independent of position, and a fluctuating component. Averaging rules are used to derive equations for velocity and concentration moments from the Equations (2.1)-(2.3). The decay equation for the variance of scalar fluctuations, obtained from Equation (2.3), is

$$\frac{d\overline{\phi^2}}{dt} = -\varepsilon_\phi = -12D\left(\overline{\phi^2}/{\lambda_\phi}^2\right), \tag{2.4}$$

where ε_ϕ is the scalar dissipation rate.

The overbar indicates an average, which can be taken over spatial points. The rate of change of the temperature variance depends on the microscale of the temper-

ature field, which is defined as

$$\lambda_\phi^2 = 6\overline{\phi^2} / \overline{\frac{\partial \phi}{\partial x_i}\frac{\partial \phi}{\partial x_i}} \tag{2.5}$$

Any single-point statistical theory must predict either the scalar dissipation rate or a microscale for dissipation. A very simple theory, due to Corrsin (1957), makes the assumption that the scalar microscale is a constant and proportional to a constant velocity length scale for stationary turbulence. Corrsin (1964) also used simplified shapes of the spectrum for fluctuations of scalar values, derived from predictions for large Reynolds number turbulence, to estimate length scales for different ranges of Schmidt (or Prandtl) numbers. The microscale for the scalar, calculated from these shapes, is

$$\lambda_O^2 = 6D \left\{ \frac{4\Lambda_\phi^{2/3}}{\varepsilon^{1/3}} + \left(\frac{\nu}{\varepsilon}\right)^{1/2} \log \mathrm{Sc} \right\} \quad \text{if Sc} >> 1 \tag{2.6}$$

or

$$\lambda_\phi^2 = \frac{24D}{3 - \mathrm{Sc}^2} \left(\frac{5\Lambda}{\pi \varepsilon^{1/2}} \right)^{2/3} \quad \text{if Sc} < 1. \tag{2.7}$$

With these expressions for the microscale, the variance can be calculated, given the rate of kinetic energy dissipation, ε, and the integral length scale of the scalar field, Λ_ϕ.

Another way to evaluate the rate of change of a scalar variance is to assume that the ratio $r = (k/\varepsilon) / \left(\overline{\phi^2}/\varepsilon_\phi\right)$, which is a ratio of time scales for the decay of turbulent kinetic energy and scalar fluctuations, is a constant. Here k is the kinetic energy, $3\overline{u^2}/2$. This form is often used in conjunction with k-ε modeling of turbulence (Pope, 1985). There is evidence both from experiments and theory, which is discussed further in a later section, that the time scale ratio is not a constant value. Newman et

al. (1979) have proposed a model for the dissipation rate of scalar fluctuations which allows r to change. A dimensionless decay rate is chosen so that r has a slow relaxation to unity from its initial value in moderate to high Reynolds number turbulence. None of these methods for scalar dissipation has any dependence on reaction rate.

Pdf methods

One method which is particularly appropriate for reactive turbulent flows is the probability density function (pdf) approach. These methods are described in detail in a review by Pope (1985) and will therefore be discussed only briefly here. The major points of concern are the treatment of molecular mixing and chemical reactions.

Before proceeding, we first review some points of probability theory. The pdf of a random variable Y, $f(y)$, is defined such that the probability that Y is in the range $(y, y-dy)$ is $f(y)dy$ and so that $f(y)$ is nonnegative and integrates to unity. Joint pdf's of more than one random variable are defined in a similar manner. The pdf can be used to calculate the expectation of any function of Y, even highly nonlinear functions such as reaction rates, as follows:

$$\langle g(Y)\rangle = \int_{-\infty}^{\infty} g(y)f(y)dy. \tag{2.8}$$

The angular brackets indicate a mathematical expectation, which is assumed to be equivalent to spatial or temporal averaging if statistical quantities are homogeneous or stationary.

A marginal pdf is obtained by averaging a joint pdf over the range of some of the independent variables. A conditional pdf of a set of random variables, given the values for a second set of random variables, is defined as the joint pdf divided by the

marginal pdf for the set of random variables that are given, if the marginal pdf is nonzero. For example,

$$f(\psi_1|\psi_2 = \phi_2) = \frac{f(\psi_1, \psi_2)}{f(\psi_2)}.$$

The conditional expectation of a random variable is defined similarly to Equation (2.8), except that the conditional pdf is used.

For our system, the local, instantaneous values of the velocity components and species concentrations are taken to be random variables. The rate of change of reactant concentrations due to chemical reaction is a function only of species concentrations and, possibly, temperature at a point in space. A joint pdf of these quantities includes all information needed to calculate the average rate of reaction. The joint composition pdf is often used as part of traditional moment closures, whereby a set of differential equations for moments of velocity and concentrations are solved. In these approaches the pdf is modeled with a parametric form that depends on a few moments of the random variables. This type of closure is discussed in more detail in Part II.

In the pdf approach, which was introduced independently by Lundgren (1967) and Monin (1967) for the joint pdf of velocity components in a turbulent flow, equations governing the development of the pdf are solved. These dynamical equations are derived from the governing equations in several ways (see Pope, 1985). The method used by Lundgren is to define a "fine-grained" distribution, which is a product of delta functions. The joint pdf is then defined by ensemble averaging the fine-grained pdf. Using different techniques, equations for the composition pdf in reacting flows were developed by Hill (1970) for stationary turbulence and by Dopazo and O'Brien (1974).

Pope (1981) developed the equation for the joint pdf of velocity and composition, $f(\mathbf{v},\vec{\psi};\mathbf{x},t)$,

$$\rho\frac{\partial f}{\partial t}+\rho v_j\frac{\partial f}{\partial x_j}+\left(\rho g_j-\frac{\partial\langle p\rangle}{\partial x_j}\right)\frac{\partial f}{\partial v_j}+\frac{\partial(\rho S_\alpha f)}{\partial\psi_\alpha}$$
$$=\frac{\partial}{\partial v_j}\left[\left\langle-\frac{\partial\tau_{ij}}{\partial x_i}+\frac{\partial p'}{\partial x_j}\middle|\mathbf{v},\vec{\psi}\right\rangle f\right]+\frac{\partial}{\partial\psi_\alpha}\left[\left\langle\frac{\partial J_{i\alpha}}{\partial x_i}\middle|\mathbf{v},\vec{\psi}\right\rangle f\right]. \qquad (2.9)$$

In Equation (2.9) the independent variables $\mathbf{v}$ and $\vec{\psi}$ correspond to the random variables $\mathbf{u}$ and $\vec{\phi}$, the pressure has been represented as a mean component $\langle p\rangle$ and a fluctuating component p', repeated Greek subscripts imply summation from 1 to n, ρ and $\mathbf{S}$ are functions of $\vec{\psi}$, and the angular brackets represent conditional expectations of random functions given that the values of the velocity and composition vectors are $\mathbf{v}$ and $\vec{\psi}$. Terms in this equation that involve multi-point phenomena—molecular diffusion and viscosity and the pressure gradient—are not closed in a single-point pdf formulation. These terms can be expressed with conditional expectations or two-point pdf's. Convective terms also require modeling if only the compositions of reacting species, and not the velocity components, are used in the pdf. The terms containing the conditional averages must be modeled before Equation (2.9) can be solved. The advantage of using Equation (2.9), rather than a set of equations for concentration and velocity moments, is that the source term appears in closed form.

The marginal pdf for the composition, $f(\vec{\psi};\mathbf{x},t)$, can be obtained by averaging Equation (2.9) over all $\mathbf{v}$, to give

$$\frac{\partial\left(\rho f\left(\vec{\psi}\right)\right)}{\partial t}+\frac{\partial\left(\rho S_\alpha f\left(\vec{\psi}\right)\right)}{\partial\psi_\alpha}=\frac{\partial}{\partial\psi_\alpha}\left[\left\langle\frac{\partial J_{i\alpha}}{\partial x_i}\middle|\vec{\psi}\right\rangle f\left(\vec{\psi}\right)\right]-\frac{\partial}{\partial x_i}\left[\left\langle u_i\middle|\vec{\psi}\right\rangle f\left(\vec{\psi}\right)\right] \qquad (2.10)$$

The last term on the right hand side of Equation (2.10) is zero in homogeneous

turbulence but presents difficulties in the modeling of nonhomogeneous flows. The other term on the right hand side, which we will refer to as the mixing term, can be expressed, for homogeneous turbulence and Fickian diffusion, in one of the following three ways:

$$\frac{\partial}{\partial \psi_\alpha}\left[\left\langle \frac{\partial J_{i\alpha}}{\partial x_i}\middle|\vec{\psi}\right\rangle f\right] = \begin{cases} \frac{\partial}{\partial \psi_\alpha}\left[\left\langle D\nabla^2\phi_\alpha\middle|\vec{\psi}\right\rangle f\right] \\ \frac{\partial^2}{\partial \psi_\alpha \partial \psi_\beta}\left[\left\langle 2D\nabla\phi_\alpha\cdot\nabla\phi_\beta\middle|\vec{\psi}\right\rangle f\right] \\ \frac{\partial}{\partial \psi_\alpha}\lim\limits_{\mathbf{r}\to\mathbf{0}} D\nabla_{\mathbf{r}}^2\left(\left\langle \phi'_\alpha\middle|\vec{\psi}\right\rangle f\right). \end{cases} \tag{2.11}$$

The unknown function that must be modeled includes the conditional expectation of a scalar dissipation rate, given a composition, or a conditional expectation of the value of a scalar at a point $\mathbf{x}' = \mathbf{x} + \mathbf{r}$, given the value at the point $\mathbf{x}$.

In order to close the Equation (2.10) for the marginal pdf, Dopazo and O'Brien (1974) proposed a linear mean square estimation (LMSE) closure for the mixing term, based on Lundgren's (1972) closure for the viscous terms. The LMSE model assumes that the conditional expectation of the fluctuations of a scalar at one point, given the value at another point, is linearly related to the fluctuations at the second point. The mixing term becomes

$$\frac{\partial}{\partial \psi}\left[\left\langle \frac{\partial J_i}{\partial x_i}\middle|\psi\right\rangle f(\psi)\right] = -\frac{6D}{\lambda_\phi^2}\frac{\partial}{\partial \psi}\left[\left(\psi - \langle\phi\rangle\right) f(\psi)\right], \tag{2.12}$$

where λ_ϕ is a length scale for the concentration field and is defined in Equation (2.5).

This relationship holds exactly for a Gaussian distribution and is easily implemented in the solution of Equation (2.9) or (2.10). One disadvantage of the LMSE model is that the closure preserves the shape of the initial pdf (Pope, 1985), so the pdf cannot evolve into a Gaussian form from arbitrarily chosen initial conditions. One

test that is often made of pdf closures is the time history of a pdf for a nonreactive scalar from an initially bimodal pdf, $f(\psi) = c\delta(\psi) + (1 - c)\delta(1 - \psi)$. The initial condition corresponds to a case where the random variable can only assume initial (nondimensional) values of 0 and 1. It is expected (Pope, 1982) that the pdf will assume an asymptotically Gaussian shape as the variance is decreased. A bimodal distribution will remain bimodal with the LMSE closure, and this is not a physically realistic model of molecular mixing. This model would seem to be best suited, rather, for cases where the pdf's are nearly Gaussian. The closure has been used in calculations by Dopazo and O'Brien (1974) and by Bonniot and Borghi (1979).

Sinai and Yakhot (1989) have recently formed a closure, very similar to the LMSE model, for a pdf of a nonreacting scalar in the long time limit when normalized moments become constant. The conditional expectation of the dissipation term, given the value of the scalar normalized with the rms value, is expressed as a Taylor series in the normalized scalar about the mean dissipation. The series is truncated with the second order term and a closed form for the normalized scalar pdf is given. The pdf agrees very well with DNS data over a larger than expected range.

C/D models

The mixing term, Equation (2.11), is most commonly modeled with coalescence-dispersion (C/D) types of models. The basis for these models is the work of Curl (1963), which has been modified for use as a pdf closure. Curl's model was developed for reactions between immiscible liquid phases and describes the concentration in liquid drops which are coalescing and then redispersing. The model can be easily applied

to turbulent mixing, although the physical basis for the model is not evident in this case. Curl's model gives the following equation for the rate of change of the pdf for a single species in homogeneous turbulence with no source term:

$$\frac{\partial f(\psi)}{\partial t} = 2\omega \left\{ 2 \int f(\psi + \psi') f(\psi - \psi') d\psi' - f(\psi) \right\}, \tag{2.13}$$

where the mixing frequency ω is defined as

$$\frac{d\overline{\phi^2}}{dt} = -2\omega\overline{\phi^2}. \tag{2.14}$$

One consequence of Curl's model is that discrete pdf's remain discrete. An initially bimodal pdf will have an ever increasing number of delta functions as the scalar variance decays, as a result of the mixing between fluid elements. This is also not physically acceptable behavior for molecular mixing.

Curl's model can be easily extended to multiple reacting species. Pope (1976, 1981) has used this model in calculations of reactive and nonreactive flows.

Dopazo (1979) and Janicka et al. (1978, 1979) proposed models which allowed the extent of mixing between the fluid elements in Curl's model to be a random variable. Equation (2.13) becomes (Pope, 1982)

$$\frac{\partial f(\psi)}{\partial t} = 2\beta\omega \left\{ 2 \iint K(\psi, \psi', \psi'') f(\psi') f(\psi'') d\psi' d\psi'' - f(\psi) \right\}, \tag{2.15}$$

where

$$K(\psi, \psi', \psi'') = \int_0^1 A(\alpha) \delta \left(\psi - (1-\alpha)\psi - \frac{\alpha}{2} \left(\psi' + \psi'' \right) \right) d\alpha. \tag{2.16}$$

In this equation, $A(\alpha)$ is the pdf of the mixing extent α, and β is a function of α that is needed to keep the definition of ω the same as in Curl's original model. The

function A is only restricted to have the properties of a pdf defined on the range (0,1). The use of a continuous function for A allows the shape of the pdf to change. Kosàly (1986) has shown the function $A(\alpha)$ should decrease monotonically with α to predict the initial rate of mixing of a bimodal scalar field, by assuming the pdf must decrease monotonically from the peak at $\psi = 0$.

Curl's model can be recovered from the above form by using the function $A(\alpha) = \delta(1-\alpha)$, whereas Janicka et al. use $A(\alpha) = 1$. Kosàly (1986) has shown the C/D closures are equivalent to the linear mean square estimation (LMSE) closure proposed by Dopazo and O'Brien when the function $A(\alpha)$ has a narrow peak at $\alpha = 0$.

C/D models are often linked to the Monte Carlo methods used in the solution of pdf equations. The Monte-Carlo procedure is more efficient than finite-difference methods because of the high dimensionality of the pdf (Pope, 1981), except in simple cases. This type of method uses an ensemble of stochastic particles, each of which are assigned composition values. At every fractional timestep during the simulation a particle may be selected at random and paired with another particle. New compositions are then assigned to the pair of particles. With Curl's model, a fraction of the particles are selected, each is paired randomly with another particle, and the new composition of each particle pair becomes the average of the previous concentrations of the two particles. In the modified forms of Curl's model, such as the model of Janicka et al., the change in concentration of each particle is a random variable which must be between zero and half the initial difference. The frequency at which particles are selected in these methods is chosen to fit the decay of the variance of an inert scalar.

Pope (1982) and Kosàly (1986) have shown that the predicted pdf from none of the C/D closures for inert species discussed above will approach a Gaussian form at long times and that the flatness factor for the inert concentration becomes infinite as the pdf approaches its asymptotic form. In order to improve this behavior, Pope (1982) has introduced a mixing model that biases the selection of stochastic particles in the Monte Carlo solution, based on the time since the particle was last chosen. This model introduces a new random variable η, the age for each stochastic particle. The Equation (2.13) for the nonreacting single species pdf becomes

$$\frac{\partial f(\psi)}{\partial t} = 2\beta\omega \left\{ 2 \iint K(\psi, \psi', \psi'') h(\psi') h(\psi'') d\psi' d\psi'' - h(\psi) \right\}, \qquad (2.17)$$

where $h(\psi)$ is the concentration pdf of the elements sampled by the age-biased procedure, and β is a function of α and η.

Pope recommends choices for A and η to give values of the flatness and superskewness factors that are finite, and to give an asymptotic shape of the pdf that is close to Gaussian. This model is used by Anand and Pope (1987) for premixed flames and Haworth and Pope (1987) for a mixing layer.

Kosàly and Givi (1987) compared the mixing models of Curl (1963), Janicka et al. (1978, 1979), and Dopazo and O'Brien (1974) for flows with infinitely fast reactions and with inert species. The shapes of the concentration pdf's predicted using Curl's model and Janicka et al.'s model are similar, except for peaks at the origin and the concentration extremes for Curl's model, for mixing of an inert species from an initially bimodal distribution in homogeneous turbulence. A Monte Carlo solution to approximate Dopazo and O'Brien's model gave sharply peaked pdf's for this case. The mean, variance, and skewness of the concentration distributions are the same for

all three models, whereas the value of the flatness factor of the pdf predicted by the Dopazo-O'Brien closure was smaller than the values predicted by either Curl's or the JKK model. It is not surprising that the models predict the same values for the first three moments of the concentration of an inert species, since the mixing frequency is chosen to fit a prescribed decay rate for the variance. The first four moments of concentration of reactants in the limit of infinitely fast reaction rate showed much more variation than in the inert case.

A time or length scale for the variance decay is a parameter required in all current single point models. Models have been proposed, however, that do not need these external scales. A multi-point pdf closure, proposed by Ievlev (1973), has been studied by Kuo and O'Brien (1981), who found that for the short-time behavior of this closure for a diffusive-reactive system the model represented molecular mixing better than single-point models. Eswaran et al. (1989) have proposed LMSE and EDQNM (eddy-damped quasi-normal Markovian) models for a two-point scalar pdf. Meyers and O'Brien (1981) modeled the equation for the joint pdf of a scalar and its gradient.

Useful Experimental Results

Since scalar dissipation in reacting homogeneous turbulent flows is interpreted or modeled using results from the decay of inert scalars in homogeneous turbulence, some pertinent experiments are summarized in this section.

The kinetic energy and the variance of temperature or concentration fluctuations in experiments with grid-generated turbulence can usually be expressed as a power

law function of the distance downstream in the wind tunnel

$$\overline{u^2} \sim x^{-n}. \tag{2.18}$$

$$\overline{\phi^2} \sim x^{-m}. \tag{2.19}$$

The ratio of time scales for the velocity and scalars, r, is the ratio of the decay exponents m/n for the power law forms.

Measured values of n in grid generated turbulence are about 1.2 (Comte-Bellot and Corrsin (1966), but a wide range of measured values of m, and therefore r, are reported. Warhaft and Lumley (1978) reviewed previous experimental results for m and n, in a study of the effects of the initial conditions on the decay rate, and used two different mechanisms to introduce temperature fluctuations in grid-generated turbulence. First, they heated the grid used to generate the velocity fluctuations, and found the scalar decay rate depended on the power input to the grid. Second, they used an array of heated wires downstream of the grid to introduce the temperature fluctuations independently of the velocity fluctuations, and found the decay rate to be a function of the length scale of the temperature fluctuations. The time scale ratio r did not change in these experiments, which developed for about one turbulence decay time.

Sreenivasan et al. (1980) studied the decay of temperature fluctuations both both heated grids and with an array of heated wires downstream from the grid. They found that the decay rate for scalar fluctuations was independent of the temperature of the grid, but it did depend on the relative length scales of the scalar and velocity fields for the heated-grid experiments. The average value of the decay exponent of 1.3 agreed with most of the results of previous work, when these results were plotted with the

same virtual origin. The decay exponent for the array of heated wires was a constant value of 2.2, independent of the position of the screen, the temperature of the wires, and the relative length scales.

Calculations by Newman and Herring (1979), using the Test Field Model, showed the temperature fluctuations approached a universal decay law for different initial conditions within one turbulence decay time, whereas calculations of Durbin (1982), using a Lagrangian dispersion theory, indicated that the decay rate was not a constant and universal behavior did not exist. The theories used temporally developing turbulence, as does the present study, while in the experiments turbulence is developing spatially. The two problems can be related by Taylor's hypothesis, but Newman and Herring discuss the difficulty in matching the initial conditions for the two problems.

McKelvey et al. (1975) studied the mixing in the type of tubular reactor used in the studies of reacting flows by Vassilatos and Toor (1965) and Mao and Toor (1970) and found the variance of the concentration of an inert species had a decay exponent of 1.5. Bennani et al. (1985) found a value of 1.3 for the decay exponent for the variance of the concentration of an inert species in grid generated turbulence, and a value of 1.5 for the decay exponent for a concentration. The variance of the concentration of a reactant increased initially, and then followed a power law decay. The microscale for the concentration of reactants could not be directly measured by Bennani.

CHAPTER 3. PROBLEM DESCRIPTION

The effects of the detailed turbulent velocity field on a single reaction have been examined in this paper by using direct numerical simulation. The particular case of interest here is the single-step, irreversible, second-order reaction, A + B → products, occurring in a decaying homogeneous turbulent flow. The velocity field is resolved down to the Kolmogorov scale, so no turbulence modeling is used. The velocity field is isochoric, with Newtonian viscosity. The concentration fields are passive quantities with respect to the velocity field.

Governing Equations

The governing equations for the problem are the incompressible Navier-Stokes equations for the conservation of momentum, for a Newtonian fluid of constant density and viscosity, and conservation equations for the mass of each reactant species,

$$\frac{\partial u_i}{\partial t} + u_j \frac{\partial u_i}{\partial x_j} = -\frac{1}{\rho}\frac{\partial p}{\partial x_i} + \nu \nabla^2 u_i, \tag{3.1}$$

$$\frac{\partial u_j}{\partial x_j} = 0, \tag{3.2}$$

$$\frac{\partial A}{\partial t} + u_j \frac{\partial A}{\partial x_j} = D_A \nabla^2 A - k_R AB, \tag{3.3}$$

with an equation for the concentration of species B that is equivalent to Equation (3.3). Fickian diffusion with a constant effective mass diffusivity, D_A, has been assumed to be the only mechanism for diffusion in Equation (3.3). The diffusivities of the reacting species are equal and the reaction rate coefficient k_R is a constant in the cases reported here.

Numerical Procedure

Pseudospectral methods are used to integrate Equations (3.1)–(3.3). These methods solve the ordinary differential equations for the coefficients of a truncated Fourier series. Convolutions of Fourier coefficients arise from nonlinearities in the governing equations but are not evaluated directly. Rather, the nonlinear terms are evaluated at collocation points in physical space and the coefficients of the nonlinear terms are evaluated. Fourier expansions are the most efficient type of basis function to use for homogeneous turbulence because Fast Fourier Transform (FFT) algorithms can substantially reduce the number of operations needed to evaluate the nonlinear terms. A general discussion of spectral and pseudospectral methods for the solution of incompressible flows is given by Orszag (1971, 1972). Pseudospectral and other methods for reacting turbulent flows are discussed by Oran and Boris (1987) and by Leonard and Hill (1989). Two different codes are used in this study. One code, developed by R. M. Kerr (see Kerr, 1985) is written in FORTRAN, while the other, developed by R. S. Rogallo (see Rogallo, 1981 and Lee and Reynolds, 1985), is written in the Vectoral language (Wray, 1989).

The velocities and species concentration are expanded in these programs as fol-

lows:

$$u_i(\mathbf{x},t) = \sum_{|\mathbf{k}|=-K}^{K} v_i(\mathbf{k},t)e^{i\mathbf{k}\cdot\mathbf{x}} \tag{3.4}$$

and

$$A(\mathbf{x},t) = \sum_{|\mathbf{k}|=-K}^{K} \hat{A}(\mathbf{k},t)e^{i\mathbf{k}\cdot\mathbf{x}}. \tag{3.5}$$

The domain in physical space is a cube of size $(2\pi)^3$, and 64 Fourier coefficients were used in each direction. The use of Fourier coefficients in the expansions requires the boundary conditions to be periodic.

The governing equations for $u_i(\mathbf{x},t)$ and $A(\mathbf{x},t)$, and the orthogonality properties of $e^{i\mathbf{k}\cdot\mathbf{x}}$, can be used to write equations for $v_i(\mathbf{k},t)$ and $\hat{A}(\mathbf{k},t)$:

$$\frac{dv_i(\mathbf{k},t)}{dt} + \nu k^2 v_i(\mathbf{k},t) = -T_i\left\{\mathbf{u}\cdot\nabla\mathbf{u}\right\} + k_i\frac{\mathbf{k}\cdot\mathbf{T}\left\{\mathbf{u}\cdot\nabla\mathbf{u}\right\}}{k^2} \tag{3.6}$$

and

$$\frac{d\hat{A}(\mathbf{k},t)}{dt} + Dk^2\hat{A}(\mathbf{k},t) = -T\left\{\mathbf{u}\cdot\nabla A + k_R AB\right\}. \tag{3.7}$$

The continuity equation, $\mathbf{k}\cdot\mathbf{v}(\mathbf{k},t) = 0$, has been used to eliminate the pressure term in Equation (3.6). Fourier transforms of nonlinear terms are denoted by $\mathbf{T}\{\ldots\}$, and are not written out explicitly here since they are evaluated in physical space. The viscous or diffusive term on the left hand side of Equation (3.6) or (3.7) is evaluated implicitly through the use of an integrating factor.

The two programs use different methods to advance Equations (3.6) and (3.7) in time. Rogallo's code uses a second-order predictor-corrector scheme, while Kerr uses a third-order Runge-Kutta method designed to minimize memory requirements. Both methods use variable time steps based on an approximate CFL criterion, $v\Delta t/\Delta x = C$, where v is the maximum value of the magnitude of the velocity, Δt is the time

step, Δx is the grid spacing, and C is a constant. Rogallo's code requires $C = 1$, while Kerr's code uses $C = 1.5$.

Evaluating the nonlinear terms in physical space normally introduces aliasing errors. To dealias the quadratic terms, Rogallo's code uses a combination of truncation of Fourier modes outside a sphere of radius $K\sqrt{(8/9)}$ and a random shift of the computational grid at every fractional timestep. The only procedure used to control aliasing in Kerr's method is the truncation of Fourier modes outside a sphere with a radius of $K\sqrt{(8/9)}$. The value of the radius could be changed to $2K/3$ to eliminate all aliasing errors. Kerr's method uses the rotational form of the Navier-Stokes equation, where $\mathbf{u} \cdot \nabla \mathbf{u} = \boldsymbol{\omega} \times \mathbf{u} + \nabla u^2/2$, to prevent instabilities that might arise because of aliasing errors. This form will conserve energy, despite aliasing errors, for an inviscid solution if there are no errors in evaluating the time derivative (Orszag, 1972).

Initial Conditions

In this section the runs that were made in this study are described. The physical parameters and initial conditions used for each of the runs are summarized in Table 3.1. Runs A–I were made with Kerr's code, while runs X, Y, Y0, and Z were made with Rogallo's code. The concentrations of two reactants and an inert species were calculated in each of the runs A–I. The concentrations of eight species were calculated in runs X, Y, Y0, and Z. The eight species for runs X and Z were two reactants and one product species, for each of two different reactions, as well as two inert species. The concentrations of two reactants, for each of four different reactions, were calculated in runs Y and Y0. In each run, the concentrations of an inert species

with the same initial conditions as the reactants were also calculated, except for runs Y and Y0, where the reactants and inert species were calculated as separate cases.

The velocity field was chosen by scaling randomly selected Fourier coefficients to give a specified energy spectrum. The form of the energy spectrum determined the intensity and length scales of the turbulence. Because the Fourier coefficients were chosen from a normal distribution, the coefficients were uncorrelated, and some statistical quantities, such as the velocity derivative skewness or spectral energy transfer rate, were not given realistic values with this initialization. Runs A–I used this condition as an initial value. The shape of the initial spectrum was given as either

$$E(k,0) \propto k^4 e^{-k^2/2k_0^2} \tag{3.8}$$

or

$$E(k,0) \propto k^3 e^{-k/k_0}. \tag{3.9}$$

The time that these statistics need to develop was reduced in runs X, Y, Y0, and Z by pre-processing the initial fields. An initial spectrum of the form

$$E(k.0) \propto \frac{(kL)^4}{\left(1+(kL)^2\right)^3} \tag{3.10}$$

was chosen. The simulation was run for a short period of time, until the energy spectrum developed a constant shape. The coefficients were saved and used as initial values for runs X, Y, Y0 and Z. The initial energy spectrum for these cases had a shape similar to the developed spectrum for runs A–I.

Two different types of initial conditions were used for the reactant concentrations. Both had a high degree of initial segregation of reactants. The first type had alternating slabs of reactant species. These slabs were oriented so that the initial

concentrations were uniform in the x_2 and x_3 directions. Square waves in the x_1 direction were damped slightly by diffusion before the simulation began, in order to prevent Gibbs' ringing of the concentration values at the points between the slabs. The degree of segregation was, therefore, not perfect at the initial time. All the runs but the one labeled Z used this type of initial condition. All these runs except runs Y and Y0 had one slab of each reactant in the domain. Runs Y and Y0 had four different cases, each with the same reaction rate coefficient (all of the species were nonreacting in run Y0) and molecular diffusivity, but with different initial conditions for the concentration fields. Each reactant in these runs had from one to four slabs in the computational domain.

The second type of initial concentration values had values for reactants A and B at points chosen randomly, using a random function with a Gaussian distribution. denoted as f. Initial length scales for the concentration field were chosen by scaling the Fourier coefficients of f to fit a prescribed concentration spectrum of the form

$$E(k,0) \propto \frac{(kL)^3}{(1+(kL)^2)^2}. \tag{3.11}$$

The function f was allowed to convect and diffuse for a period of time. This pretreatment was intended to create realistic spatial structure for the reactant concentrations, which were defined based on the local values of f, while correlations between Fourier coefficients of the velocity field were developing. The concentration of species A was assigned a value of 2 in the regions of space where f was positive and the concentration of species B was defined as 2 regions where f was negative. These initial conditions were damped, as with the initially anisotropic conditions, before the simulation was begun. The two conditions are shown schematically in Figure 3.1. The first method

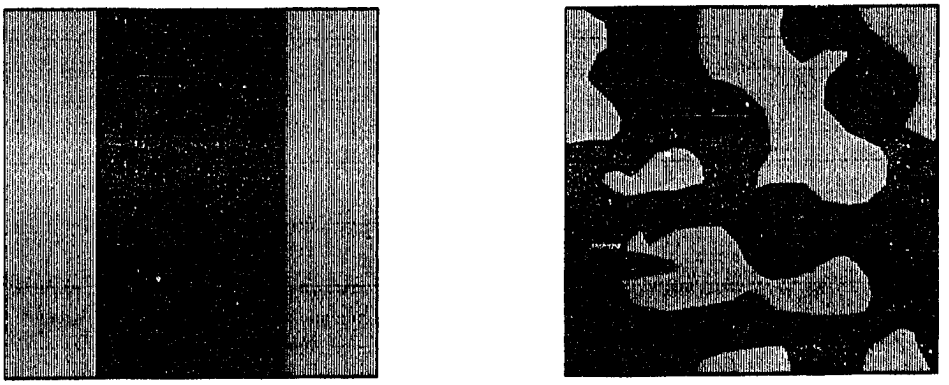

(a) (b)

Figure 3.1: Schematic illustration of initial conditions for the reactants. Reactant A is shown in gray and reactant B in black. (a) Runs A–I, X–Z. (The reactants in run Y have more than one slab of each reactant in the domain.) (b) Run Z

allows for easy examination of reaction zones, whereas the second method is more statistically isotropic.

Table 3.1: Summary of the initial conditions and parameters used in the simulations

run[a]	ν	u'	R_λ	$E(k,0)$[b]	k_R	$\overline{a^2}$, $\overline{b^2}$, $-\overline{ab}$	Da
A	0.01	0.942	65.8	Eqn. (3.8)	1.0	0.856	1.0
B	0.015	0.942	43.9	Eqn. (3.8)	1.0	0.856	1.0
C	0.02	0.942	32.9	Eqn. (3.8)	1.0	0.856	1.0
D	0.01	0.942	65.8	Eqn. (3.8)	5.0	0.856	5.0
E	0.02	0.942	32.9	Eqn. (3.8)	5.0	0.856	5.0
F	0.015	0.825	32.3	Eqn. (3.9)	1.0	0.839	1.0
G	0.015	0.825	32.3	Eqn. (3.9)	5.0	0.839	5.0
H	0.015	0.825	27.4	Eqn. (3.9)	1.0	0.839	0.88
I	0.015	0.825	27.4	Eqn. (3.9)	5.0	0.839	4.4
X	0.02	1.03	19.7	Eqn. (3.10)	2.0, 8.0	0.898	1.6, 6.4
Y[c]	0.02	1.03	19.7	Eqn. (3.10)	2.0	0.961, 0.921 0.882, 0.842	1.6, 6.4
Y0	0.02	1.03	19.7	Eqn. (3.10)	0.0	0.961, 0.921 0.882, 0.842	0.0
Z[d]	0.02	1.03	19.7	Eqn. (3.10)	2.0, 8.0	0.748	1.6, 6.4

[a] All simulations were performed with 64^3 coefficients on a domain of size $(2\pi)^3$. Runs A–I were made with Kerr's code on a Cray X-MP computer at NCSA, whereas runs X–Z were made with Rogallo's code on a Cray 2 computer at NAS. The initial mean reactant concentrations were 1.0 and the value of the Schmidt number was 0.7 in all runs.

[b] Eqn. (3.10) indicates that the preconditioned velocity field was used. The initial statistics reported here are for the beginning of the simulation, after the preconditioning.

[c] The initial concentration fields in this run and in run Y0 had from one to four stripes of each reactant in the domain. The four values for the initial concentration variances are those for each of the cases with a different number of stripes.

[d] The initial concentration fields were chosen to be statistically isotropic in this run with $\bar{A} = 1.03$ and $\bar{B} = 0.97$.

CHAPTER 4. RESULTS AND DISCUSSION

Results from the direct simulations, in the form of statistical quantities, are presented in this section. Volume averages are performed over the entire physical domain of a single realization, as opposed to taking averages over many realizations of an ensemble of experiments. In this chapter we first describe some features of the computed velocity fields. Next, the development of microscales for the dissipation of concentration fluctuations of inert and reacting scalars are examined. Finally, predictions of C/D models for the mixing of reacting and nonreacting scalars are compared to the DNS results.

Velocity Fields

Runs A–E use the same initial velocity field, which is defined to have an initially Gaussian-like energy spectrum (Equation (3.8)), but they have different initial Reynolds numbers, since the values of the molecular viscosity differ. The initial energy spectrum used in these runs is that often assumed for final period turbulence, where the viscous effects dominate the inertial effects (Hinze, 1975). The energy spectra for the initial and later times are shown in Figure 4.1 for run A and run C. The shapes of the spectra have adjusted from their initial values after one turnover time and remain similar for the remainder of the run. The spectrum for run C falls

off more rapidly with the wavenumber k after one turnover time than does that for run A.

This transitional period, that occurs primarily during the first eddy turnover time, is also seen in the development of the Taylor microscale for the velocity field, λ_g, in Figure 4.2 for run C. The linear part of the curve is used to find the virtual origin and the power law exponent for the decay of the kinetic energy. Both the virtual origins and decay exponents are nearly the same for runs A and C. The kinetic energies for these two cases are shown in Figure 4.3. The decay exponent for both cases is approximately 2.5, which is the value predicted for final period turbulence (Hinze, 1975), in contrast with the experimentally observed value of 1.3 (Comte-Bellot and Corrsin, 1966) for grid-generated turbulence in a wind tunnel.

A preconditioned velocity field was used in runs X, Y, and Z in order to give a more realistic initial shape to the energy spectra and eliminate the transitional period seen in runs A–E. The development of the energy spectrum for these runs is shown in Figure 4.4. The microscale for these runs grows as the square root of time and is again used to calculate the parameters in Equation (2.18). The decay of the turbulent kinetic energy can be fit with a power law over the entire range of the data (Figure 4.5). The decay exponent for these runs is 1.5, which is somewhat larger than experimental measurements, but the agreement is much better than with the other velocity fields used. Despite the fact that the Reynolds number decays more slowly for the preconditioned fields, runs X, Y, and Z were not carried out as far as runs A–E, because the initial Reynolds number for the preconditioned velocity field was much lower than the value used in runs A–E, and the value of the Reynolds

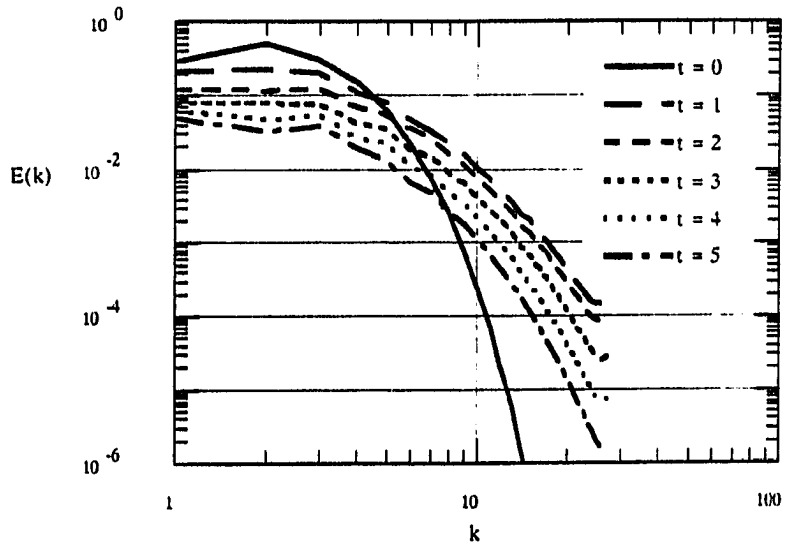

(a)

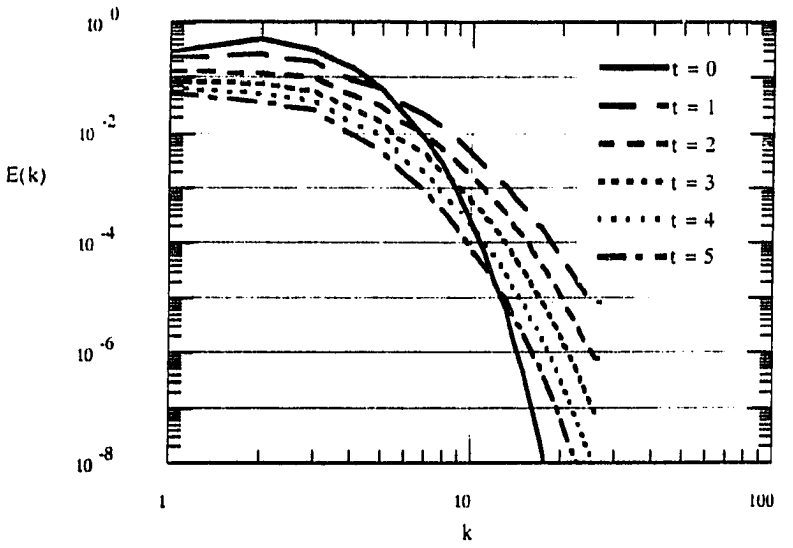

(b)

Figure 4.1: Development of the kinetic energy spectra for runs A and C. (a) Run A; (b) Run C. The initial Reynolds number is 65.8 in run A and 32.9 in run C

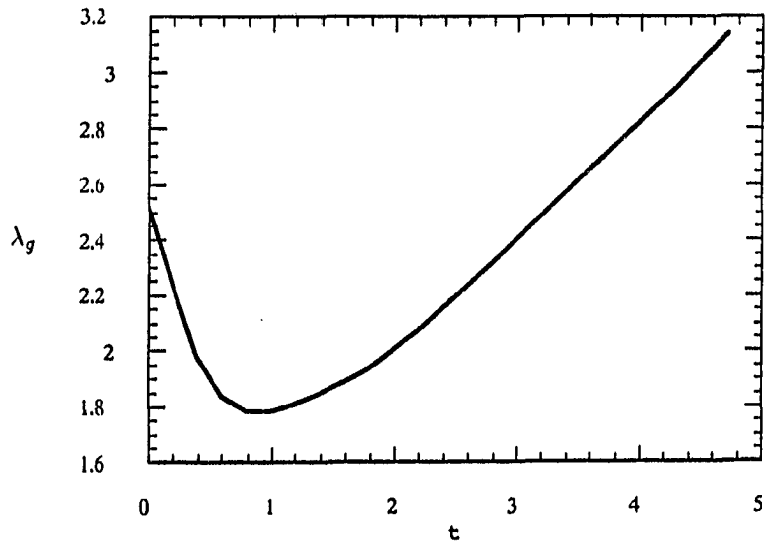

Figure 4.2: Development of the Taylor microscale for the velocity field for run C. ($R_\lambda = 32.9$)

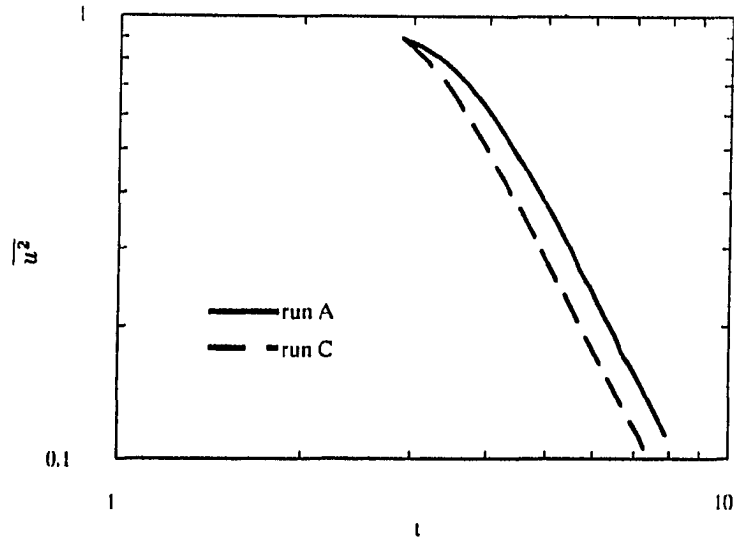

Figure 4.3: Development of the mean square velocity fluctuations for runs A and C

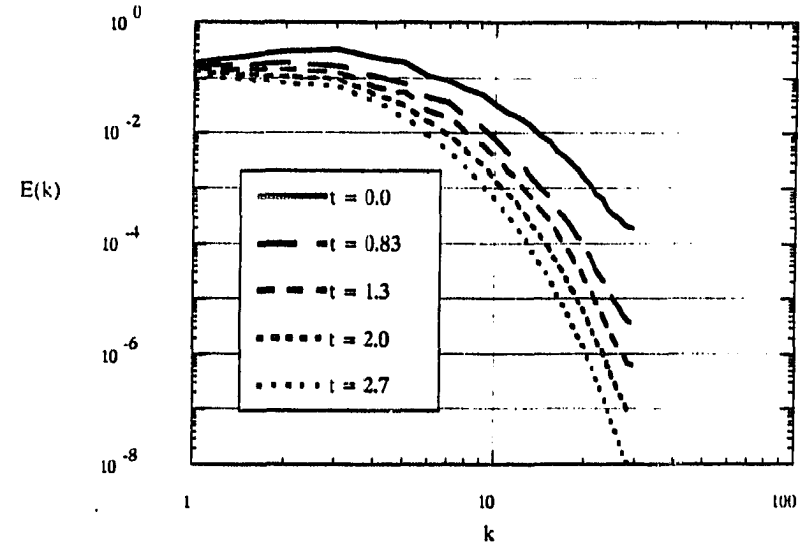

Figure 4.4: Development of the kinetic energy spectrum for runs X, Y, and Z with an initial R_λ of 19.7. The velocity field has been preconditioned in these runs

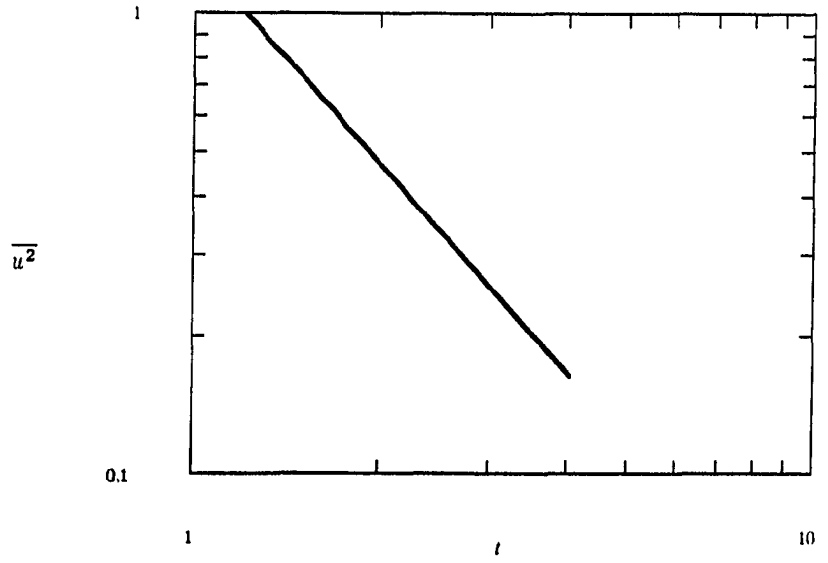

Figure 4.5: Development of the mean square velocity fluctuations for runs X, Y, and Z

number became too small at later times.

Concentration Fields

Mixing of scalar quantities is often interpreted in terms of concentration microscales, and we present results for the time dependence of these scales in this section. The microscales can be used as parameters in pdf models, and we also examine different methods for modeling pdf equations in this section.

Microscales

The rate of change of the variance of an inert species can be expressed in terms of a Taylor microscale for the concentration field (Corrsin, 1951b),

$$\frac{d\overline{\phi^2}}{dt} = -\varepsilon_o = \frac{-12D\overline{\phi^2}}{\lambda_\phi^2}. \tag{4.1}$$

The microscale λ_ϕ is defined for an isotropic turbulent concentration field as $\lambda_\phi^2 = 12D\overline{\phi^2}/\varepsilon_\phi$. Not all of the concentration fields used in the simulations are isotropic, but there are no mean gradients when the averages are performed over the domain of the simulation. Microscales in each direction can also be defined as

$$\begin{aligned} \frac{1}{\lambda_\phi^2} &= \frac{1}{(\lambda_1)^2} + \frac{1}{(\lambda_2)^2} + \frac{1}{(\lambda_3)^2} \\ &= \frac{\overline{(\partial\phi/\partial x_1)^2}}{6\overline{\phi^2}} + \frac{\overline{(\partial\phi/\partial x_2)^2}}{6\overline{\phi^2}} + \frac{\overline{(\partial\phi/\partial x_3)^2}}{6\overline{\phi^2}}. \end{aligned} \tag{4.2}$$

The power law decay of the scalar variance that is seen in most experimental measurements corresponds to growth in the average microscale as the square root of

time,

$$\lambda_\phi = \sqrt{12Dt/m}, \tag{4.3}$$

whereas an exponential decay corresponds to a constant microscale.

Inert species The time development of the average microscales for the concentration of the inert species from runs A–E, which have three different initial values for the Reynolds number, are shown in Figure 4.6. Since the molecular diffusivities differ for these cases, the values are plotted as $\lambda_\phi^2/12D$ in Figure 4.7. With this scaling the curves for different values of the molecular diffusivity are similar after a short time. This indicates that, after a transitional period, the decay rate of the scalar variance is relatively independent of the value of viscosity used in the simulations and has a power law of the form

$$\overline{\phi^2}/\overline{\phi^2}_0 = a(t - t_0)^{-m}. \tag{4.4}$$

The virtual origin t_0 must be used to take into account the transitional period. The linear part of the curves for runs A and C in Figure 4.7 give a decay exponent m of about 3.2, which is larger than that usually observed in experiments of grid-generated turbulence with temperature decay. The curve for run B gives a decay exponent of about 5.0, which is much larger than experimental measurements (Warhaft and Lumley, 1978; Sreenivasan et al., 1980).

The concentration fields in runs A–E all have the same initial conditions and are not statistically isotropic. The reactants in the four cases in run Y0 have different initial length scales (but are still anisotropic), whereas the species in run Z have isotropic distributions. The development of the square of the average microscale for

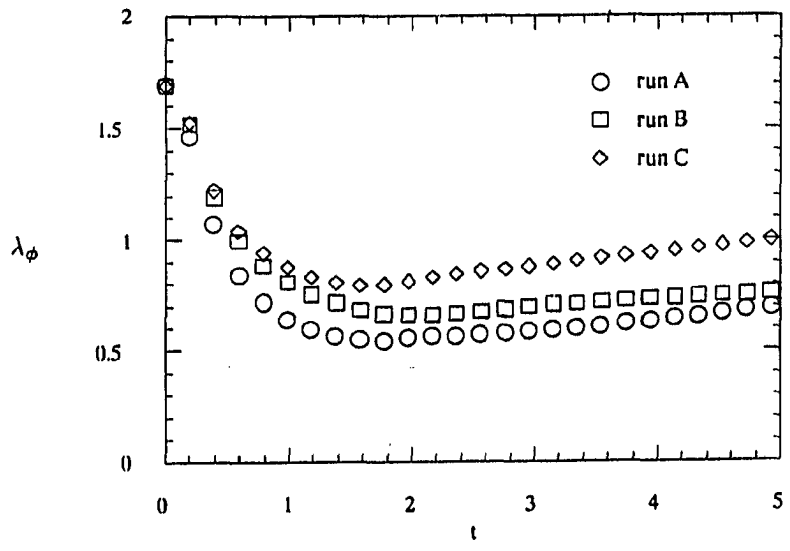

Figure 4.6: Time development of the average microscale for the concentration of an inert species ϕ in runs A–C. The initial R_λ is 65.8 in run A, 43.9 in run B, and 32.9 in run C

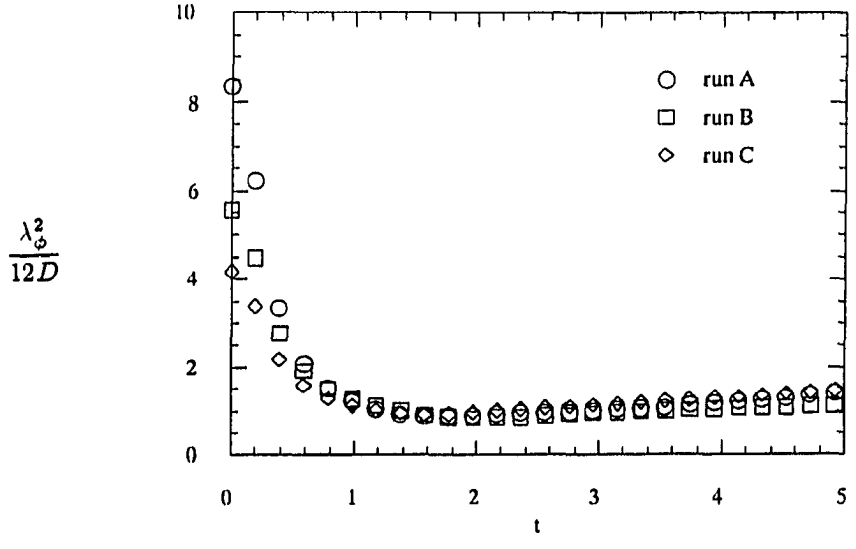

Figure 4.7: Time development of the squared microscale for the concentration of an inert species in runs A–C, normalized with the mass diffusivity

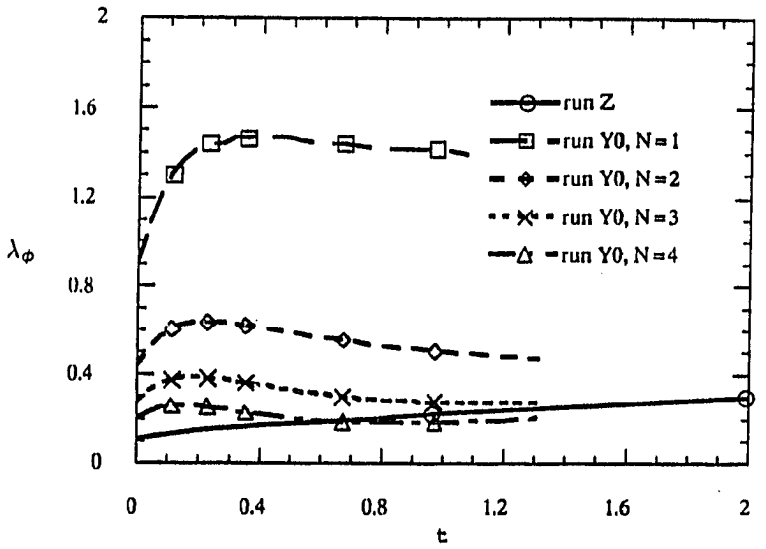

Figure 4.8: Time development of the squared concentration microscales for inert scalars in runs Y0 and Z. The initial concentration fields for run Z are isotropic, while the species in run Y0 have from one to four slabs in the domain. (The number of stripes is indicated by N in the legend)

each of the inert species from run Y is shown in Figure 4.8, along with the square of the isotropic microscale for the inert species in run Z. There is a linear increase of λ_ϕ^2 with time for run Z, but not for any of the species in run Y. The slope of the curve for the microscale in run Z indicates a decay exponent $m = 1.6$ for the scalar variance, which is slightly higher than most experimental measurements but within the range of observed values (Warhaft and Lumley, 1978; Sreenivasan et al., 1980). Each of the microscales for run Y increases initially, reaches a maximum value, decreases, and then—for the species with the smallest scales in run Y—begins to increase at later times. The microscales for runs A–E require a transitional period between one and two turnover times before increasing as $t^{1/2}$, but run Y was not carried past this point.

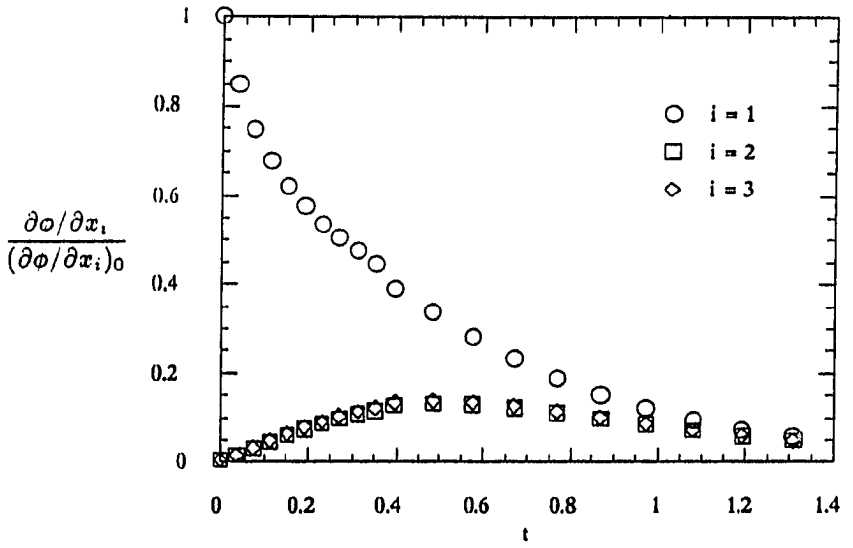

Figure 4.9: Time development of the mean square concentration derivatives in each coordinate direction, normalized with the initial mean square derivative in the x direction, for the species with three slabs in run Y0

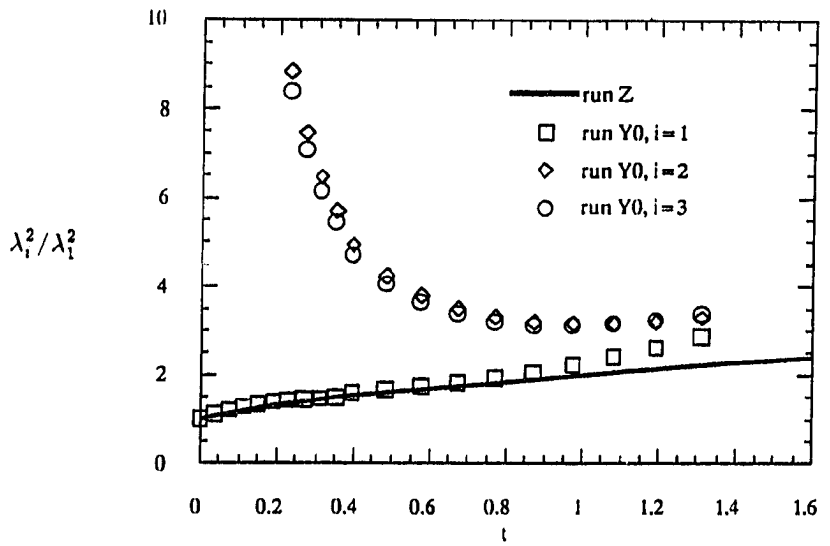

Figure 4.10: Time development of the directional concentration microscales defined in Equation (4.2) for run Y0 and of the average microscale in run Z

Since most of the species concentrations are not isotropic, the development of the microscales for each coordinate direction, rather than the average value, is more appropriate. The mean square concentration derivatives in each direction for one of the inert species in run Y0, normalized with the initial mean square derivative in the x direction, (Figure 4.9) show a decrease in the x direction and an increase from a zero initial value for the y and z directions, with a rate of change that depends on the initial length scale. The mean square derivatives in each direction have become almost the same by the end of the run for the species with the smallest initial scales. Normalized length scales in each direction, as defined in Equation (4.2), are shown for these conditions in Figure 4.10. The values of λ_x have approximately the same growth rate as in run Z, but do not have a strictly linear growth rate. The length scales in the y and z directions for the scalar with the smallest initial scales seem to approach the average length scale for run Z at the end of the simulation, as the concentration field becomes more isotropic.

Reacting species It is expected that chemical reaction will decrease the concentration microscales somewhat, since depletion of reactants in the reaction zone will increase the concentration gradients. An earlier study (Leonard and Hill, 1989), however, although carried out with lower precision than was used in the present one, indicated the rate of reaction has a very small effect on the concentration microscales. The average microscales for case Z and for the species with the smallest initial scales in case Y are shown in Figure 4.11 for different values of the Damköhler number. The Damköhler number is defined here as $k_R A_0 \Lambda / u'$, where A_0 is the initial mean concentration, Λ is the initial integral length scale for the velocity field, and u' is the

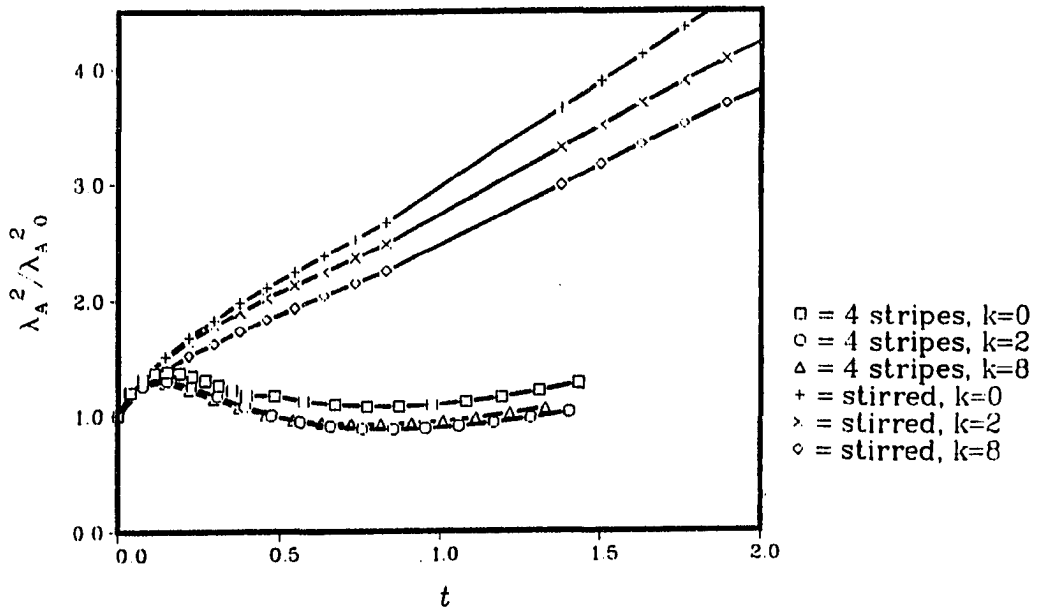

Figure 4.11: Development of the average microscale for the concentration of reactant A in runs Y and Z. The initial concentration fields for run Z are isotropic, while the species in run Y have from one to four slabs in the domain

initial turbulence intensity. The growth of the concentration microscales is retarded by the chemical reaction, but the effect is less pronounced for the anisotropic cases. The deviation of the concentration microscales for reacting species is about 10%–20% from the inert species microscales in both cases.

C/D models

Pdf's of the species concentrations are evaluated from DNS data for both reactive and inert flows. The evolution of joint composition pdf's for the two-species reaction, marginal pdf's of each species, and pdf's of inert species or conserved scalars are compared to solutions of modeled equations for the pdf's. The terms in the pdf equations that require modeling are evaluated directly from the DNS data. In this

way shortcomings of the models may be seen.

The modeled pdf equations have been solved with a Monte Carlo method to compare their predictions with the DNS results. It should be noted that such a solution with a C/D model does not give a pdf as a direct result. The pdf must be obtained by averaging over stochastic particles, in the same manner as it is obtained from the DNS data.

C/D models require a parameter to fit the decay rate of an inert species variance. One such parameter is the mixing frequency ω, which is defined as $\omega = 12D/\lambda_\phi^2$, and does not depend on the model. It is determined in this work from the DNS results for inert species. Physical considerations were not used in determining ω. Rather, the effect of incorporating a finite-rate chemical reaction was studied for a model which predicted the proper rate of mixing of an inert species (as measured by the variance decay). For each velocity field used in the simulation, an inert species was computed in addition to the reactive species. The decay of the variance for the inert species in each run was used to estimate ω for the purpose of testing the pdf models.

The Monte Carlo solution approximates the joint pdf for the concentrations of species A and B. The DNS used a square wave to define the initial reactant concentrations in all runs except run Z, but with the Fourier coefficients damped at large wavenumber to eliminate Gibbs' ringing. The initial pdf for each species in the DNS method was, therefore, a continuous function which was approximately bimodal. A beta function was chosen as the initial condition for the marginal pdf of each species in the Monte Carlo solution. Composition values for species A for each stochastic particle were taken from the beta distribution and multiplied by 2

to match the range of concentrations from the DNS, and then the concentrations for species B were evaluated as $2-A$. The initial variances of reactant concentration from the DNS were used to determine the parameters for a symmetric beta distribution. Values of the mixing frequency and the reaction rate coefficient were supplied to match conditions for each simulation.

Three C/D models, proposed by Curl (1963), Janicka et al. (1978, 1979) (which will be referred to as the JKK model), and Pope (1982), are used in the Monte Carlo calculations. All three models are implemented by the algorithm suggested by Pope (1982). The models differ in the bias in selecting particles (the Curl and JKK model have none) and in the effectiveness of mixing for each pair of particles. The number of particles used in the calculations was 2^N, with $N = 14$, and the time step was set so that $\omega t \approx 10^{-4}$. Pope's (1982) algorithm for selecting stochastic particles with an age bias by giving each particle an age and a life expectancy is more efficient to implement for the Curl and JKK models, which do not have an age bias, than an algorithm which randomly selects a fraction of particles for mixing.

Conserved scalar variance decay

Previous studies (Hsieh and O'Brien, 1986; Kosàly and Givi, 1987; McMurtry and Givi, 1989) have used constant values of ω in their Monte Carlo calculations. The values of the variance of an inert species concentration, $\overline{\phi^2}$, predicted by C/D modeling, using Pope's model with a constant mixing frequency determined from DNS data, are compared to the results of the DNS for run A in Figure 4.12. The time scaling has been made dimensionless with the eddy turnover time, defined in

terms of the initial intensity and integral length scale of the turbulence. The variance is made dimensionless with the initial mean concentration of the reactant species. The initial variance of the inert and reacting species are the same, and not equal to one, because the square wave initial conditions were damped somewhat. Since ω is constant, the C/D results show an exponential decay in the variance with the same average frequency as the DNS results. The C/D results are lower than the DNS results because the best fit of an exponential decay to the DNS data does not give the proper initial value for the variance. The initial values of the variance for the C/D methods were chosen to match values from the DNS data, rather than to give the best overall fit of the data. This initialization will be more important for the calculation of reacting scalars discussed later, where the initial rate of reaction depends on the degree of segregation. The different C/D models predict the same rate of decay of the variance of an inert species.

The problem of determining the proper value of ω, while important, is circumvented by using the results of the DNS to find the value for each case. The DNS data in Figure 4.12 show a transition period, preceding the exponential decay of the inert species, that cannot be accounted for by a constant mixing frequency. The predictions for the inert species variance are compared to the DNS results for a simple time-dependent fit of the mixing frequency in Figure 4.13. In Figure 4.13, ω initially increases linearly and then remains constant. This simple change in the form of ω can improve the agreement with the data at initial times, but the comparison at later times is poorer than for the constant value of ω. Unfortunately, no assumptions based on physical arguments were used to fit ω. The actual time dependence of the

mixing frequency in the DNS could be used, but this much detail will not generally be available when C/D methods are used. In addition, the choice of ω will not affect the shape of the pdf's for the nonreacting case, because the selection of stochastic particles, not the pairing between them, depends on ω.

The scalar microscale for case Z, which has an initially isotropic distribution for the initial concentration field, grows with the square root of time, instead of the nearly constant behavior seen in the other cases. The corresponding time dependence of the mixing frequency is $\omega = (at + b)^{-1}$, where the constants a and b are evaluated from the DNS data for use in the Monte Carlo calculations. The three models again produce virtually indistinguishable results for the variance decay (Figure 4.14), but overestimate the DNS results. The form of the mixing frequency does not fit the data at small times well, so the initial predictions of the rate of change of the variance are different for the C/D models and the DNS data, even though the variance decays at the same rate for both the models and the DNS data after a small time.

Shape of the pdf

Since all of the C/D models that are tested here predict the same rate of change of the inert species concentration variance, other comparisons must be made to evaluate the theories. The average of any function $Q(A, B)$ can be evaluated from the stochastic system, but functions of the gradients of A and B, such as the unknown conditional expectations, cannot because the particles have no information about length scales. The pdf's can be evaluated at different times and the rate of change approximated, but the pdf's tend to be noisy functions in both time and composition

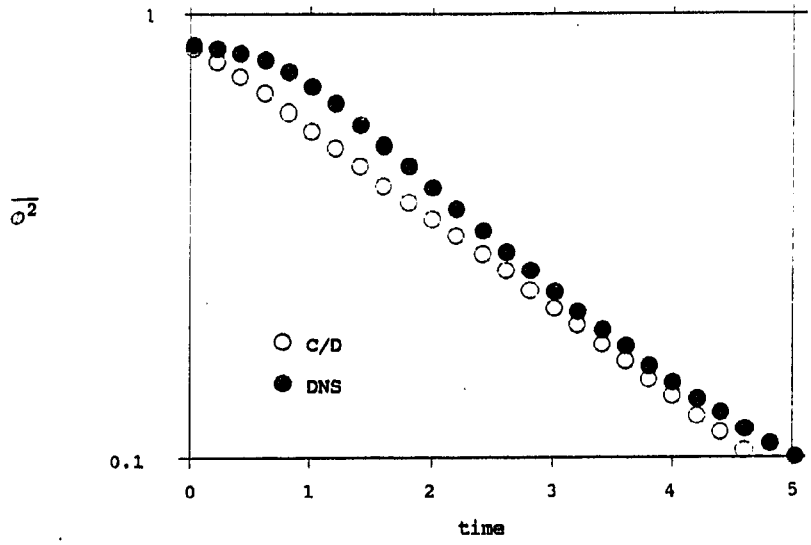

Figure 4.12: Concentration variance of an inert species, $\overline{\phi^2}$, calculated from DNS and C/D modeling for run A. The initial value of the Reynolds number is 65.8

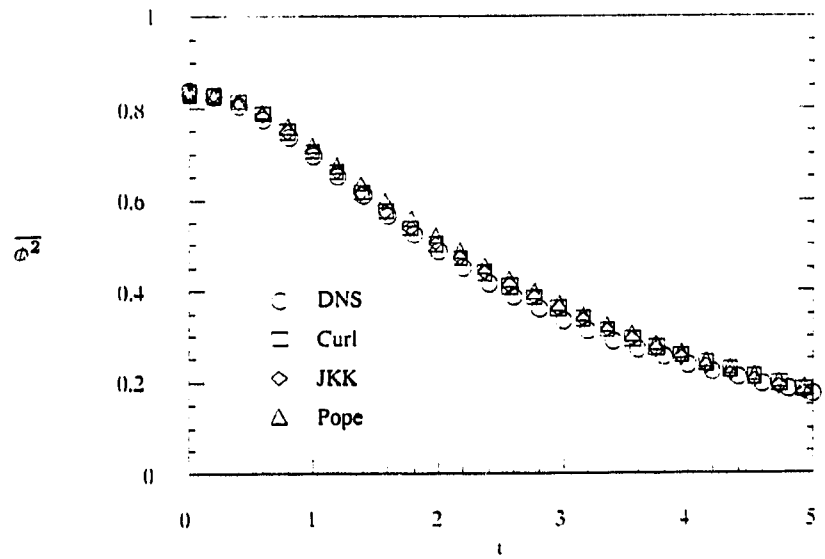

Figure 4.13: Concentration variance of an inert species, calculated from DNS and C/D modeling with a variable mixing frequency for run A

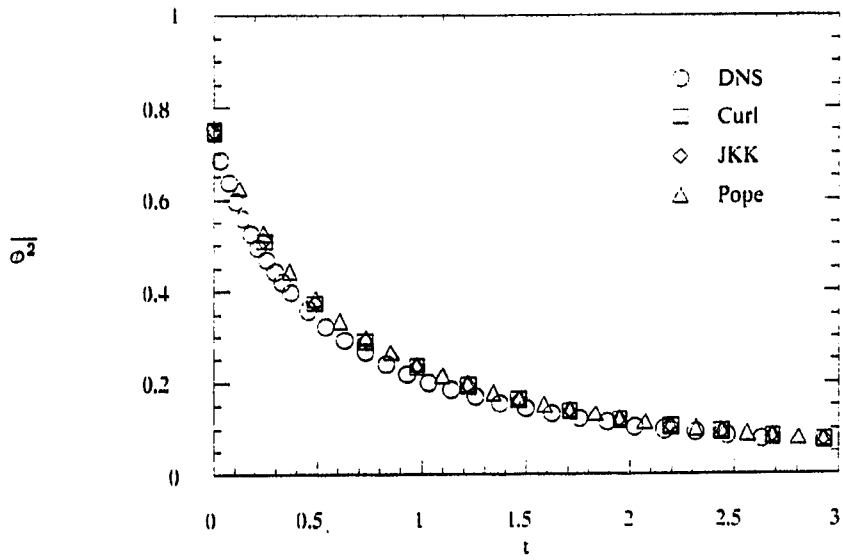

Figure 4.14: Concentration variance of an inert species, calculated from DNS and C/D modeling for run Z. The concentration fields are isotropic and the initial Reynolds number is 19.7

space. Rather than evaluating the instantaneous rate of change of the pdf in this manner, a series in time shows the evolution of the pdf from both the C/D models and the simulations. The term that requires modeling in the differential equation for the pdf is evaluated in the next section.

Inert flows The evolution of the inert species pdf, $f(\psi)$, calculated from the DNS data of run G, is shown in Figure 4.15. The pdf's were calculated with 64 sample bins without smoothing. The shapes are very similar to the data of Eswaran and Pope (1988) and McMurtry and Givi (1989). The pdf's calculated in those studies become self-similar by a dimensionless time of about $\omega t = 1.5$. whereas the pdf's in this study do not achieve a Gaussian shape during the simulation. It is known (Pope, 1982) that the C/D models do not yield Gaussian pdf's at long times. Pope's (1982) model gives

an asymptotic shape that is closest to Gaussian, but the curve is narrower and has a larger peak value. The present study considers the transition of the initial bimodal pdf, rather than the long-time behavior.

The pdf's shown in Figure 4.15 are compared to those obtained from the Monte Carlo solutions at two different times in Figure 4.16. Curl's model produces unacceptable behavior for the evolution of the pdf. It was noted in the earlier review of C/D models that a pdf which is initially discrete will remain so with Curl's model. Even though the initial pdf was continuous in this case, the use of Curl's model results in large peaks between the composition extremes. Also, the peaks at 0 and 2 decay more slowly with Curl's model than in either of the other models or than the simulation data, because the peak in probability in the center must be balanced by larger values at the extremes in order to give the same variance. The pdf's produced with the JKK model and Pope's model, on the other hand, are nearly identical, except that Pope's model gives a slightly flatter pdf. The peaks in probability at the extremes decrease much too slowly for all of the C/D models.

The extent of mixing for the stochastic particles is too large in these models to accurately predict the shape of the pdf during the transition period. Curl's model, which completely mixes the stochastic particles, produces the worst agreement. None of the methods use a pdf of the mixing extent which is a monotonically decreasing function, as suggested by Kosàly (1986), and all overpredict the probability of the concentration at the mean value. It is not clear what the form of the pdf for the mixing extent should be, or even whether it should be a constant function of time. The LMSE closure corresponds to a C/D model with the mixing extent chosen to peak

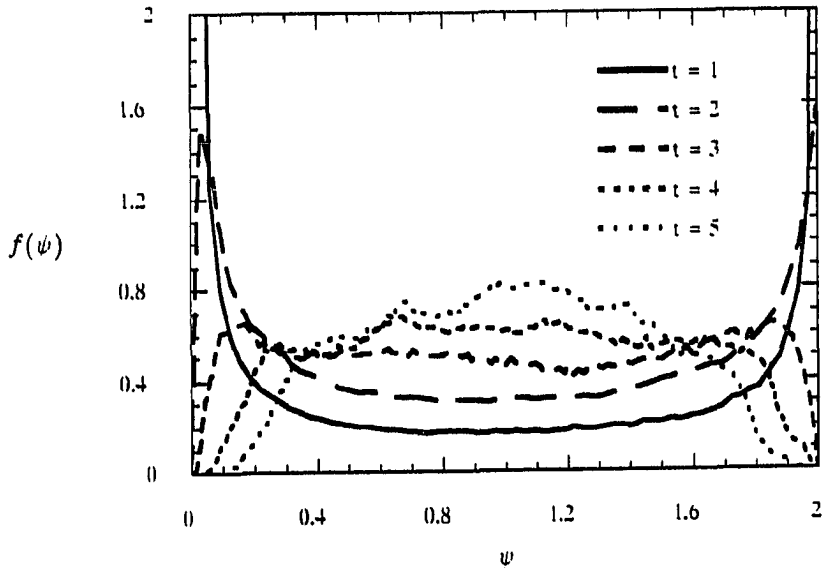

Figure 4.15: Evolution of the pdf of an inert species concentration in run G. The initial Reynolds number is 32.3 and Equation (3.9) is used for the initial energy spectrum. The time $t = 5$ corresponds to $\omega t = 0.875$

sharply at zero (Kosàly, 1986) and was shown by Kosàly and Givi (1987) to best fit the initial rate of change of concentration for an infinitely fast reaction, but the LMSE is known to preserve the shape of the initial pdf. The peaks at the extremes will be preserved with this model, but will move closer together as the variance decreases. This may be appropriate for the earliest stages of mixing, but does not agree with the DNS data for most of the mixing period.

The shape of the pdf's of the inert species evaluated from run Z are compared with predictions from Pope's model at similar times in Figure 4.17. The DNS data show the pdf to be centered about a value of ψ slightly greater than one, because the initial conditions were not precisely stoichiometric and the mean value of ϕ is 1.03. The C/D models, however, assumed the initial mean concentrations were stoichio-

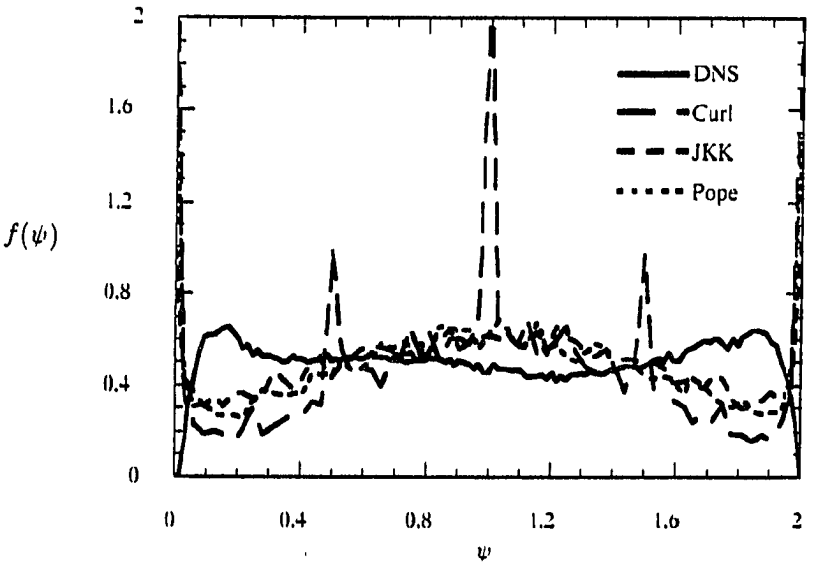

(a)

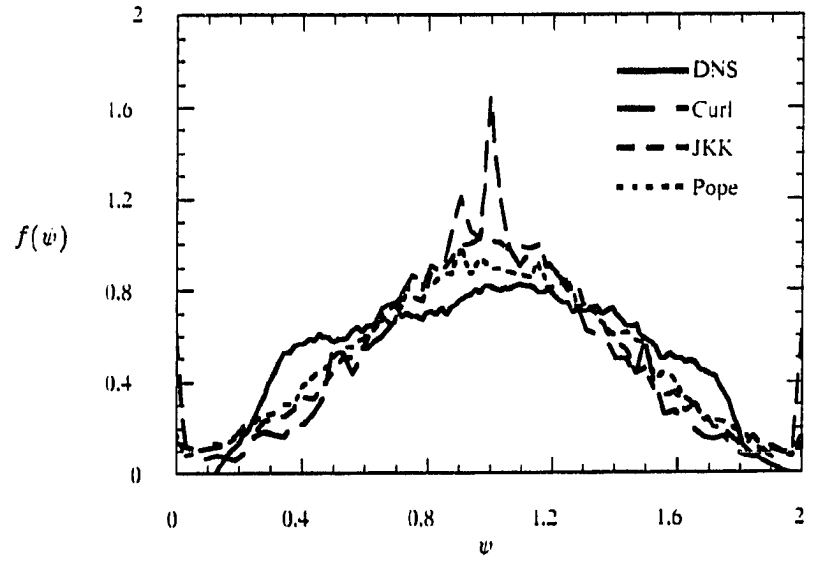

(b)

Figure 4.16: Comparison of C/D model predictions for the pdf an inert species concentration with the DNS data from Run G. (a) $t = 3$, (b) $t = 5$

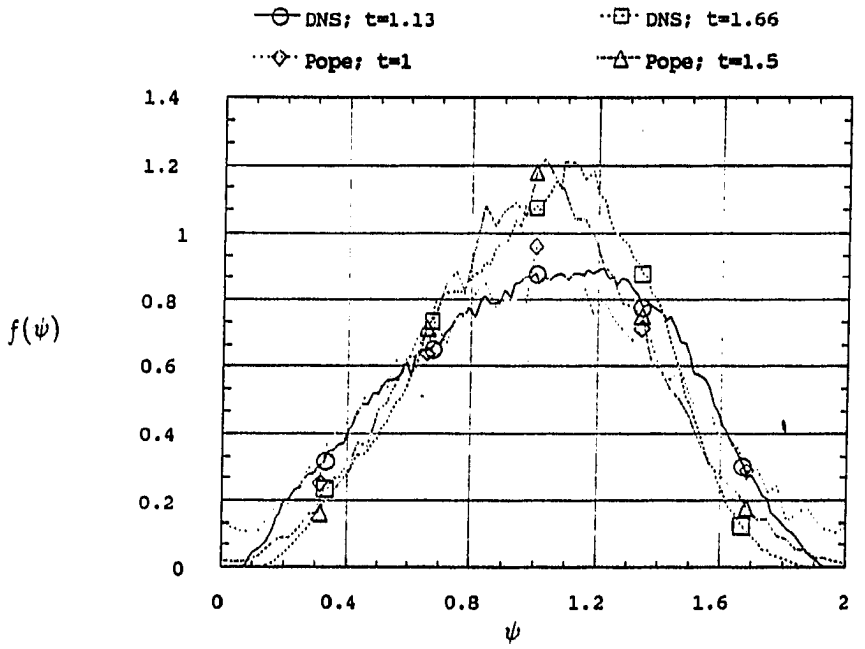

Figure 4.17: Comparison of C/D model predictions with Pope's method for the pdf of the concentration of an inert species with the DNS data from Run Z. The concentration field is isotropic

metric. The disagreement in the shapes of the pdf's cannot be attributed to the type of initial conditions used in runs A–E, X and Y, however. As in the anisotropic cases, the C/D models predict a peak value that is too large.

Reacting flows The evolution of the marginal pdf for the concentration of reactant A, $f(\alpha)$, from run G is shown in Figure 4.18. The joint pdf of the concentrations of reactants A and B is needed to calculate the average reaction rate. The marginal pdf is obtained by integrating the joint pdf over all concentration values for reactant B, and is shown here in order to make a comparison with the inert species. The differences between the inert and reactive cases do not become evident until after $t = 2$. A sharp peak in the probability at the origin persists because of the consumption of reactant A. The reaction causes a transport of probability to the origin, and

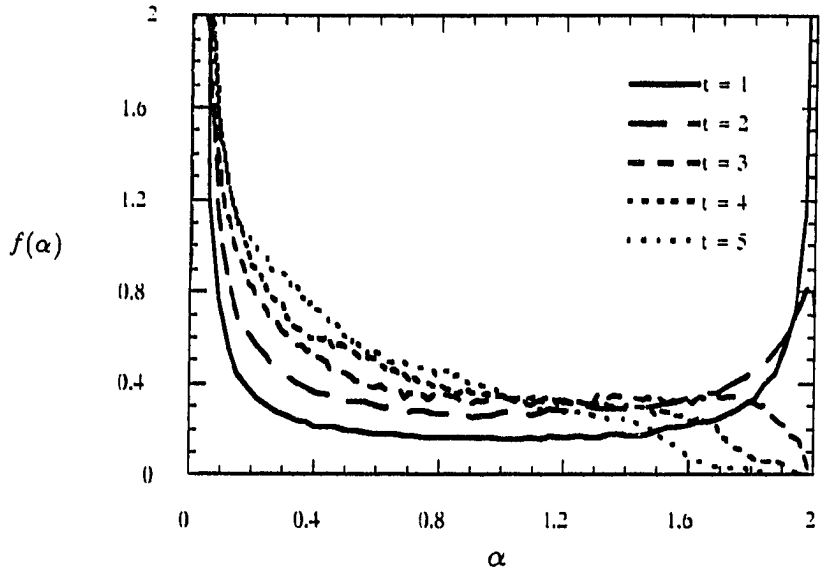

Figure 4.18: Evolution of the pdf of the concentration of reactant A in run G. ($R_\lambda = 32.3$, Da = 5)

the final distribution will eventually be a delta function at $\alpha = 0$.

The predicted marginal pdf's for the concentration of reactant A from the C/D models are compared with the DNS data in Figure 4.19. The difference in shape between the model predictions and the simulation results is less pronounced in the reacting case than in the inert case. There is still a tendency for the C/D models to predict a peak that persists at $\alpha = 2$. This corresponds to regions of the fluid containing species that have not been mixed and cannot react with species B. This peak at large concentration values results in probability values for $0 < \alpha < 2$ that are too small, because the total probability is unity. Curl's model develops peaks, as in the case with an inert species, but these peaks represent well mixed regions with a high reaction rate and are, therefore, reduced in the reactive case.

The marginal pdf of the concentration of either reactant does not contain enough

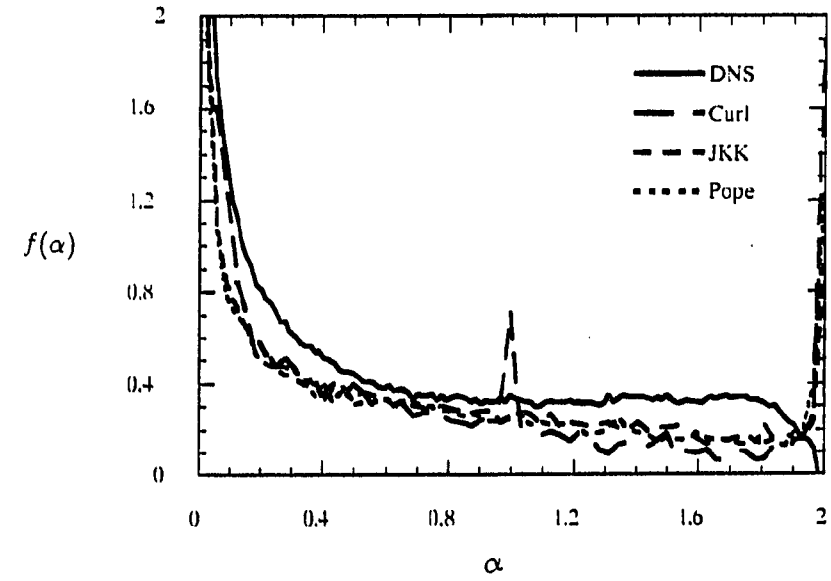

(a)

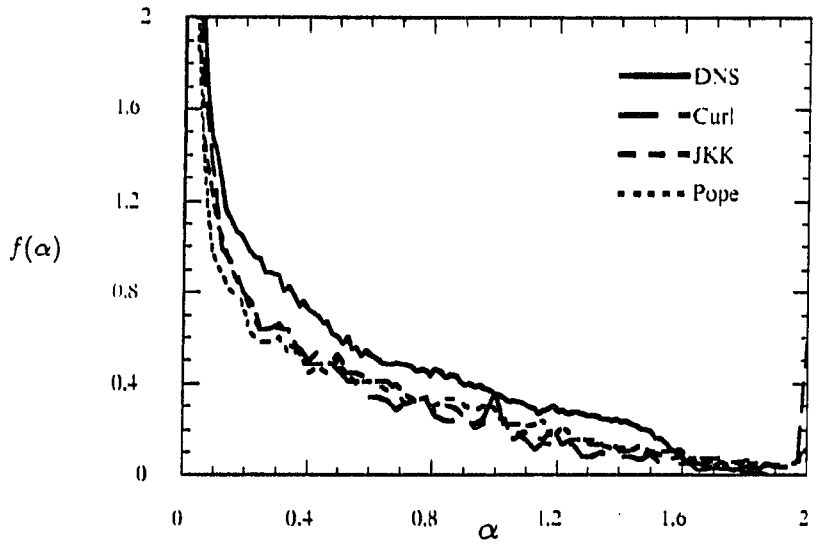

(b)

Figure 4.19: Comparison of C/D model predictions for the pdf of the concentration of reactant A with the DNS data from Run G. (a) $t = 3$, (b) $t = 5$

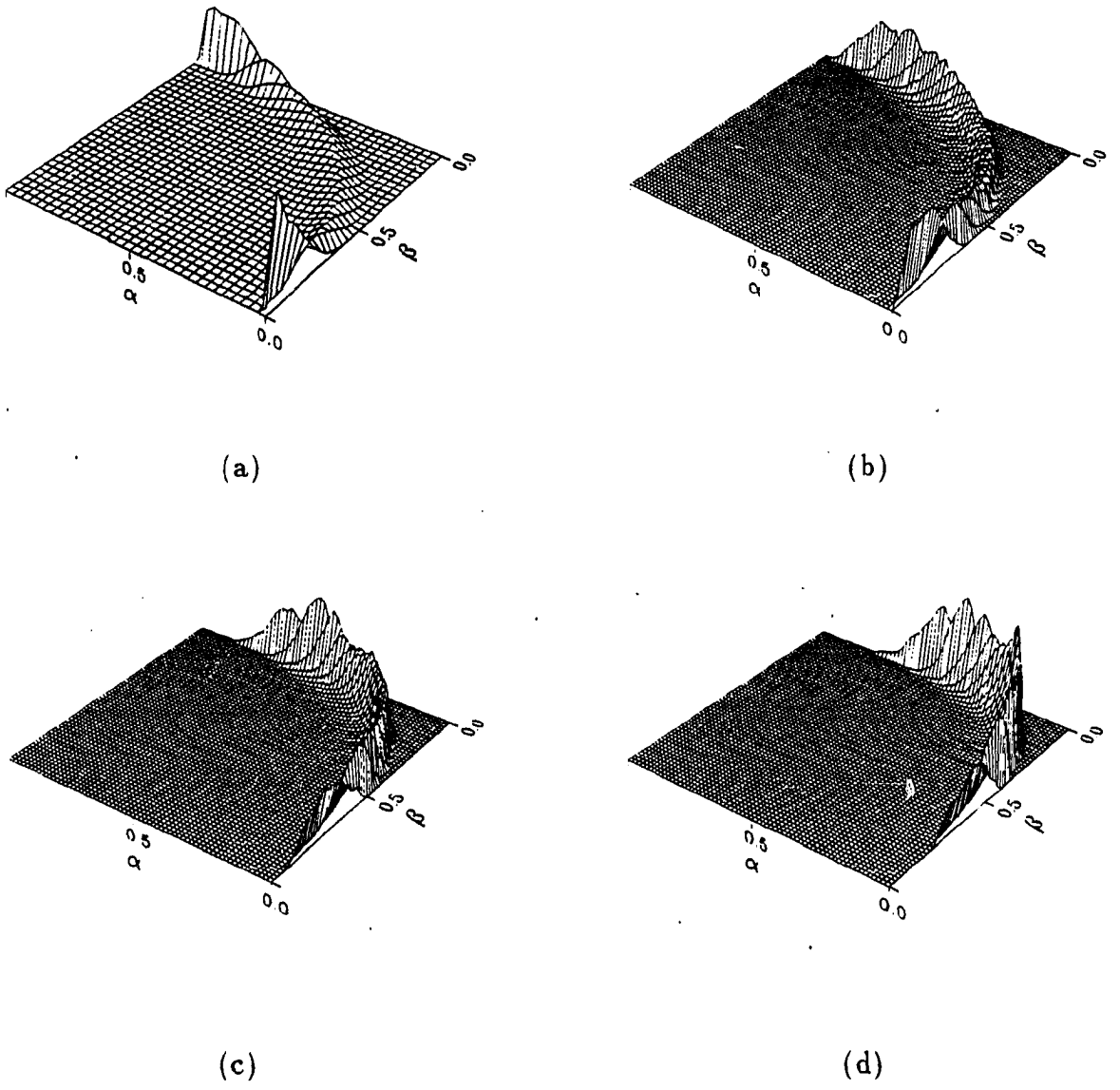

Figure 4.20: Development of the joint reactant concentration pdf in Run A. The origin in the α, β plane is at the right corner in each figure. (a) $t = 2$, (b) $t = 3$, (c) $t = 4$, (d) $t = 5$

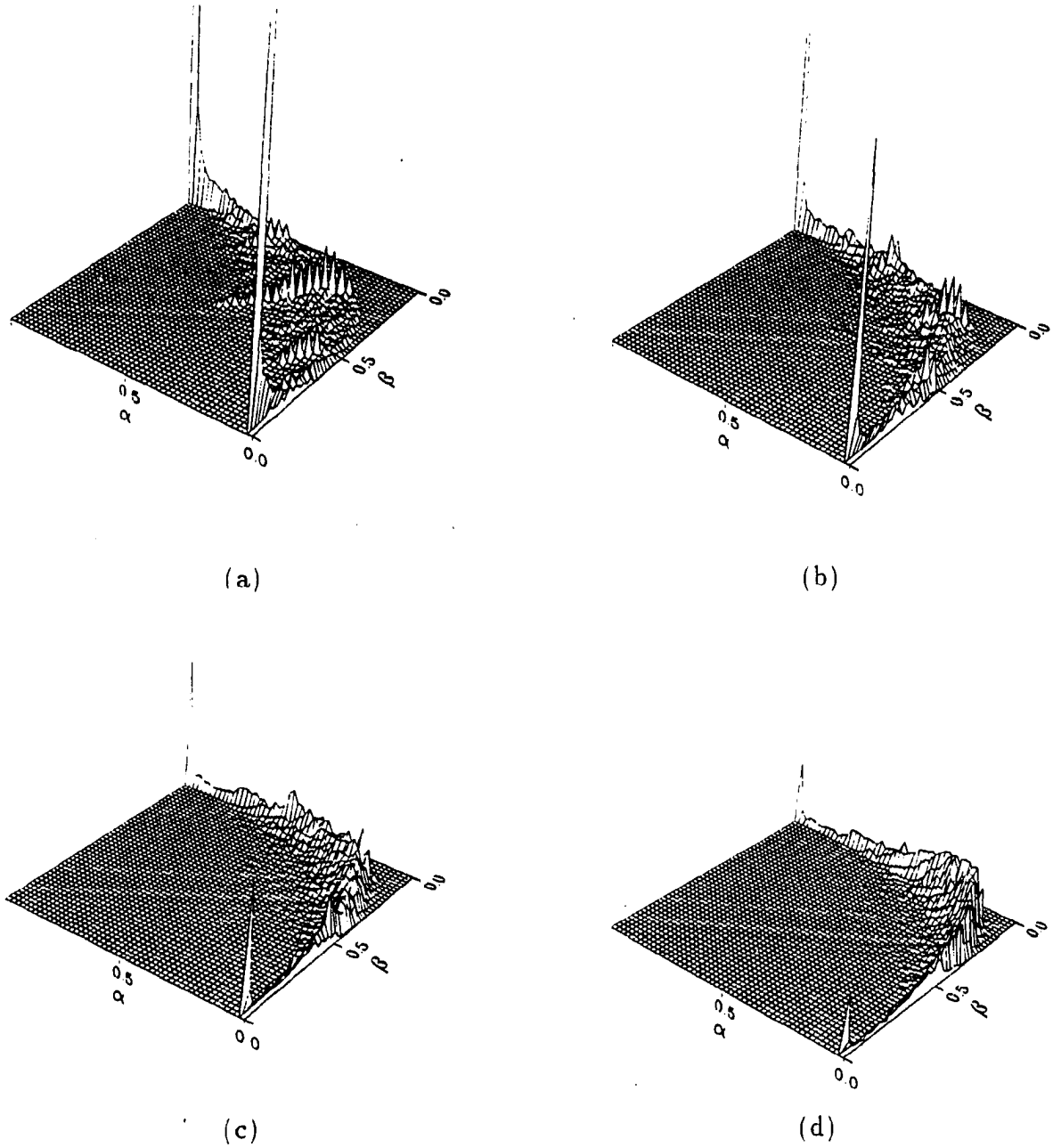

Figure 4.21: Prediction of the joint reactant concentration pdf with Curl's model for Run A. The peaks in the pdf have been truncated in (a) and (b). (a) $t = 2$, (b) $t = 3$, (c) $t = 4$, (d) $t = 5$

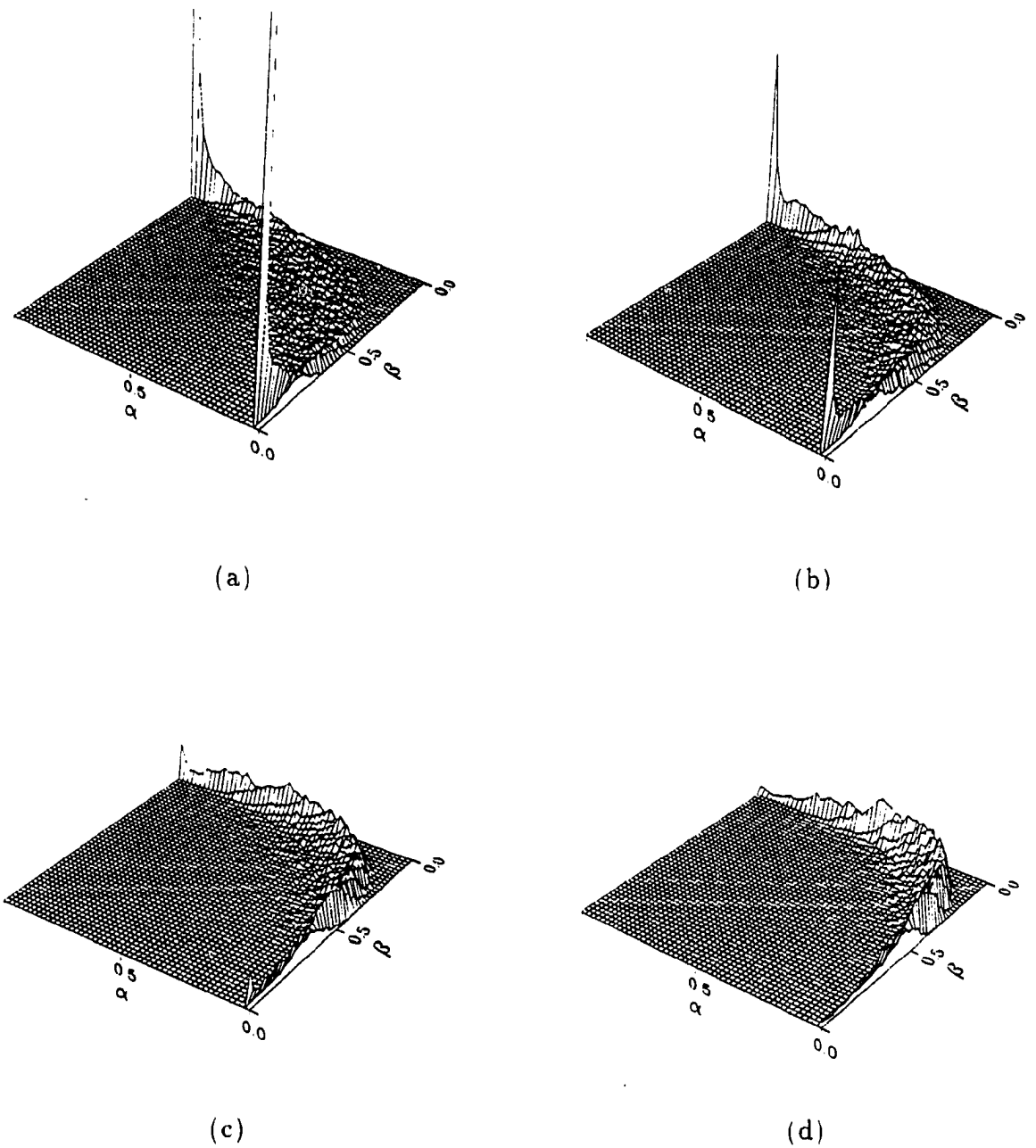

Figure 4.22: Prediction of the joint reactant concentration pdf with Pope's model for Run A. The peaks in the pdf have been truncated in (a). (a) $t = 2$, (b) $t = 3$, (c) $t = 4$, (d) $t = 5$

information to determine the average reaction rate. The joint pdf of the concentration of the two reactants in run A is shown at various times in Figure 4.20. The transport of probability in the (α, β) composition space due to mixing and chemical reaction can be seen, but the contributions from each of these mechanisms cannot be determined. This question will be addressed in the next section. The predictions of Curl's and Pope's models for the shape of the pdf are shown in Figures 4.21 and 4.22 for the same sequence of times used in Figure 4.20. The spikes that are produced by Curl's model in the pdf of the inert species become ridges of high probability in the joint reactant concentration pdf. Peaks in the pdf at the initial pdf location persist until the end of the calculation with Curl's model, whereas smaller peaks are seen in the joint pdf with Pope's method. The shape of the pdf predicted using Pope's model is similar to that calculated from the DNS data, with the largest differences occurring at the relatively high concentrations of either reactant. There was very little qualitative difference between the predictions of Pope's and JKK's models.

The mean concentration of reactant A in run G is compared to the predictions of the C/D models in Figure 4.23. The C/D models can accurately predict the mean reactant concentration for finite rate chemistry when the mixing frequency is chosen properly. A time-dependent mixing frequency was needed to match the initial rate of mixing, which determines the initial rate of change of the mean concentration. The variance of reactant concentration is not predicted as accurately as the mean, but the slower decay rate due to the effects of reaction is accounted for, despite the fact the mixing frequency was calculated from data for the inert species. Predictions of the mean reactant concentration for case Z (with isotropic concentration fields) also

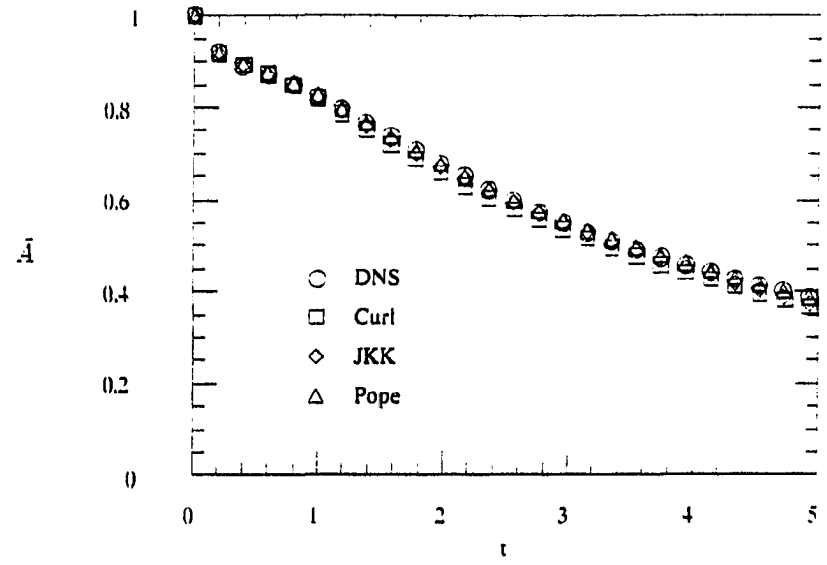

Figure 4.23: Comparison of the prediction of mean reactant concentration from C/D modeling with the DNS data for run G. (R_λ = 32.3, Da = 5)

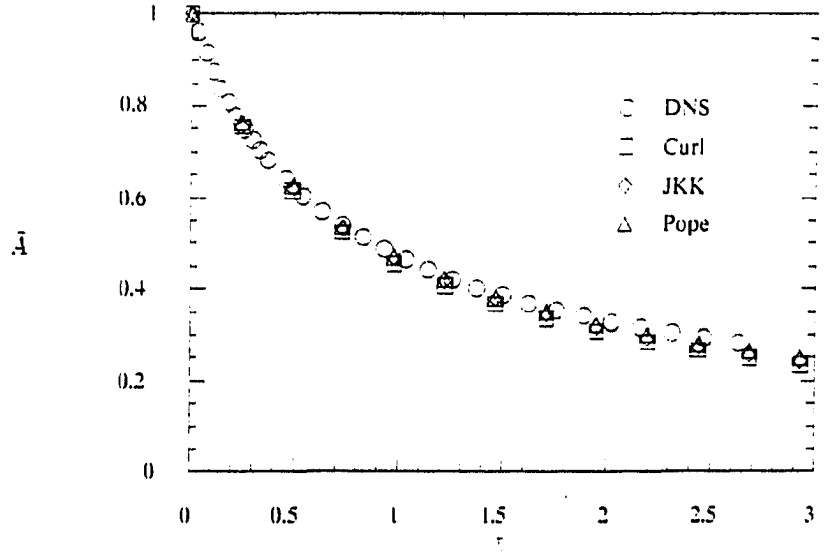

Figure 4.24: Comparison of C/D model predictions for the mean concentration of reactant A with the DNS data from Run Z. (R_λ = 19.7, Da = 6.4, isotropic concentration fields)

agree well with the DNS data (Figure 4.24) for all three models and both reaction rates, although the agreement is better at lower reaction rates. The pdf methods all predict the rate of change of the variance of the reacting species to be too low.

There is little difference between either the predicted shape of the pdfs or the mean concentration, when calculated with the Pope and JKK models. Pope's method is an improvement over other C/D models, in the sense that the self-similar pdf for an inert scalar at long times is more nearly Gaussian. However, closures that are based on asymptotic behavior of the pdf of an inert species may not show any improvement in predicting reacting flows, since the reaction may have reached completion before the asymptotes are reached. The reaction is more than 60% complete by the end of the calculation in this study, while the pdf is still in transition from a bimodal to a Gaussian distribution.

The mixing term

The instantaneous rate of change of the pdf can be calculated by evaluating the right hand side of Equation (2.10). The mixing term for the pdf, shown in Equation (2.11), is a first- or second-order derivative of the product of the pdf and a conditional expectation. The pdf's and conditional averages of the Laplacian of an inert species were calculated from saved scalar fields for runs X, Y, and Z, which were all of short duration, in order to calculate the rate of change of the pdf for a conserved scalar. The entire term in Equation (2.11), rather than just the conditional expectation, is modeled in the C/D methods as an integral in composition space. One reason for this is to prevent instabilities that might result from a numerical method

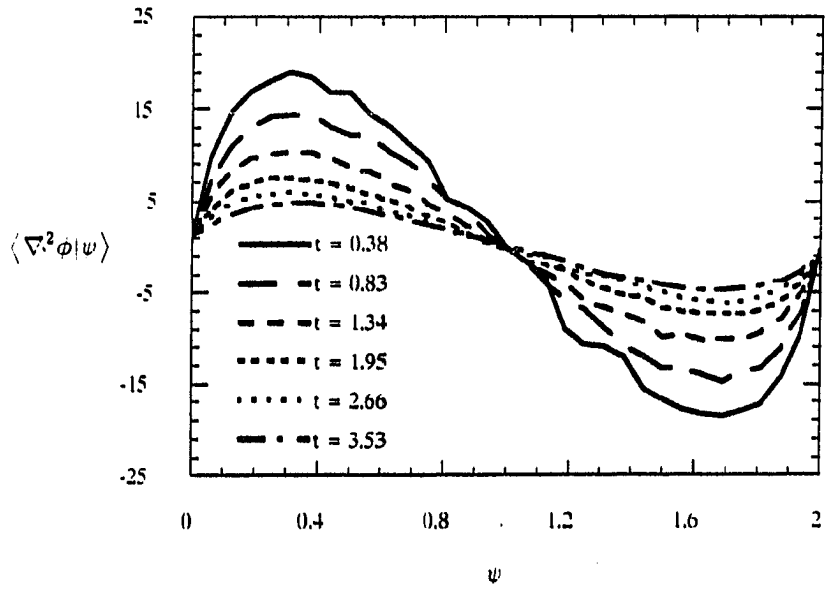

Figure 4.25: Development of $\left\langle \nabla^2\phi \middle| \psi \right\rangle$ for run X. ($R_\lambda = 19.7$, slab initial conditions)

required to approximate derivatives (Janicka et al., 1978).

Inert flows The development of the conditional expectation of $\nabla^2\phi$ for small times is shown in Figure 4.25 for case X. The product of the pdf and the conditional expectation, shown in Figure 4.26, is independent of time over most of its range during this simulation. The magnitude of the slope of $\left\langle \nabla^2\phi \middle| \vec{\psi} \right\rangle f(\vec{\psi})$, which is proportional to the rate of change of the pdf, $\partial f/\partial t$, is greatest near the peaks and is nearly constant near the center of the range. The maximum rate of decrease of probability occurs at the location of the peaks of the pdf. The maximum rate of increase of probability occurs very near the peaks, indicating a local rate of transfer in composition space.

The rate of change of the pdf, evaluated by calculating the slope of the curve

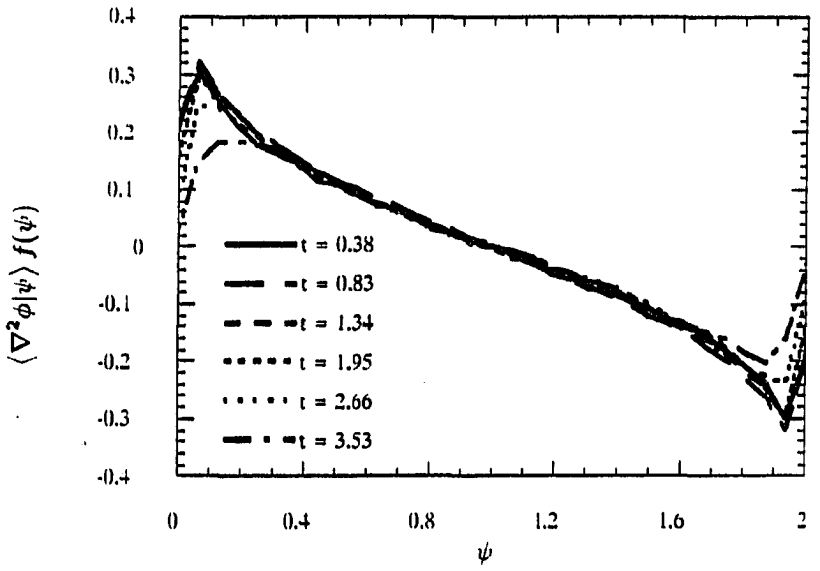

Figure 4.26: Development of $\langle \nabla^2 \phi | \psi \rangle f(\psi)$ for run X

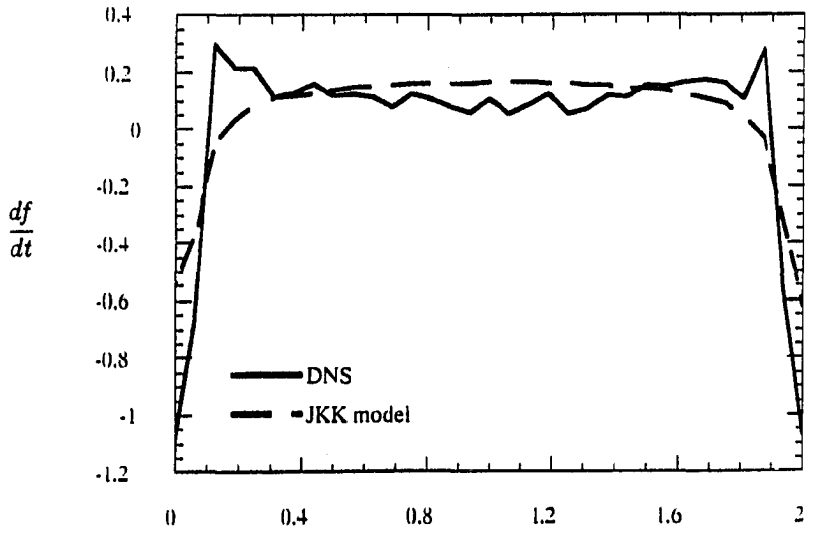

Figure 4.27: Comparison of the instantaneous rate of change of the pdf of an inert species concentration, as predicted by the JKK model, with the DNS data from run X at time $t = 3.5$

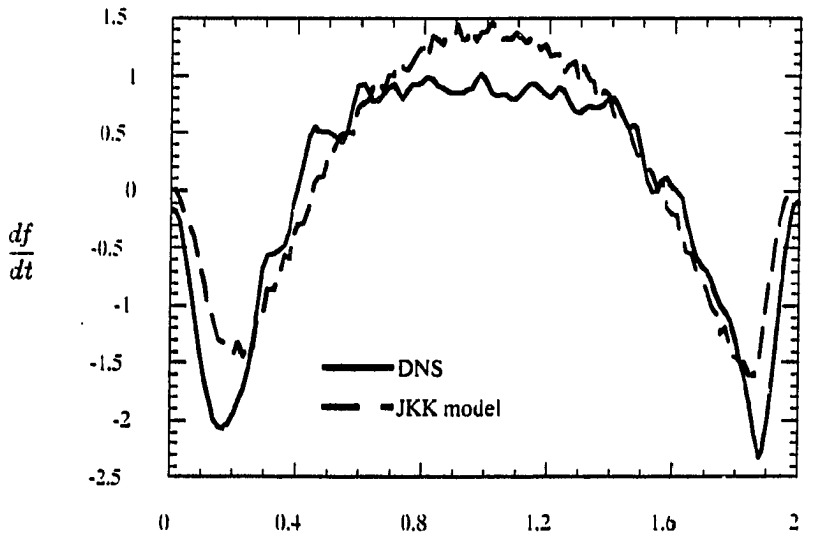

Figure 4.28: Comparison of the instantaneous rate of change of the pdf of an inert species concentration, as predicted by the JKK model, with the DNS data from run Y0

in Figure 4.26 for $\omega t = 0.35$, is compared with the prediction of the JKK model in Figure 4.27. The model predictions were calculated by using the pdf evaluated from the DNS in the right hand side of Equation (2.15) rather than a pdf evaluated with the Monte Carlo solution with the model. The predicted rate of decrease of the peaks of the pdf are too small, and the predicted rate of increase of the pdf near the mean value is too large. Figure 4.28 shows a comparison, at time $t = 1.3$, between the calculated rate of change of the pdf and the predictions using the JKK model for the inert species with the largest initial mixing frequency in run Y0 (four bands of each reactant in the domain). The model predicts the rate of change of the pdf around the mean value to be too large and the rate of change near the peaks of the pdf to be too small. This behavior is consistent with an observation by Pope (1982), that the pdf

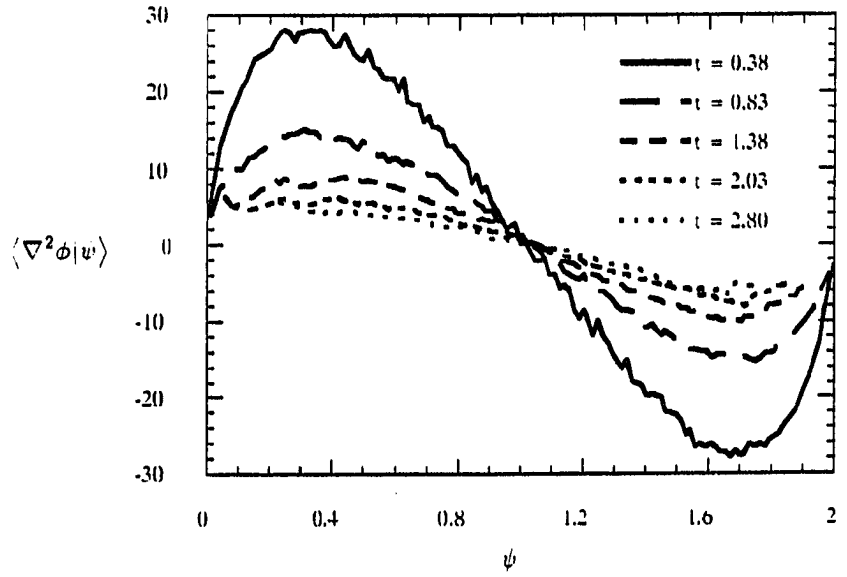

Figure 4.29: Development of $\langle \nabla^2\phi | \psi \rangle$ for an inert species concentration from run Z. ($R_\lambda = 19.7$, isotropic concentration fields)

determined with a modified Curl model, such as the JKK model, becomes peaked too sharply about the mean, and moments normalized with the variance become infinite for the JKK model.

The conditional expectation of $\nabla^2\phi$ is shown at various times in Figure 4.29 for case Z (isotropic concentration fields). The curves at small time resemble those for the cases with the slab geometry in Figure 4.25. The product of the conditional expectation and the pdf shows more time dependence (Figure 4.30) than in the other cases, but the concentration fields have evolved further in run Z.

The integral form for the mixing term in the JKK model is evaluated at different times and compared to the derivative of the curves in the previous figure in Figure 4.31. The curves show a decreasing agreement in time between the DNS results and the model predictions. The pdf at the mean composition is predicted to grow

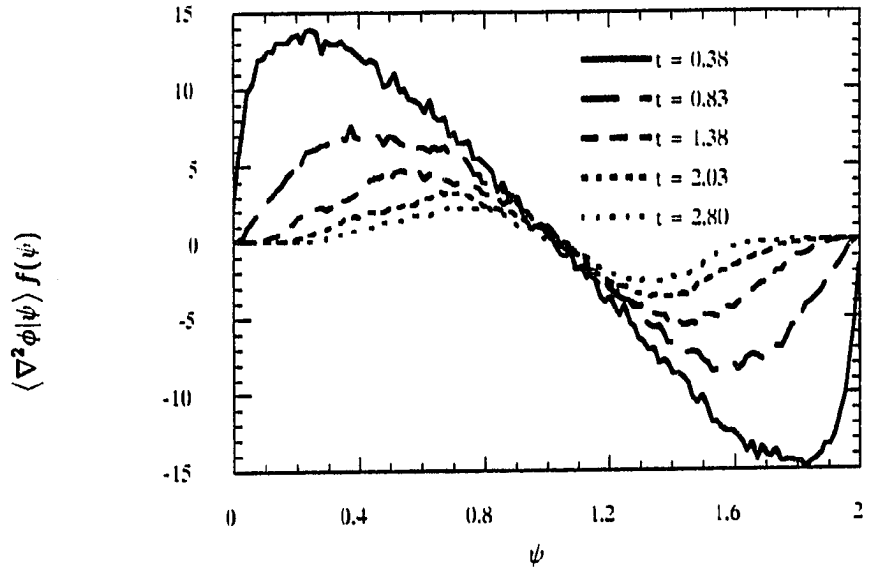

Figure 4.30: Development of $\left\langle \nabla^2\phi \middle| \psi \right\rangle f(\psi)$ for an inert species concentration from run Z

at an increasing rate in the JKK model, but at a fairly constant rate from the DNS data. Points in composition space where the net change of the pdf is zero agree well at the later time, however.

Reacting flows The effects of mixing and reaction on the rate of change of the joint pdf of reacting species can be considered as fluxes in composition space, since the right hand side of Equation (2.10) is a sum of divergences of vectors in composition space. The reaction flux

$$\mathbf{S}(\vec{\psi})f(\vec{\psi},t) \tag{4.5}$$

is known, given the value of the pdf, but the mixing flux

$$\left\langle D\nabla^2\vec{\phi} \middle| \vec{\phi} = \vec{\psi} \right\rangle f(\vec{\psi},t) \tag{4.6}$$

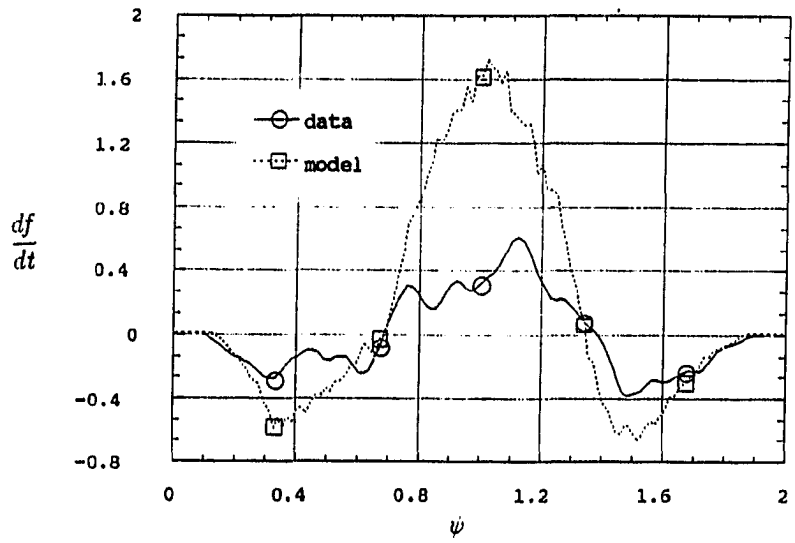

Figure 4.31: Comparison of the instantaneous rate of change of the pdf of an inert species concentration, as predicted by the JKK model, with the DNS data from run Z

must be modeled.

These fluxes are evaluated at $t = 2.1$ from the results of run Z (isotropic concentration fields) and shown with the corresponding joint pdf of the reactant species in Figure 4.32. The length of the reaction flux vectors are proportional to $\alpha\beta f(\alpha, \beta)$, and they all have the same orientation. The magnitude and direction of the mixing vectors at each point in composition space, however, depend on the conditional expectation of each species. The only model that we have discussed that attempts to predict these mixing vectors is the LMSE model (Dopazo and O'Brien, 1974), in which the mixing vector points towards the point $(\bar{A}, \bar{B})$ and with a magnitude that is proportional to the distance to this point. If the calculations were continued with no further change due to chemical reaction, the final state of the system would have

uniform concentrations at the current mean values, or a delta function in composition space. The instantaneous mixing fluxes, as shown in Figure 4.32, however, are not necessarily directed toward the current mean values, so the LMSE closure cannot predict the rate of change of the pdf properly for this case. The maximum deviation in the direction of the mixing fluxes occurs at the extremes of the concentration values, where the magnitudes of the fluxes are greatest. The divergence of the mixing flux shown in Figure 4.32 is modeled by the C/D methods and can be calculated from DNS data, but the mixing fluxes cannot be determined from the C/D models.

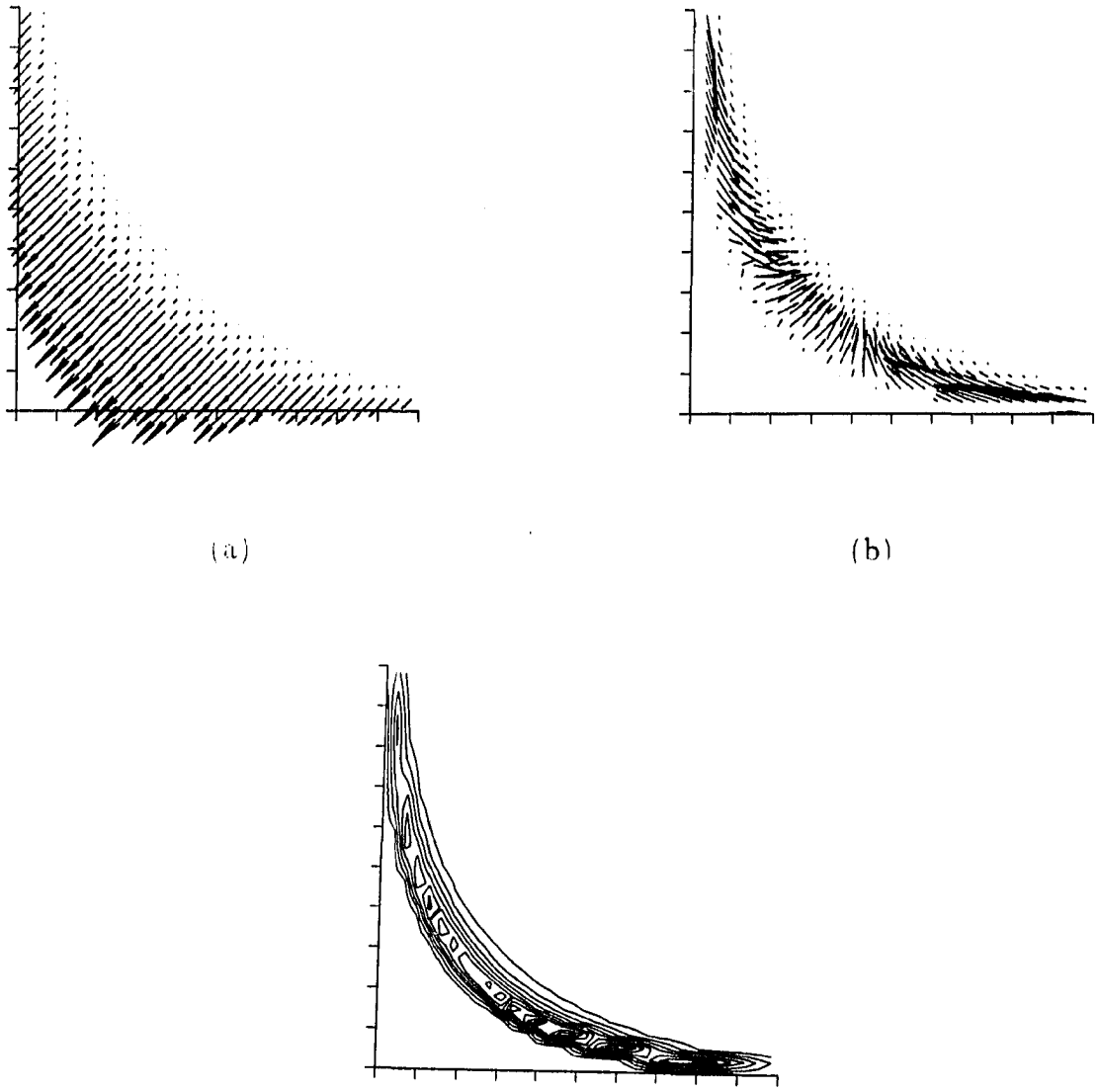

(a)

(b)

(c)

Figure 4.32: Composition fluxes of probability for run Z. (a) Reaction flux; (b) Mixing flux; (c) $f(\alpha,\beta)$

CHAPTER 5. SUMMARY AND CONCLUSIONS

Direct simulations of an irreversible, second-order, isothermal reaction between initially segregated reactants were made in order to evaluate some statistical quantities that must be modeled in statistical theories of turbulent reacting flows. Of particular interest here are terms that are obtained from diffusive terms in the governing equations. The simulations performed in this study used different values of the Reynolds and Damköhler numbers, and different initial conditions for the velocity and concentration fields.

The velocity fields used in this study developed quite differently. The velocity field that was chosen from a Gaussian distribution and scaled to fit a specified energy spectra at the initial time required approximately one turnover time to develop. After the transitional period the kinetic energy decayed at a rate that is seen for final period turbulence. The preconditioned velocity field fit a power law decay of $\overline{u^2}$ over the duration of the simulation with a decay exponent, n, of 1.5.

The microscale for the decay of concentration fluctuations was examined for different initial conditions and Damköhler numbers. The case for isotropic initial conditions showed a power law decay of the variance with an exponent of $m = 1.6$. The anisotropic cases, in which the scalar fields consist of slabs of reactants, showed length scales in the direction of the initial gradients to behave similar to the average

microscale in the isotropic case, but the length scales in the other direction decrease from initially infinite values. This is consistent with the fact that the concentration gradients are initially zero in two directions, but increase as the rotation and straining of the fluid distort the isoconcentration surfaces.

The microscales show a small dependence on the reaction rate, but the values for inert flows were used in calculation of the pdf's of reactant concentrations. In the C/D models studied here, all the effects of the turbulence on the rate of change of concentration gradients and, hence, the molecular mixing, are incorporated through the scalar microscales.

The three C/D models tested produced nearly identical behavior in the low order moments examined. The shapes of the pdf's, which determine moments of all orders, are different for the three methods. Curl's model demonstrated the well-known physical shortcomings associated with the simplest C/D model. The JKK model and Pope model produced very similar results for the shape of the pdf. Pope's model was introduced to provide better asymptotic behavior for the pdf of an inert species. The long-time behavior was not examined, because the focus here was on the evolution of the reaction between two segregated species. The reaction will be nearly complete or may be dominated by kinetics when the pdf of a conserved scalar becomes Gaussian.

There is little reason to distinguish between the JKK and Pope models for the results of the simulation. Curl's model is unsuitable, based on the the predicted shapes of the pdf. Since Pope's model has been shown to provide better behavior for long times (Pope, 1982) and is no more difficult to implement than the JKK model, it is recommended as the choice for a C/D model if one is used.

Pope's model includes two arbitrary functions that have recommended choices to predict a shape that is close to Gaussian. These choices were used in this study, but may not be the most appropriate forms for the transition from the initial pdf to a Gaussian pdf. The similarity in shapes between our results for the inert species pdf and those in other studies indicates that general forms of these functions may be possible. Since one of the functions, $A(\alpha)$, is related to the early shapes of the pdf's, but is roughly optimized for long-time behavior, the shape of $A(\alpha)$ may not be constant.

The actual shapes of the mixing terms in the differential equation for the rate of change of the pdf, as well as the conditional expectations which are included in these terms, have been evaluated from the simulation. With these data available, more accurate models may be possible.

PART II.

EVALUATION OF CLOSURE MODELS FOR TURBULENT REACTING FLOWS

CHAPTER 6. INTRODUCTION

The details of turbulent flows cannot be predicted because uncertainties that are present in initial and boundary conditions are rapidly amplified, yet average quantities can often be measured and are reproducible. Furthermore, the full details of the flow are really too much information, since the range of scales in turbulent flows is so large. The desired description of the flow is usually in terms either of a few statistical moments, such as the means and rms values of quantities such as velocities or temperature, or of the probability distributions for these quantities.

The rates of chemical reactions are affected by concentration fluctuations caused by turbulent motion when time scales for the reactions are of the same order or faster than the time scales for mixing, and when the order of the reaction is greater than one. The mean reaction rate cannot generally be calculated using the mean concentrations of the reactants. The manner in which reactants are introduced determines whether the turbulent fluctuations increase or decrease the mean reaction rate. Only when the reaction rate is much slower than the rate of mixing and concentration fluctuations are, thus, removed by molecular diffusion can the kinetic expressions for a nonlinear reaction rate be evaluated with mean concentrations.

In this paper statistical methods used to predict the average reaction rates in turbulent reacting flows are reviewed, and the predictions of the statistical methods

are compared to data from direct numerical simulations (DNS's). With the DNS, the unsteady, three-dimensional differential equations governing the flow are solved without modeling. Preliminary results of tests of reaction rate closure models with DNS data have been reported in Leonard and Hill (1986, 1988, 1989). A similar study has been made recently by McMurtry and Givi (1989) who used DNS's to evaluate one of the models examined here, as well as the probabilistic models examined in Part I.

CHAPTER 7. BACKGROUND

Results from numerical simulations are used in this paper to evaluate models used for the mean rate of reaction in a chemically reacting turbulent flow. These models are discussed in this section, as well as experimental work and previous numerical simulations which have been used to validate some of the models. Statistical treatments of turbulent reacting flows have been reviewed by Hill (1976), Jones and Whitelaw (1982), O'Brien (1986), and Borghi (1988). direct simulations of reacting flows have been reviewed by Oran and Boris (1987), Jou and Riley (1987), and Givi (1989).

Statistical Methods

Because of the large range of scales in turbulent flows, it is not practical to perform full simulations for all cases of interest. In most cases it is only necessary to know the largest scales or the lowest order statistical quantities. The equations governing the flows are used as a basis for statistical treatments, but the effects of turbulence are then modeled so that a finite number of equations can be used to describe the system.

Statistical methods are divided into two categories here: probability and moment methods. Probability methods are those which use equations for probability density

functions (pdf's) that are generated from the conservation equations governing the system, while moment methods involve various kinds of approximations of the statistical moments, although they may use an assumed shape of a pdf as part of a model. Only single-point methods are considered here.

Probability methods

Joint single-point probability density functions (pdf's) of the reactant concentrations contain all the information needed to calculate single point statistics of the concentration fields, including the mean reaction rate. Dynamical equations for these pdf's can be derived directly from the governing differential equations for the system. For details, see Pope (1985). Source terms from chemical reactions appear in closed form in the pdf equations, so the method will not be discussed in this part. Molecular effects, on the other hand, must be modeled in this approach. These methods were discussed in Part I.

Moment methods

The equations governing the transport of mass and momentum are typically averaged using Reynolds averaging or, in the case of variable density flows, Favre, or density weighted, averaging (Favre, 1965). Averaged conservation equations have been the most commonly used type of statistical treatment. Closure models for these equations vary in the level of sophistication but have been well developed for non-reacting flows. Among the reviews of these methods are Reynolds (1976), Reynolds and Cebeci (1978), Launder (1978), and Lumley (1980). Reacting flows, on the other

hand, present certain unique problems when treated with moment methods. For example, concentration values, unlike velocity values, are bounded and positive, and the pdf's of the concentrations are therefore generally far from Gaussian. Also, correlations between species concentrations and exponential functions of temperature are possible for nonisothermal cases because of Arrhenius forms for the reaction rate.

The Reynolds averaged form of the governing equation for species A in homogeneous turbulence is

$$\frac{d\overline{A}}{dt} = -k_R \left(\overline{A}\,\overline{B} + \overline{ab} \right), \tag{7.1}$$

where A and B, the concentrations of species A and B, are decomposed into means, $\bar{A}$ and $\bar{B}$, and deviations, a and b, from the means. Transport terms do not appear because the fields are homogeneous. Equation (7.1) and a corresponding equation for the mean value of species B contain a covariance of the concentrations of the two reactants. Higher order moment equations can be derived from the governing equations using averaging rules. For example, equations for the variance and covariance of the reactant concentrations are

$$\frac{d\overline{a^2}}{dt} = -2D\overline{\frac{\partial a}{\partial x_j}\frac{\partial a}{\partial x_j}} - 2k_R \left(\overline{a^2 B} + \overline{ab}\,\overline{A} + \overline{a^2 b} \right), \tag{7.2}$$

and

$$\frac{d\overline{ab}}{dt} = -2D\overline{\frac{\partial a}{\partial x_j}\frac{\partial b}{\partial x_j}} - k_R \left(\overline{a^2}\overline{B} + \overline{b^2}\overline{A} + \overline{ab}(\overline{A} + \overline{B}) + \overline{a^2 b} + \overline{ab^2} \right), \tag{7.3}$$

where we have assumed that the diffusivity D is the same for the two species. The equation for the variance of species B is given from Equation (7.2) by interchanging the variables for the concentrations of species A and B (Toor, 1969).

The closure problem for reacting flows is similar to that of ordinary turbulence theory: even with the simplifications of statistical homogeneity, the number of statistical quantities is greater than the number of equations. Relationships between the statistical quantities, in addition to the moment equations derived from the governing equations, are therefore postulated, in order to obtain a closed system of equations. Only the terms that arise in the moment equations because of the source terms in the governing equations are considered in this paper. Terms involving molecular mixing, such as the first term on the right hand side of Equation (7.2) or (7.3), and the effect of reaction on these terms, have been discussed in Part I.

Assumed pdf models One way to model the mean reaction rate and other single-point statistics of the concentration fields is to model the joint pdf of the concentrations of the reacting species. A simple form of the pdf with a small number of parameters can be assumed, instead of solving a differential equation, and can be used to calculate the average reaction rate in a moment method. Moment methods using this type of closure will be referred to as "assumed-pdf" models. The goal in assuming a form for the pdf is to find a realistic shape with as few parameters as possible. Some of these models are discussed in this section. A general review can also be found in Borghi (1988).

For the simple two-species reaction that is being considered here, either the joint pdf of A and B or the joint pdf of A and the conserved scalar variable $(A - B)$ can be used to calculate the mean reaction rate. The latter may be preferable, since the marginal distribution of $(A-B)$ will be independent of reaction rate if the diffusivities of the two species are equal.

Fast chemistry models The assumed-pdf approach is often used in the limiting case of very fast chemistry. In this case, only a one-dimensional pdf for the conserved scalar is needed for a single-step reaction. It is much easier to specify a one-dimensional form than a multi-dimensional form. Suggested forms for the conserved scalar pdf include Gaussian, clipped Gaussian, beta, uniform, bimodal, and trimodal distributions (see the reviews by Jones and Whitelaw (1982) or Borghi (1988)).

Typical eddy models Pdf's can be continuous or discrete functions, or a combination of both. A discrete form of the pdf implies that the domain can be divided into a number of representative samples or "typical eddies", as proposed by Donaldson (1975) and Donaldson and Varma (1976). There are three variables associated with each of these "eddies" or "environments", in the terminology of Tarbell's mechanistic closures (Tarbell and Mehta, 1986), that are possible for a joint pdf of two reactants. These are the concentrations of each reactant in the representative sample and the probability of the event itself. The representative samples will be referred to as environments, rather than typical eddies, in this section for each of the models.

The joint pdf can be written for n environments as

$$f_{AB}(\alpha,\beta;t) = \sum_{i=1}^{n} c_i \delta(\alpha - \hat{\alpha}_i)\delta(\beta - \hat{\beta}_i), \tag{7.4}$$

where $\hat{\alpha}_i$ and $\hat{\beta}_i$ are the concentrations in each of the environments. If a low-level closure is desired, then the number of events must be kept small, and some mechanisms must be proposed to relate some of the variables.

One example of a discrete pdf has been proposed by Patterson (1981). Three

Table 7.1: Parameters for Patterson's model

environment	c_i	$\hat{\alpha}_i$	$\hat{\beta}_i$
1	$\frac{\overline{a^2}}{\overline{A}^2+\overline{a^2}}$	$\frac{\overline{A}^2+\overline{a^2}}{\overline{A}}$	0
2	$\frac{\overline{b^2}}{\overline{B}^2+\overline{b^2}}$	0	$\frac{\overline{B}^2+\overline{b^2}}{\overline{B}}$
3	$1-c_1-c_2$	$\frac{\overline{A}^2+\overline{a^2}}{\overline{A}}$	$\frac{\overline{B}^2+\overline{b^2}}{\overline{B}}$

environments are possible. In the first environment only A is present, in the second only B, and in the third both A and B are present. This model has nine variables, but the probabilities of the environments must add to one, and the concentration of one reactant has been specified in two of the environments. The model further stipulates that the concentration of A or B in the environment where both are present is the same as in the environment where it is present alone. The parameters in Equation (7.4) for this model are summarized in Table 7.1. This pdf will result from one-dimensional top-hat concentration profiles for each species that overlap. With these restrictions, the model has four parameters. The mean and variance of the model can be calculated in terms of these parameters and the system inverted to give the parameters in terms of the means and variances of the concentrations of the two reactants.

Patterson's closure requires the solution of Equations (7.1) and (7.2) for the mean and variance of the concentration of each reactant. The second-order term $\overline{ab}$ and the third order terms $\overline{a^2b}$ and $\overline{ab^2}$ are modeled with the pdf. The unknown moments of reactant concentration on the right hand sides of Equations (7.1) and (7.2) can

Table 7.2: Parameters for Tarbell's model

environment	c_i	$\hat{\alpha}_i$	$\hat{\beta}_i$
1	$I_s/2$	$2\bar{A}_0$	0
2	$I_s/2$	0	$2\bar{B}_0$
3	$1-I_s$	$\overline{A}$	$\overline{B}$

be expressed in terms of the moments on the left hand side, giving the reactant concentration covariance as

$$\overline{ab} = -\overline{a^2}\,\overline{b^2}/\overline{A}\,\overline{B}. \tag{7.5}$$

Patterson recommends using $\overline{a^2b} = 0$ and $\overline{ab^2} = 0$ instead of the form predicted with the pdf.

$$\overline{a^2b} = \frac{\overline{a^2}\,\overline{b^2}}{\bar{B}}\left(1 - \frac{\overline{a^2}}{\bar{A}^2}\right), \tag{7.6}$$

in order to improve the prediction of the model. The dissipation term must still be modelled, as the pdf form makes no assumptions about concentration gradients. Patterson recommends using Corrsin's (1964) form for the microscale for the dissipation rate of concentration fluctuations of a nonreacting species in an isotropic mixer.

Another discrete pdf has been proposed by Dutta and Tarbell (1989) and was derived from a mechanistic model of mixing (Tarbell and Mehta, 1986). The form is similar to Patterson's in that there are three "environments". Two environments contain only species A or B and the third contains both. In Tarbell's model, however, the concentrations in the environments containing only one species remain the same, and the probabilities of the occurrence of the environment (or the volume fraction of the environment) decay exponentially, with a characteristic time determined by the

mixing of an inert species ϕ:

$$I_s = \frac{\overline{\phi^2}}{\overline{\phi^2}_0} = e^{-t/\tau} \tag{7.7}$$

The characteristic time, τ, is the only parameter in the model. The probability of occurrence of the third environment is fixed by the requirement that the total probability be unity. The concentrations in the third environment is assumed to be at the mean concentration of the reacting species. The parameters appearing in Equation (7.4) for Tarbell's model are summarized in Table 7.2.

Tarbell's closure requires the solution of Equation (7.1) for the mean concentration of each species. A time scale for mixing, or the microscale for the inert species concentration, must be supplied for this model. This time scale can also be used to close the dissipation term. The unknown term in Equation (7.1) can be written in terms of the mean reactant concentrations and a characteristic time as

$$\overline{ab} = e^{-t/\tau}\left(\overline{A}\,\overline{B} - \overline{A}_0\overline{B} - \overline{A}\,\overline{B}_0\right). \tag{7.8}$$

We have used a slightly modified version of Tarbell's model since the mean concentration, when evaluated from the assumed form of the joint pdf, does not change. This does not mean that the rate of change is zero when Equation (7.8) is used to close the moment equations, but this form is not really consistent with the three-environment model. We use, instead,

$$\overline{ab} = \frac{I_s}{1 - I_s}\left(\bar{A}\bar{B} - \bar{A}\bar{B}_O - \bar{A}_0\bar{B} - I_s\bar{A}_0\bar{B}_0\right), \tag{7.9}$$

which is obtained by requiring the assumed form for the pdf to predict the correct mean reactant concentration.

Toor's model One of the older models that has received a great deal of attention is one proposed by Toor (1969), which used the limiting cases of very fast and very slow reactions to form a closure for intermediate rates. Toor considered a multi-jet reactor with two feed streams, whereby each stream is introduced in a fraction of the inlets with fixed concentrations of the two species, A and B. The reactants A and B are assumed to have identical mass diffusivities. The conservation equations and the initial conditions for the two species are made identical with a simple change of variables. These equations are identical to the conservation equation for an inert species as the reaction rate approaches zero. The variance of an inert species, the variance of reacting species, and the covariance of reacting species, therefore, all decay at the same rate if the reaction rate is very slow and if the diffusivities of the reactants are equal. Defining the normalized variance of the concentration of an inert species to be ${\sigma_m}^2 \equiv \overline{\phi^2}/\overline{\phi^2}_0$ and the normalized covariance of reactant concentrations to be ${\psi}^2 \equiv \overline{ab}/\overline{ab}_0$, then

$$\psi^2 = {\sigma_m}^2. \tag{7.10}$$

The zero subscript denotes an initial value, and the subscript m refers to a process with mixing in the absence of reaction.

In the fast chemistry limit Toor (1962) used a Gaussian pdf for the conserved scalar variable $(A - B)$ to relate the mean concentration of each reactant for a stoichiometric mixture to the variance of the value of the conserved scalar.

$$\frac{\overline{A}}{\overline{A}_0} = \sigma_m. \tag{7.11}$$

The covariance can be expressed in terms of the mean concentrations if the reactants are completely segregated, $\overline{ab} = -\overline{AB}$, and so the covariance is again related to the

conserved scalar variance

$$\psi^2 = \sigma_m{}^2. \tag{7.12}$$

Since the expressions are the same for the very fast and very slow cases, Toor (1969) proposed that the relationship may hold for intermediate cases and, therefore, that reactant concentration covariance is independent of the reaction rate.

The initial conditions for most of the cases considered in this paper—complete initial segregation of reactants A and B—have discrete initial joint pdf's for A and B, with only two possible events. The pdf of the conserved scalar is bimodal in this case. Kosàly (1987) has shown that the asymptotic behavior of Toor's model for the reactant covariance can be modified for the case of very fast chemistry where the initial pdf for the conserved scalar is not Gaussian. (This dependence was noted earlier and parenthetically in a paper by Miyawaki et al., 1974.) If it is assumed that the pdf approaches a Gaussian shape at long times, as shown from DNS's by Eswaran and Pope (1988), a simple multiplicative factor that depends on the shape of the initial pdf (in this case, $2/\pi$) is needed to correct Toor's theory for long times, but values at intermediate times are not predicted. No predictions can be made about the behavior of finite rate chemistry, although Kosàly assumes that the fast and slow cases are limits between which the intermediate results should lie. McMurtry and Givi (1989) have shown from DNS that the ratio of the reactant covariance to the conserved scalar variance is between one and $2/\pi$ for finite-rate chemical reactions, as well as for the limiting case of infinitely fast reaction rate.

The fast chemistry limit of Toor's theory holds when the shape of the standardized pdf, $f' = \sigma f(z)$, where $z = (\psi - \mu)/\sigma$ and μ and σ are, respectively, the mean

and standard deviation, is constant (Givi and McMurtry, 1988). In order to illustrate the behavior of Toor's model for a case where the conserved scalar pdf has a form that can be expressed in terms of the first two moments and that changes shape, assume the pdf of the conserved scalar is a beta distribution.

$$f(\psi) = \frac{\Gamma(p+q)}{\Gamma(p)\Gamma(q)}\psi^{(p-1)}(1-\psi)^{(q-1)}. \tag{7.13}$$

The beta distribution is only defined on the range (0,1), so the conserved scalar must be scaled accordingly. The mean value of the conserved scalar, given by this pdf, is $p/(p+q)$ and the variance is $pq/(p+q)^2(p+q+1)$. The ratio p/q must be a constant, since the mean value of the conserved scalar does not change. The parameters of the beta distribution can be expressed in terms of the mean and variance of the conserved scalar concentration. If the initial concentrations of the reactants are in stoichiometric proportion, then

$$p = q = \frac{1}{8\sigma_m^2} - \frac{1}{2}. \tag{7.14}$$

The decay rate of the conserved scalar, therefore, determines the parameters p and q and the shape of the pdf. As p and q go to zero the pdf approaches two delta functions, at $\psi = 0$ and $\psi = 1$, and as p and q become infinitely large, the pdf approaches a Gaussian shape. Toor's theory can, therefore, be used to evaluate the mean reactant concentrations and the reactant covariance for the fast chemistry limit in terms of the incomplete beta function. The ratio of the reactant covariance to the conserved scalar variance is plotted in Figure 7.1 as a function of ωt, where the conserved scalar variance is given by $\sigma_m = e^{-\omega t}$. The asymptotic limit of $2/\pi$ is approached only after the variance has decayed to a value that results in greater than 90% completion of the reaction. While Kosàly's remarks about Toor's theory are

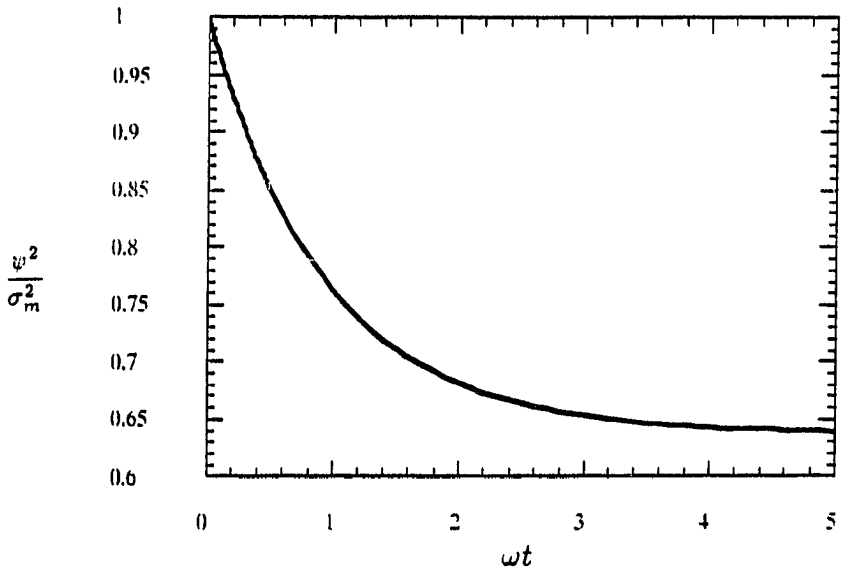

Figure 7.1: Predictions of Toor's theory, assuming a beta distribution for the conserved scalar

correct, it is difficult to incorporate them into a closure model since they hold only for the asymptotic behavior of the infinite rate limit.

Other models Concentration values must be positive and concentration moments are subject to some inequality rules. For example, $\overline{ab} \leq -\overline{AB}$. Inequalities such as these can be used as a basis for a closure model. Lin and O'Brien (1972) have proposed such a model for third order moments, but different choices for the coefficients used in the model that all meet the inequality restrictions can give results differing from each other by an order of magnitude and, in some cases, with opposite signs (O'Brien, 1986).

Bilger (1980) has used a variable representing the departure of the concentration of a reactant species from its value in the case of infinitely fast reaction. The mean

reaction rate is then expressed as a function of this variable and a conserved scalar. Neglecting the fluctuations in the perturbation variable and including a transport equation for its mean value completes the closure.

Borghi (1988), in a recent review of turbulent combustion modeling, remarks that the moment approach has been abandoned as a failure. Closures, such as Toor's, that attempt to model the mean reaction rates directly in terms of low order moments of concentration and temperature may be not be suitable for nonisothermal reactions, but combustion modeling is currently done with the assumed-pdf forms of the moment methods.

Previous Experimental Work

Several experimental studies have been performed with simple second-order reactions. These studies are summarized in Table 7.3.

Vassilatos and Toor (1965) studied reactions with a wide range of kinetic time scales in a tubular multi-jet reactor. The rates for acid-base neutralization reactions were controlled by mixing, whereas the rate of hydrolysis of methylformate was controlled by the kinetics. The time scales for mixing and reaction were comparable for an intermediate case of CO_2 + NaOH. The results of the experiments with the very rapid reactions supported Toor's 1962 theory relating mixing to conversion.

Mao and Toor (1970) studied acid-base reactions between the moderate (Da = O(1)) and very fast (Da = $O(10^7)$) reaction speeds of Vassilatos and Toor's earlier work. The reactor was the same as that used by Vassilatos and Toor, but the mixing device was improved by adding more tubes to feed the reactant streams. In both of

these studies small temperature rises were measured and related to the conversion of reactant species. Turbulence statistics were not measured. The invariant hypothesis of Toor (1969) was tested by using the fastest reaction to calculate the mixing characteristics of the reactor. The experimental data supported Toor's predictions, although there was enough scatter in the data to also support the correction, made by Kosàly (1987), to Toor's theory.

McKelvey et al. (1975) studied the velocity fields and mixing in a model of the reactor used by Vassilatos and Toor (1965) and Mao and Toor (1970). Complicated flow patterns near the inlet of the reactor were found, indicating the flow was not truly homogeneous. The variance of an inert species decayed as $t^{-3/2}$, as predicted by Hinze (1975) for initial period turbulence. A more stringent test of Toor's hypothesis was made by using the measured velocity and mixing data to integrate the mean concentration equations. The results showed that Toor's model could be used to predict the mean concentration for finite reaction rates, in support of his 1969 theory.

Bennani et al. (1985) studied the very slow alkaline hydrolysis of ethyl acetate and the fast hydrolysis of methylformate, using grid generated turbulence with injectors for one of the reactants located in the grid. The methylformate reaction was studied by both Bennani et al. and Vassilatos and Toor (1965). This reaction has different speeds for the two studies, relative to the mixing rate, because the reactor used by Vassilatos and Toor was more efficient in mixing the reactants. Conductivity probes were used to infer the concentrations of the reactants. Power law decays of the turbulence intensity and of the concentration variance of an inert species were in agreement with previous studies (Sreenivasan et al., 1980). The data for the fast

reaction case supported Toor's (1969) hypothesis.

Ajmera et al. (1976) and Mudford and Bilger (1984) have studied the gas-phase reaction between ozone and nitrous oxide. Mudford and Bilger used a turbulent smog chamber for the nitrous oxide-ozone reaction. Opposing jets containing the reactants entered one end of a long cylindrical bag. Ajmera et al. used an annular reactor for this reaction that was designed to provide less rapid mixing than the reactors that were used by Vassilatos and Toor (1965) and by Mao and Toor (1970).

Ajmera et al. concluded that Toor's model applies to gases as well as liquids, and that the mixing data from very fast liquid reactions can be used in the design of gas-phase reactors. Mudford and Bilger used the results of their experiments to test closure theories for the mean reaction rate. Joint pdf's of the composition were obtained from chemiluminescent analysis. The model that gave the best agreement with their data was the one based on perturbations from the fast chemistry limit (Bilger, 1980).

Previous Numerical Simulations

Previous studies that have used DNS's to study chemically reacting turbulent flows will be reviewed in this section. These simulations have either been made either for turbulent mixing layers or for isotropic turbulence. The studies of reactions in the mixing layer (Riley et al., 1986; McMurtry et al., 1986; Givi et al., 1986; Givi and Jou, 1988; and Riley and McMurtry, 1989) have addressed the questions of flame extinction, of the effects of heat release on the velocity field, and of coherent structures. The results of these studies were not used to evaluate closures for the mean

Table 7.3: Summary of chemical reactions and Damköhler numbers used in experimental studies

Work	Reaction (A + B)	Damköhler number $k_R A\lambda^2/D$
Vassilatos and Toor (1965)	NaOH + HCl	10^7
	LiOH + HCl	
	2LiOH + HOOCCOOH	
	LiOH + HCOOH	
	CO_2 + 2NaOH	1
	CO_2 + NH_3	10^{-2}
	$HCOOCH_3$ + NaOH	10^{-3}
Mao and Toor (1970)	HCl + NaOH	10^7
	Maleic Acid + OH^-	10^4
	Nitrotriacetic Acid + OH^-	10^3
	CO_2 + 2NaOH	1
Bennani et al. (1985)	$CH_2COOC_2H_5$ + NaOH	0.1
	$HCOOCH_3$ + NaOH	40
Mudford and Bilger (1984)	O_3 + NO_3	1
Ajmera et al. (1976)	O_3 + NO_3	1

rate of reaction. The data from Riley et al. (1986) were consistent with similarity theory.

DNS's of a bimolecular reaction in isotropic turbulence has been used in previous studies by Hamlen (1984), Leonard (1988), Leonard and Hill (1986, 1988, 1989), and McMurtry and Givi (1989) to test closure models for the mean rate of reaction. The models proposed by Toor (1969) and Patterson (1981) were tested with the data from the simulations made by Leonard and Hill, which used a lower resolution than in the present study. The form of the reactant covariance, $\overline{ab}$, predicted by Toor's theory was in better agreement with the DNS results than was the form predicted by Patterson's theory. The predictions for the mean reactant concentration are also better when Toor's model is used to close the moment equation. McMurtry and Givi used simulations of forced isotropic turbulence to test Toor's model. The resolution of the simulation was the same as used in the present study, but larger Reynolds and Damköhler numbers were used. The ratio of the reactant covariance to the variance of a conserved scalar,

$$\frac{\overline{ab}/\overline{ab}_0}{\overline{\phi^2}/\overline{\phi^2}_0},$$

(which is assumed by Toor to be unity for all reaction rates) approaches $2/\pi$ for the limiting case of very fast chemistry (which is the value predicted by Kosàly (1987)). The deviation of this ratio, which is called the unmixedness ratio by McMurtry and Givi, from unity is small for small values of the Damköhler number, and appears to be approaching zero for long times. The tendency for the unmixedness ratio to approach unity at long times was seen earlier by Hamlen (1984) and by Leonard (1988) in low resolution simulations.

Leonard and Hill (1988, 1989) showed that the microscale for the concentration of reactants was not sensitive to the value of the reaction rate. Borghi et al. (1989) have also studied the effects of finite-rate chemical reaction on length scales. In this study a nonlinear single-species reaction was used, and the microscale for the reactant concentration did have a significant dependence on the rate of reaction.

CHAPTER 8. PROBLEM DESCRIPTION

The effects of the detailed turbulent velocity field on a single reaction have been examined in this paper by the use of direct numerical simulations, and the adequacies of some simple statistical closure theories applied to the reaction term have been tested. The particular case of interest here is the single-step, irreversible, second-order reaction A + B $\rightarrow$ products with the rate of reaction given by $S = -k_R AB$. The reaction rate coefficient k_R is considered to have a constant value in this study, but in general it will vary with time and position and have a temperature dependence.

Statistically homogeneous, decaying turbulence was used in the present study. In this case there are no mean spatial gradients, and so we were able to focus on the chemical reaction term in the statistical equations. Initial turbulence levels were given, instead of considering the problem of how the turbulence was generated. The velocity field was resolved down to the Kolmogorov scale, so no turbulence modeling was used. The velocity field was isochoric, with constant Newtonian viscosity, and the concentration fields were assumed to be passive quantities with respect to the velocity field.

Governing Equations

The governing equations for the problem are the incompressible Navier-Stokes equations for the conservation of momentum and conservation equations for the mass of each reactant,

$$\frac{\partial u_i}{\partial t} + u_j \frac{\partial u_i}{\partial x_j} = -\frac{1}{\rho}\frac{\partial p}{\partial x_i} + \nu \nabla^2 u_i, \tag{8.1}$$

$$\frac{\partial u_j}{\partial x_j} = 0, \tag{8.2}$$

and

$$\frac{\partial A}{\partial t} + u_j \frac{\partial A}{\partial x_j} = D\nabla^2 A - k_R AB, \tag{8.3}$$

with an equivalent equation for the concentration of reactant B. Fickian diffusion with a constant effective mass diffusivity, D, has been assumed. In all calculations reported here it was assumed that the diffusivities of the reacting species are equal. The reaction rate coefficient was also constant, independent of temperature, in the cases reported here, and so the energy equation did not need to be solved.

Numerical Method

A pseudospectral method was used to integrate the governing equations. (See Kerr, 1985, and Hamlen, 1984, for more details about the procedure.) In these methods, the variables are expressed as truncated Fourier series, and the ordinary differential equations for the expansion coefficients are then solved. Convolutions of Fourier coefficients, which arise from quadratic nonlinearities, were not evaluated directly. Rather, the nonlinear terms were evaluated at collocation points in physical space,

and the coefficients of the nonlinear terms were then evaluated. Fourier expansions are the most efficient type of basis function to use in homogeneous turbulence because Fast Fourier Transform (FFT) algorithms can substantially reduce the number of operations needed to evaluate the nonlinear terms.

The velocities and species concentrations are expanded as follows:

$$\mathbf{u}(\mathbf{x},t) = \sum_{|\mathbf{k}|=-K}^{K} \mathbf{v}(\mathbf{k},t)e^{i\mathbf{k}\cdot\mathbf{x}}, \tag{8.4}$$

$$A(\mathbf{x},t) = \sum_{|\mathbf{k}|=-K}^{K} \hat{A}(\mathbf{k},t)e^{i\mathbf{k}\cdot\mathbf{x}}, \tag{8.5}$$

where $\mathbf{v}$ and $\hat{A}$ are the Fourier coefficients to be integrated forward in time. The governing equation for $\mathbf{u}(\mathbf{x},t)$ and $A(\mathbf{x},t)$ and the orthogonality properties of $e^{i\mathbf{k}\cdot\mathbf{x}}$ can be used to write equations for $\mathbf{v}(\mathbf{k},t)$ and $\hat{A}(\mathbf{k},t)$:

$$\frac{dv_i(\mathbf{k},t)}{dt} + \nu k^2 v_i(\mathbf{k},t) = T_i\{\mathbf{u}\times\boldsymbol{\omega}\} - k_i\frac{\mathbf{k}\cdot\mathbf{T}\{\mathbf{u}\times\boldsymbol{\omega}\}}{\mathbf{k}^2} \tag{8.6}$$

and

$$\frac{d\hat{A}(\mathbf{k},t)}{dt} + Dk^2\hat{A}(\mathbf{k},t) = T\left\{-\mathbf{u}\cdot\nabla A - k_R AB\right\}. \tag{8.7}$$

The convective term in Equation 8.1 has been written in rotational form in this expression, and the continuity equation, $\mathbf{k}\cdot\mathbf{v} = 0$, has been used to eliminate the pressure term. Fourier transforms of the nonlinear terms are denoted by $T\{\ldots\}$. The rotational form of the Navier-Stokes equations is used to prevent instabilities arising from aliasing errors. The only method of controlling aliasing that is used in this method is to truncate Fourier coefficients outside a sphere of radius $K\sqrt{(8/9)}$.

Equations (8.6) and (8.7) are integrated with a third-order Runge-Kutta method, with a time step that is based on a CFL stability criterion. The viscous or diffusive

Table 8.1: Summary of initial conditions and parameters used in the simulations

run[a]	k_R	ν	$3\overline{u^2}/2$	R_λ	$\overline{a^2}$, $\overline{b^2}$, $-\overline{ab}$
A	1.0	0.01	1.33	65.8	0.856
B	1.0	0.015	1.33	43.9	0.856
C	1.0	0.02	1.33	32.9	0.856
D	5.0	0.01	1.33	65.8	0.856
E	5.0	0.02	1.33	32.9	0.856

[a] All simulations were performed with 64^3 coefficients on a domain of size $(2\pi)^3$. The value of the Schmidt number was 0.7 and the initial mean concentration of each reactant was 1.0 in all runs.

term on the left hand side of the equations is evaluated implicitly through the use of an integrating factor. The domain for the simulations is a cube of size $(2\pi)^3$, with periodic boundary conditions. The calculations in this study were performed with 64^3 Fourier coefficients on a Cray X-MP supercomputer at the National Center for Supercomputing Applications (Urbana, Illinois). Initial conditions, which are discussed in the next section, and physical parameters are summarized in Table 8.1.

Initial Conditions

The reactant distributions are specified, initially, to be slightly damped square waves in the x_1 direction and uniform in the x_2 and x_3 direction.

$$A(\mathbf{x},t) = 1 + \sum_{|k_1|<K} \frac{1}{k_1} \sin\left(\frac{k_1\pi}{2}\right) \cos(k_1 x_1)\, e^{(-Dk^2 t^*)}, \qquad (8.8)$$

where k_1 is an integer. The initial conditions for the concentration field are not statistically isotropic, but the volume averages of the concentration gradients are zero and the reaction zones are well defined. Two reaction zones exist because the boundary conditions for the reactant concentrations are periodic. The square waves are damped because the Fourier expansion is not accurate for sharp discontinuities in the concentrations.

The initial velocity field is chosen by scaling randomly selected Fourier coefficients to give a specified energy spectrum. The form of the energy spectrum determines the intensity and length scales of the turbulence. Because the Fourier coefficients are chosen from a normal distribution, the coefficients are uncorrelated, and some statistical quantities, such as the velocity derivative skewness or spectral energy transfer, are not given realistic values with this initialization. The initial energy spectrum for each case is of the form

$$E(k) = 16\sqrt{\frac{2}{\pi}}\frac{u'^2 k^4}{k_0^5} e^{-2k^2/k_0^2}. \tag{8.9}$$

The peak wavenumber k_0 was 2.86, which gives an initial Taylor microscale λ_g of 0.70.

CHAPTER 9. RESULTS AND DISCUSSION

The results of direct simulation of turbulent reacting flows are used to test closure theories for moment equations by comparing the predicted forms of the unknown terms and the results of integrated moment equations with DNS data. Various Reynolds and Damköhler numbers are used in this study. In this chapter we first present results on the development of statistics of the concentration field, and then present results on the tests of the closure models.

Reynolds and Damköhler Number Effects

The mean concentration of reactant A is shown in Figure 9.1 for runs A–E. These five runs have three different values for the initial Reynolds number and two different values of the Damköhler number. Also shown in Figure 9.1 is the mean concentration in the limit of infinitely fast reaction, calculated from the conserved scalar $(A - B)$ in run B. The initial value of $\bar{A}$ in this limiting case is not one, because the reactants for the finite-rate chemistry cases were not perfectly segregated. A step change occurs in the mean concentrations for the infinitely fast reaction at $t = 0$, since the reactants cannot coexist.

The mean concentration, $\bar{A}$, decreases faster for the two cases with the larger Damköhler number, but not as fast as in the limiting case. The time scales for mixing

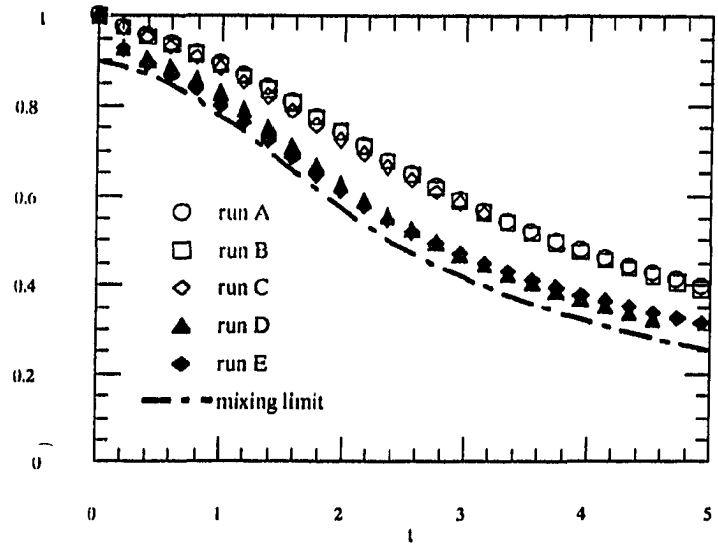

Figure 9.1: Mean concentration of reactant A for runs A–E. The initial R_λ is 65.8 for runs A and D, 43.9 for run B, and 32.9 for runs C and E. The initial Damköhler number is 1 for runs A–C and 5 for runs D and E

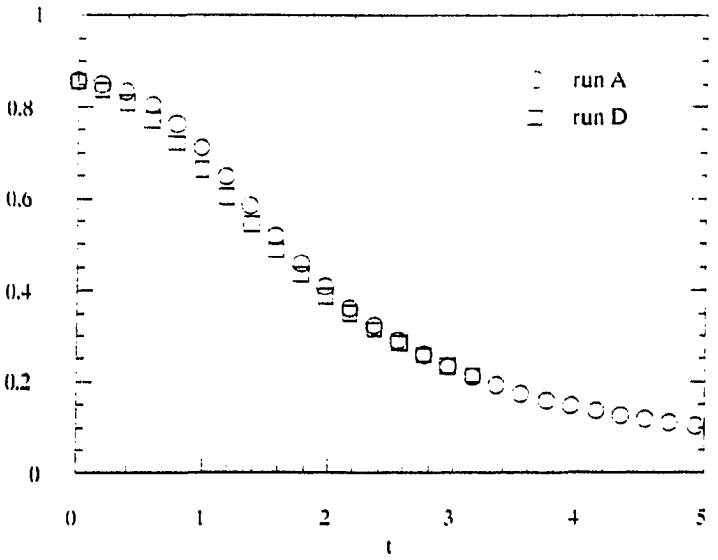

Figure 9.2: Development of the variance of the concentration of reactant A for runs A and D

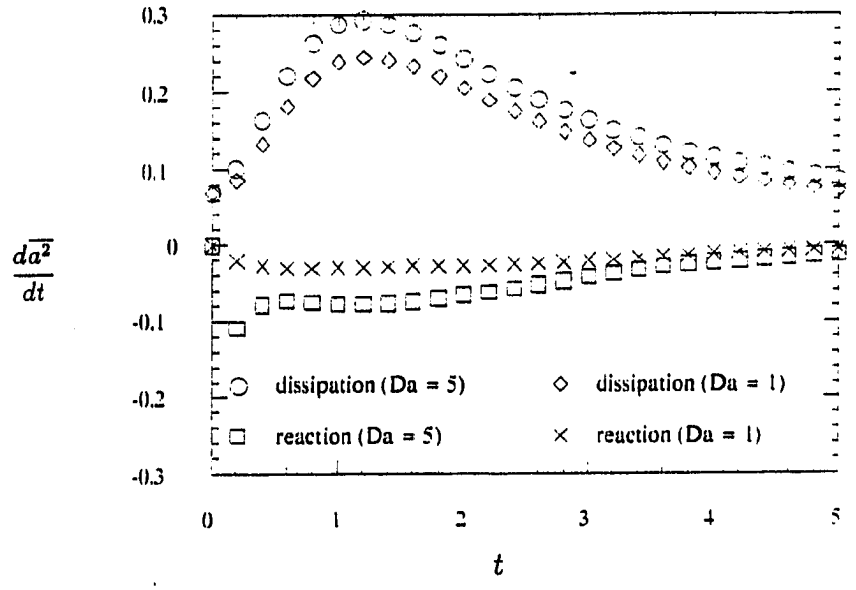

Figure 9.3: Development of the contributions to the rate of change of the variance of the concentration of reactant A for runs A and D

and reaction are comparable in these cases and the Damköhler numbers are, thus, moderate to high. It is for these cases, where the mean reactant concentration cannot be predicted from either the kinetics expression or from an inert tracer species (i.e, the conserved scalar), that proper modeling in the closure theories is most important. The mean values of the reactant concentrations are barely changed when the viscosity is changed by a factor of two. The change in viscosity changes the length scales of the velocity and the scalar fields, rather than affecting directly the rate of decay of kinetic energy and concentration variance. The behavior of the length scales is treated in Part I.

The time evolution of the variance of the concentration of reactant A in runs A and D is shown in Figure 9.2. The reaction rate coefficient differs by a factor of 5 for these runs, but the variance, $\overline{a^2}$, is almost unchanged. There are two terms

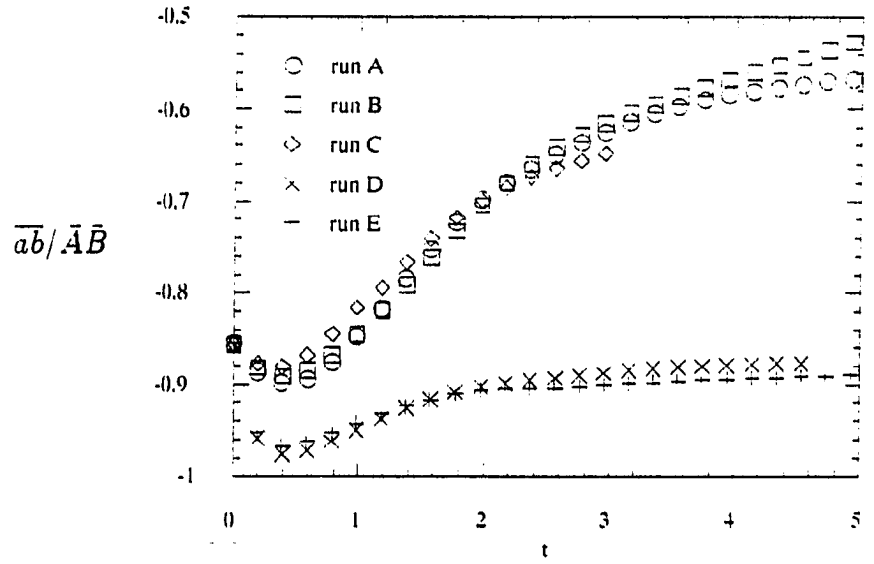

Figure 9.4: Development of the segregation coefficient, $\overline{ab}/\bar{A}\bar{B}$, for runs A–E

on the right hand side of Equation (7.2) that contribute to the rate of change of the reactant concentration variance—scalar dissipation and chemical reaction. The contributions to the rate of change of the variance due to each of these terms are shown in Figure 9.3. The largest of the two terms is the scalar dissipation rate, which is a factor of 3 to 4 greater in magnitude than the reaction term. Even though the magnitudes of both terms increase when the Damköhler number is increased, the signs of the two terms are different, so the net change is small. Consequently, the scalar variance is dominated by molecular dissipation and is not very sensitive to the Damköhler number.

The segregation coefficient, $\overline{ab}/\bar{A}\bar{B}$, is shown in Figure 9.4 for runs A–E. This parameter is a measure of the difference in the reaction rate from the case with

uniform concentrations, as shown by a simple rearrangement of Equation (7.1),

$$\frac{d\overline{A}}{dt} = -k\overline{A}\,\overline{B}\left(1 + \frac{\overline{ab}}{\overline{A}\,\overline{B}}\right). \tag{9.1}$$

The magnitude of the segregation coefficient increases initially, then decays slowly for cases A–C, with the lower Damköhler number, and remains nearly constant for runs D and E, with the higher Damköhler number. The initial reaction rate is abnormally large, as a result of the smoothing of the initial conditions and the consequent lack of complete segregation, but adjusts rapidly. The rate of change of the mean concentration, compared to the rate for uniform concentration fields, will be less than half of the value for the lowest Damköhler number and about 10% for the highest Damköhler number. This illustrates the importance of modeling the source term. Assuming that the mean reaction rate is a function of mean concentrations will most likely produce serious errors.

Tests of Closure Models

The closure models of Toor (1969), Patterson (1981), and Dutta and Tarbell (1989) are tested in two different manners. First, DNS data are used to evaluate the concentration covariances for each model, and the model covariances are compared to the actual covariances from the simulations. Second, the moment equations are integrated with each model in order to obtain mean concentrations as a function of time. The predicted mean concentrations are also compared to the actual values from the DNS.

Instantaneous tests

The predicted form for the reactant concentration covariance, normalized with the actual values from the simulation, is shown as a function of time for each model for runs A–I in Figures 9.5 and 9.6. The same reaction rate coefficient is used in runs A, B, and C, but the viscosity is different for each run. Runs D and E used the same viscosity as runs A and C, respectively, but a higher value of the reaction rate coefficient was used in the former. The means and variances of the concentration of reactants are insensitive to this change, as are the predictions of the models when data from the simulation are used to estimate the covariances.

Of the three models, Toor's shows the smallest deviation from the DNS data. The form used here for Toor's theory does not account for the changing shape of the conserved scalar pdf. The value of the covariance ratio for an infinitely fast reaction should approach 1.25 (Kosàly, 1986), as the trend for the larger Damköhler number data indicates. The predictions of Toor and Tarbell are similar for both values of the Damköhler number, but Patterson's predictions are greater than the simulation results for the higher Damköhler number and lower for the lower Damköhler number. Patterson's model would be expected to be more accurate for higher Damköhler numbers, since it corresponds to spatially segregated reactants. However, the model assumes that the concentration of a reactant will have the same value in a reaction zone as in a region containing only that reactant. Characteristic compositions in the reaction zone will actually be much less than the values outside the reaction zone for fast reactions. Neither Tarbell's nor Patterson's model predicts the proper initial value for the covariance, because the reactants are not completely segregated in the

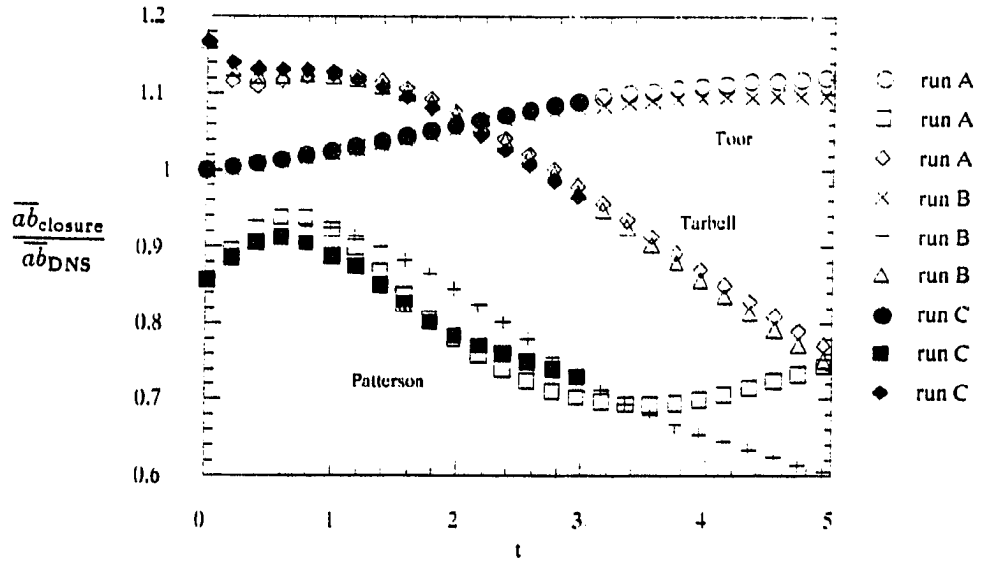

Figure 9.5: Instantaneous predictions of closure theories for the reactant covariance, normalized with the actual value, for runs A–C. (Da = 1)

simulation, but that may be a defect of our procedure rather than a defect of their models. This lack of initial agreement does not affect the agreement at later times in Figures 9.5 and 9.6, however, since the curves are calculated using the instantaneous statistics. It will, however, affect the initial rate of change of the moments when the statistical equations are integrated, and can, therefore, affect the predictions for moments at all times.

In order to determine if the anisotropy in the initial conditions for the concentration of reactants was responsible for the failure of the closure theories to predict the reactant covariance, a run with a more isotropic initial condition for the concentration fields (run Z of Part I) was used to evaluate the theories. The velocity field in this run was not the same as those for the runs discussed in this part of the paper. The initial velocity field was well developed, but had a lower Reynolds number. The values of

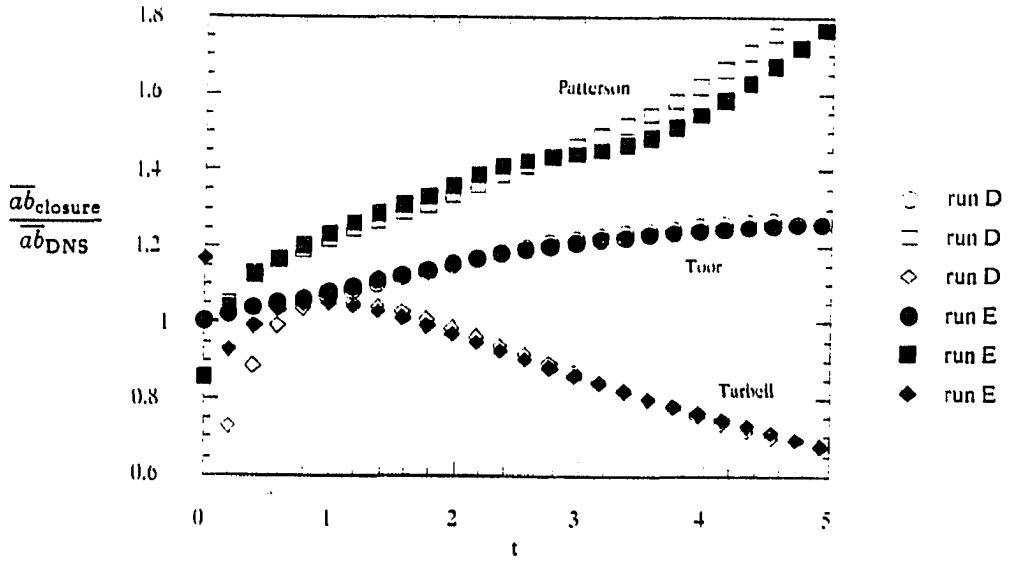

Figure 9.6: Instantaneous predictions of closure theories for the reactant covariance, normalized with the actual value, for runs D and E. (Da = 5)

the Damköhler number for the two cases were 1.6 and 6.4. The instantaneous tests of the closure models are for this run are shown in Figure 9.7. The same trends seen in runs A–E are seen for the model predictions for this case, including the fact that Patterson's model predicts the covariance to be too high for large Da and too small for small Da.

Kosàly's (1986) remarks on Toor's (1969) theory were not taken into account in the preceding tests of the closure, because the rate of change of the conserved scalar pdf from a bimodal to a Gaussian distribution cannot be predicted *a priori*. The initial pdf, however, can be defined to be Gaussian in the simulations. Toor's derivation for the covariance in the limit of slow reactions assumed an initially bimodal pdf, and so it is really not valid for such initial conditions. Nevertheless, several 32^3 simulations were performed with initially segregated reactants and a Gaussian pdf

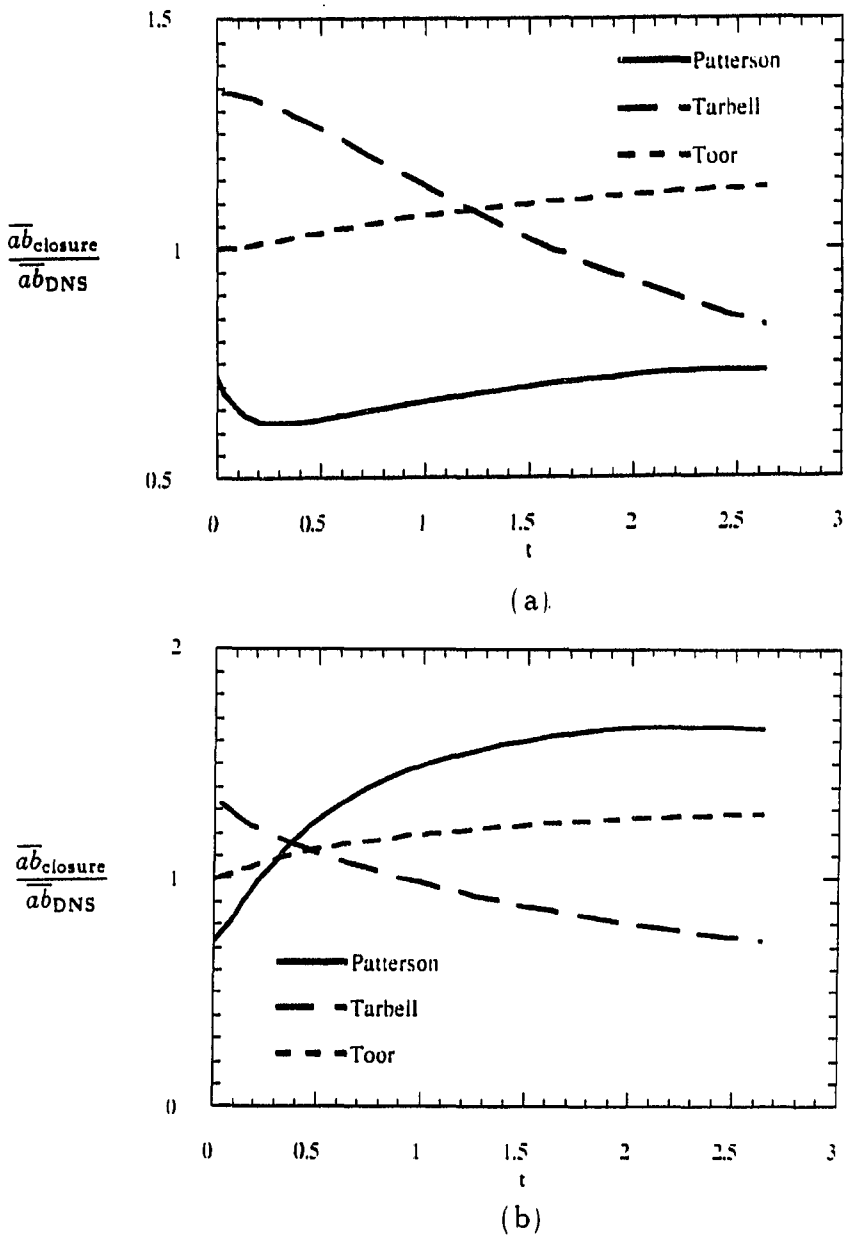

Figure 9.7: Instantaneous predictions of closure theories for the reactant covariance, normalized with the actual value, for isotropic initial concentrations. (a) Da = 1.6, (b) Da = 6.4

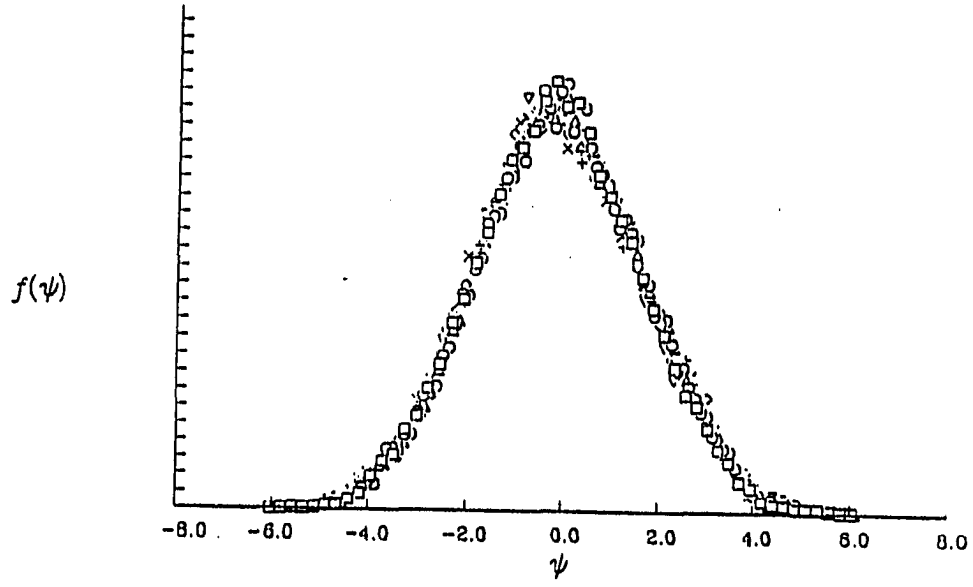

Figure 9.8: Development of the standardized pdf of the conserved scalar from a 32^3 simulation

for the conserved scalar. The conserved scalar pdf remained Gaussian during the simulation. The standardized pdf, $f'(z) = \sigma f((v - \mu)/\sigma)$, is shown in Figure 9.8 for various times. The initial variances and length scales are almost, but not exactly, the same for each reactant, because the concentrations are chosen from a random distribution. The initial length scale for the covariance, however, is significantly different than the length scales for the concentration variances. The slow-reaction limit of Toor's theory does not hold for the nonreacting case, as mentioned above. The form of the covariance predicted by Toor's theory is shown in Figure 9.9 for different values of the Damköhler number. The covariance is not independent of the reaction rate for these conditions, and the agreement of the predictions of the theory and the DNS results are poorer than for any of the cases with the initially bimodal pdf for the conserved scalar.

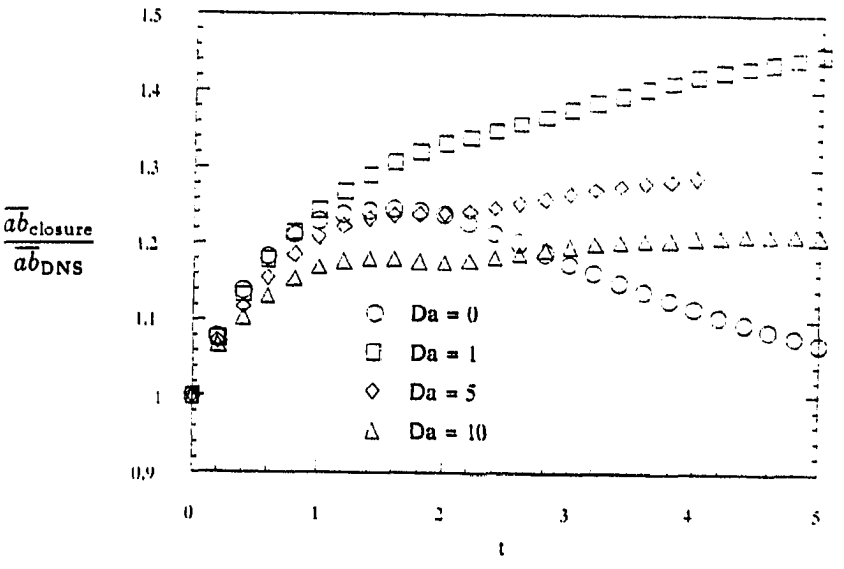

Figure 9.9: Development of Toor's prediction for the covariance when the initial conserved scalar pdf is Gaussian from 32^3 simulations

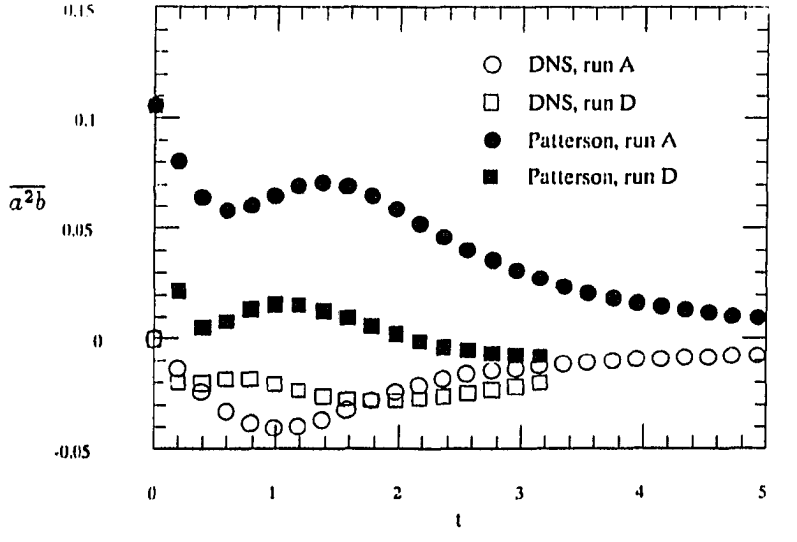

Figure 9.10: Development of instantaneous predictions of Patterson's closure theory for the third-order moment $\overline{a^2b}$, compared to the actual value, for runs D and E

Finally, Patterson's model also requires a prediction for the third-order concentration moments $\overline{a^2b}$ and $\overline{ab^2}$, since the reactant variances are used in the covariance approximation instead of the inert species variance. The deviation from the DNS data of the prediction of Patterson's model for the contribution of reaction to the rate of change of the reactant variance is shown in Figure 9.10. The simulation results support Patterson's suggestion that the triple moments should be neglected, and also show that the actual values of $\overline{a^2b}$ are of the opposite sign than predicted by Patterson's model.

Integral tests

The accuracy of the predicted forms of the modeled terms using the DNS data was presented in the previous section, but this only suggests how well the models will predict the mean concentrations and, in the case of Patterson's model, the reactant concentration variance. In order to test the model predictions, the ordinary differential equations for the means and variances of the reactant concentrations and the variance of the concentration of an inert species were integrated with the three models discussed above, for each of the DNS studies. The time scale needed for the closures was supplied by specifying the scalar dissipation microscale as a function of time for each of the runs. With the mixing properly accounted for, the models were only tested on their ability to model the terms due to reaction. The results of runs A and D are selected as representative of the data as a whole, since the value of the viscosity did not affect the agreement between the DNS data and the integrated moment equations.

Toor's model shows excellent agreement with the DNS results for the moderate Damköhler number case (Figure 9.11) and reasonably good agreement for the high Damköhler number case (Figure 9.12). The correction factor to Toor's theory discussed by Kosàly was not included in the calculations because it cannot be incorporated in the closure model. Tarbell's model shows fairly good agreement with the DNS data for run A, but poorer agreement for run D. Patterson's model does not agree well with the data for either Damköhler number.

The shortcomings of Patterson's model can be seen further by comparing the reactant concentration variance to the DNS results (Figure 9.13). The modeled form for the rate of change of the variance due to reaction is not accurate, and the variance decay rate is much too rapid. Also, modeling the joint composition pdf as three delta functions is extremely crude, as shown by plots of the joint composition pdf in Part I. The conserved scalar pdf, which is independent of the reaction rate, will presumably approach an asymptotic Gaussian shape. In the fast reaction limit the joint pdf must be zero when both species concentrations are nonzero. All the probability must be spread along the axes in composition space and will be transported towards the origin. This picture is at odds with the forms assumed by both Tarbell and Patterson.

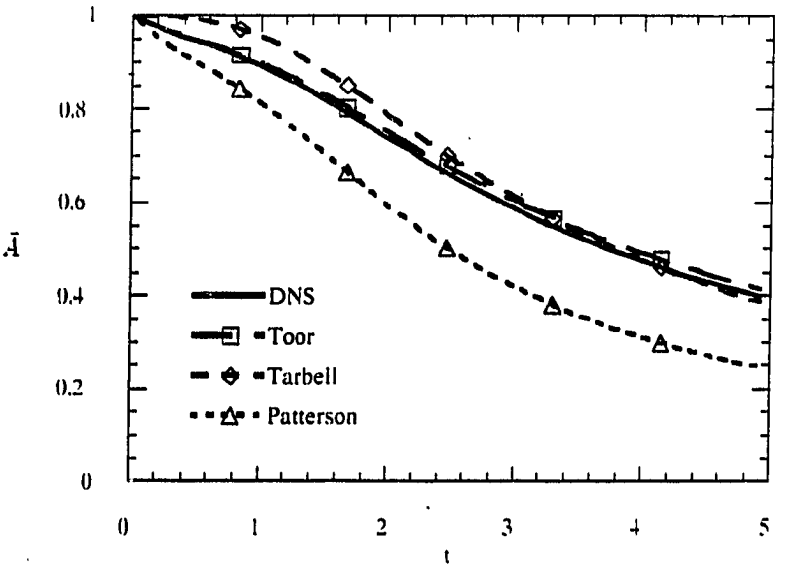

Figure 9.11: Predictions of closure models and DNS results for the mean concentration of reactant A from run A. (Da = 1)

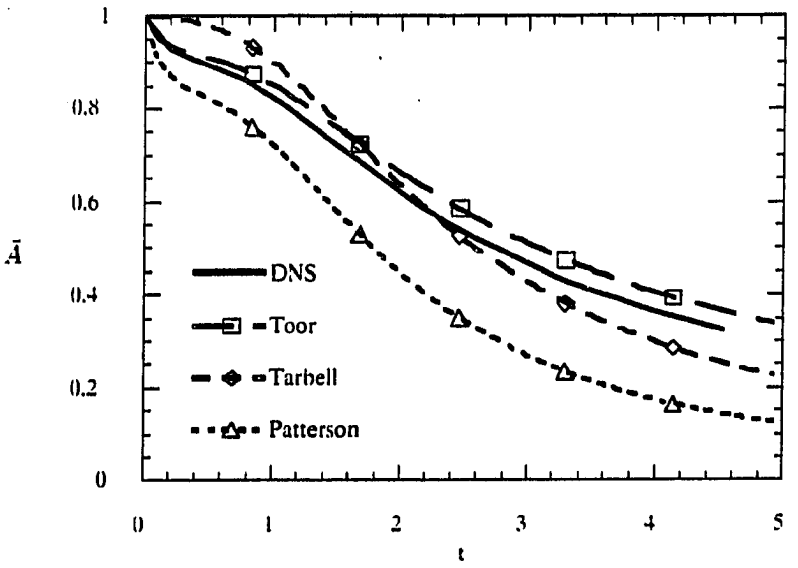

Figure 9.12: Predictions of closure models and DNS results for the mean concentration of reactant A from run D. (Da = 5)

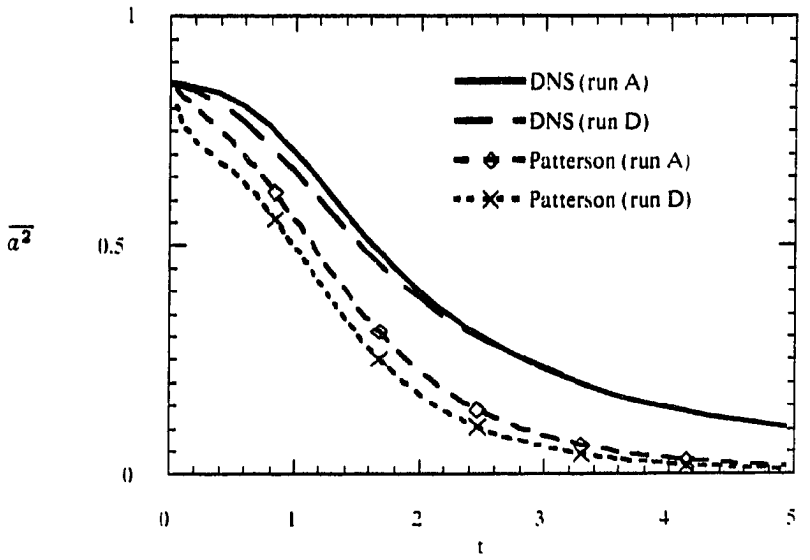

Figure 9.13: Predictions of Patterson's closure model and DNS results for the variance of the concentration of reactant A from runs A and D

CHAPTER 10. SUMMARY AND CONCLUSIONS

Direct numerical simulations of finite-rate chemical reactions in decaying homogeneous turbulence were carried out for different initial Damköhler and Reynolds numbers. Moderate and high values of the Damköhler numbers were used, and the Reynolds numbers were moderate.

The values of the initial Reynolds number had no effect on the development of the mean or variance of the concentration of either reactant or of an inert species. The reactant concentration variance showed very little sensitivity to Damköhler number, since its rate of change was dominated by molecular dissipation. The segregation coefficient, on the other hand, showed a marked change for different Damköhler numbers. At high values of Da, the segregation coefficient maintained a fairly steady value close to -1.

The mean concentration was predicted much better when Toor's model was used to close Equation (7.1) than for the other closure models examined here. Tarbell's model was able to predict the mean concentration adequately for a moderate value of the Damköhler number, but not for a high value. Patterson's model, the only one that predicted both the mean and variance of the reactant concentrations, was the least satisfactory of the three models tested. The influence of the Damköhler number on the reactant concentration variance was incorrectly predicted, which contributed

to errors in predicting the mean value.

One disadvantage of moment methods is that they need to be formulated for a specific case, such as the two-species, second-order reaction studied here. The presumed pdf method does have the advantage that any concentration moments can be evaluated, but simple forms are used to restrict the dimensionality and domain of the pdf. The alternative to using moment methods is to solve a modeled pdf equation. Moment methods are generally easier to use, but the full pdf method is better suited to the calculation of reacting turbulent flows, since the models for mean reaction rate can be avoided. The pdf equations can be very computationally demanding, on the other hand, because of the higher dimensionally of the problem. In addition, the assumptions used in modeling the pdf are hard to evaluate based on intuition, since they involve the approximations of transport terms in composition space, as discussed in Part I. As more data, especially from DNS, are available to attempt to validate the pdf models, the moment approach may, in fact, be abandoned, but for the present, both methods will be used. The evaluation of some simple models in this study indicates that care needs to be taken in the selection of the model.

PART III.

KINEMATICS OF THE REACTION ZONE IN HOMOGENEOUS TURBULENCE

CHAPTER 11. INTRODUCTION

The understanding of the structures in turbulent reacting flows is important in understanding the physics behind the turbulent mixing process and in developing models based on characteristics of the flows. The ability of turbulent motions to stretch material lines and surfaces, to bring material surfaces closer together, and to increase gradients of convected quantities has long been recognized (Batchelor, 1952). These important features have been incorporated into models for mixing and reaction in turbulent flows, such as the flamelet approach (Williams, 1975) in combustion or the lamellar models (Ranz, 1979) in chemical engineering. By mixing, we mean the reduction of fluctuations of scalar quantities, such as temperature or concentration of a chemical species, caused by a reduction in the length scales for the scalar field.

In this work we examine a simple chemical reaction in numerically simulated turbulence and study the effects of kinematical quantities on the local, instantaneous reaction rate. Visualization of the flow is accomplished by examining contours of properties in two-dimensional slices of the domain and contour surfaces in three dimensions. As we shall see, the fronts that separate unmixed reactants tend to become aligned normal to the direction of the most compressive strain rate in these simulations. The highest local reaction rates occur where the alignment between the reactant concentration gradients and the direction of the most compressive straining—and the

magnitude of the strain rate—are highest. The most intense values of the reaction rate are not reduced by high strain rates for temperature-dependent kinetics in this study. The temperature dependence of the reaction rate, in this case, was not strong enough for the reaction to be extinguished at low temperatures. The reaction fronts showed more organization for flows with a mean shear, and the concetration gradients were also much more highly amplified by the straining motion.

CHAPTER 12. BACKGROUND

The nature of organized motions in turbulent flows is discussed briefly in this section. Recent numerical studies of the structure of homogeneous turbulent flows, and a set of criteria that have been proposed to identify characteristic structures in turbulent flows, are described. Some physical mechanisms that are used to explain the mixing of scalars in turbulent flows and chemically reacting turbulent flows are reviewed. Finally, the kinematical quantities that affect the local reaction rate are identified from the local rates of change of the reaction rate and the dissipation rate of reactant concentrations, which are themselves derived from the equations for conservation of mass and momentum that govern the system.

Coherent Structures

It has been realized within the last 20 years that, while randomness and unpredictability are important characteristics of turbulence, many flows are characterized by large-scale organized structures. It is hoped that the study of coherent structures will yield information that will be of use in efforts to model turbulent flow. The concepts of coherent structures and more traditional statistical quantities can be used together in two different manners, as pointed out by Kim and Moin (1986): Either the two-point velocity correlation function can be used to test the consistency of a

model of a coherent structure, or else a structure can be extracted from the correlation function by methods such as the orthogonal decomposition proposed by Lumley (1967, 1981) or the stochastic estimation proposed by Adrian (1979).

Definitions of coherent structures are usually based on the nature of the vorticity field in the flow (Hussain, 1986), but there has been considerable controversy involving the definition. Other definitions incorporate the concept of helicity (Moffatt, 1985) or a requirement for flow patterns to survive phase averaging processes (Coles, 1981). For reviews of the study of coherent structures in turbulence see Hussain (1986) and Cantwell (1981).

Most of the studies of coherent structures in turbulence have been made for inhomogeneous flows such as boundary layers, mixing layers, jets, wakes, and pipe flows. Rogers and Moin (1987) have used DNS's to show that characteristic structures can also be found in homogeneous shear flows. In the present study, we are examining the influence of kinematical variables on the local reaction rate in homogeneous turbulent reacting flows, so we will discuss in detail only the studies of organized motion or structure in homogeneous flows.

Homogeneous turbulent flows

Rogers and Moin (1987) performed direct numerical simulations of homogeneous turbulent shear flows, and conjectured that hairpin vortices were characteristic of all turbulent shear flows, not just inhomogeneous flows. They found a significant tendency for vorticity vectors in a homogeneous shear flow to be aligned at a 45° angle to the mean flow for low Reynolds number calculations and at a 35–40° angle

to the mean flow for a higher Reynolds number flow. Vorticity is stretched by the mean extensional rate of strain, which is at an angle of 45° to the mean flow. The angle of alignment is reduced in the higher Reynolds number calculations by the mean rotation of material lines and, therefore, vortex lines. The alignment of vorticity, and the correlations of spanwise velocity, suggest the existence of vortical structures which are inclined to the mean flow. Structures resembling hairpin vortices were seen in plots of instantaneous vorticity vectors and vortex lines. These apparent hairpin vortices tended to be located in regions of high kinetic energy production, which indicates that the structures are important dynamically. Homogeneous flows with a mean nonrotational strain do not show a tendency to develop hairpins, which indicates that the mean shear is necessary for the development of hairpin vortices.

Kerr (1985) studied the small scale structure of isotropic turbulence with DNS's. Three dimensional plots were made of the most intense vorticity, scalar gradient, and most compressive rate of strain. The most intense regions of the vorticity field seemed to be concentrated in thin vortex tubes. The most intense scalar gradients and compressive strain rates tended to lie in sheets which were wrapped around these vortex tubes. Correlations of scalar gradients and vorticity, as well as plots of their instantaneous values, indicated that the scalar gradient and vorticity vectors tended to be perpendicular to each other, but their magnitudes were uncorrelated. The scalar gradient was aligned with the most compressive principal direction of the rate of strain tensor.

Ashurst et al. (1987) further analyzed Kerr's and Rogers and Moin's data and found tendencies for the vorticity to align with the direction of intermediate rate of

strain and for the scalar gradient to align with the most compressive direction of the rate of strain in both studies. Ashurst et al. concluded that the most characteristic structures in the isotropic turbulent flow are stretched vortex tubes. As the vortex tubes are stretched, vorticity is amplified as a consequence of the conservation of angular momentum. The average ratio of the three eigenvalues of the rate of strain tensor in regions of high straining is 3:1:−4. The structures are consistent with an Eulerian model of Vieillefosse (1984) and a strained spiral vortex model by Lundgren (1982).

Kinematic structures

A method of defining characteristic regions of the flow has been proposed by Hunt et al. (1988). The regions are defined as eddies, streams, and convergences zones, based on the local values of the strain rate, vorticity, pressure, and kinetic energy. Hunt et al. (1988) have suggested that regions of high local reaction rate in a turbulently reacting flow would likely be identified with the convergence zones for fast reactions. Briefly, Hunt defined an eddy region to be one of strong rotation and low pressure, a convergence zone to be a region of high strain and high pressure, and a stream to be a region of high kinetic energy that is neither rotational nor strained. The precise definition of each region is summarized in Table 12.1. The regions are defined in such a manner that they are mutually exclusive, and there are points in the flow which do not fit the classification for any of the regions. One of the criteria is based on a so-called second invariant of the velocity gradient tensor,

$$II \equiv \frac{\partial u_i}{\partial x_j}\frac{\partial u_j}{\partial x_i} = e^2 - \omega^2/2. \tag{12.1}$$

Table 12.1: Definitions of kinematic structures

Zone	Criteria[a]	
Stream	$u > c_{1s}\, u'$	$\lvert II\rvert < c_{2s}\, II'$
Eddy	$p < -c_{1e}\, p'$	$II < c_{2e}\, II'$
Convergence	$p > c_{1c}\, p'$	$II > c_{2c}\, II'$

[a]The values of the parameters that are suggested by Hunt et al. (1988) are $c_{1s} = 1$, $c_{1e} = 0.2$, $c_{1c} = 1$, $c_{2s} = 1$, $c_{2e} = 2$, and $c_{2c} = 1$.

This quantity is not invariant to rigid rotation, and so regions of high strain rate that are imbedded in large scale swirling motions may not be recognized as convergence zones. One of the other criteria is the root mean square value of the pressure fluctuations. Pressure is a nonlocal quantity, however, and the nature of regions in the flow may therefore be determined by events that are not near these regions.

Mechanisms for Mixing of Scalars

Several physical mechanisms for the mixing of scalars in turbulent flows have been used to propose shapes for the scalar energy spectrum in large Reynolds number turbulence. Batchelor (1959) assumed that for large Prandtl (or Schmidt) numbers, the scalar gradient becomes aligned with the compressive rate of strain for length scales smaller than the Kolmogorov length scale, $(\nu^3/\varepsilon)^{1/4}$. The compressive strain rate amplifies scalar gradients until balanced by diffusion. This mechanism leads to a scalar spectrum of the form $E(k) \propto k^{-1}$ for wavenumbers above the Kolmogorov wavenumber. The scalar spectrum has an exponential cutoff at the Batchelor scale, $(D/\gamma)^{1/2}$.

Batchelor et al. (1959) consider this mechanism to be irrelevant for small Prandtl

numbers, where the length scales for the scalar field are much larger than the scales for the velocity field. Gibson (1968a) proposed an alternative mechanism that is supposed to be applicable for all Prandtl numbers and predicts a different behavior for the scalar energy spectrum in the low Prandtl number case between the Corrsin scale, $(D^3/\varepsilon)^{1/4}$, and the Batchelor scale. In Gibson's mechanism, scales of motion larger than the Corrsin length scale can cause unstable configurations of scalar gradients. Regions of zero scalar gradients are then split by straining motions to generate more extrema. The scalar spectrum base on this mechanism is predicted to be $E(k) \propto k^{-3}$ for wavenumbers between the Corrsin scale and the Batchelor scale (Gibson, 1968b).

Gibson et al. (1988) proposed another mechanism that is supposed to be valid for all values of the Prandtl number and to be effective for large scalar gradients. In this mechanism, the strain rate is proposed to be aligned with the most compressive rate of strain, and the strain rate is proposed to be correlated over distances comparable to the Corrsin scale, rather than the Kolmogorov scale, as assumed by Batchelor (1959). Gradients are then amplified by the alignment with the rate of strain. This mechanism is also consistent with Gibson's (1968b) prediction for the scalar energy spectrum.

Consequences for reacting flows

There are several models that incorporate the concepts of structures in the velocity or concentration fields for reacting flows. Some of these will be described briefly here to give an idea of the use of coherent structures in the prediction of reacting turbulent flows, and to provide some motivation for this study of the kinematics of

the reaction zone.

Turbulent diffusion flames are often described as a collection of laminar diffusion flamelets which are distributed throughout the flow (Williams, 1975; Liew et al., 1984; Peters, 1984, 1986). The flamelet structure is assumed to be one-dimensional and in a quasi-steady state, and is parametrized by a conserved scalar and the scalar dissipation rate. The local concentration of a species Y_α in the flamelet can be determined in terms of the conserved scalar Z and the source term w_α by the following equation:

$$w_\alpha = -\rho D \left(\frac{\partial Z}{\partial x_i}\right)^2 \frac{\partial^2 Y_\alpha}{\partial Z^2}. \tag{12.2}$$

The effects of turbulence in this model are included in the conserved scalar dissipation term, $(\partial Z/\partial x_i)^2$, which provides a local time scale for diffusion. A laminar calculation of the reaction is needed to provide the dependence of each species on the value of the conserved scalar and of the dissipation rate of the conserved scalar. Mean concentrations can then be determined from the joint pdf of a conserved scalar and its dissipation rate. These variables are often assumed to be independent, and the pdf of the dissipation rate is often assumed to be a lognormal distribution (Liew et al., 1984).

Another approach that postulates a characteristic structure of scalar fields is the lamellar model for mixing and reaction that have been proposed by Ranz (1979), Ottino et al. (1979) and Ottino (1980). It is assumed in this model that the scalar fields have a lamellar structure. The interfacial area per unit volume of laminae and the distance between the laminae are related to a single kinematical quantity in these studies: A warped time, which includes the effect of a time-dependent straining

motion on the laminae in a Lagrangian reference frame,

$$\tau = \frac{D}{\ell^2} \int_0^t \left(\exp\left(2 \int_0^{t'} \alpha(t'')\, dt'' \right) \right)^{-1} dt', \tag{12.3}$$

where ℓ is a striation thickness and α is the rate of strain normal to the lamina.

In a somewhat similar approach, but one which leads to a quantitative estimate of the effect of reaction rate on concentration spectra, Lundgren (1985) assumed the reaction zones for a fast bimolecular reaction were spiral lamellar regions that are being wound around a stretched vortex, and calculated the spectrum for the concentration of the product of the reaction. Previously, Lundgren (1982) proposed a strained spiral vortex model for the fluid motion that gives a $k^{-5/3}$ behavior for the energy spectrum. For the concentration field, however, there is a peak in the spectrum at the Batchelor number because the thickness of the product layer is maintained at the Batchelor scale by the balance of the molecular diffusion and the straining motion. The concentration spectrum has a k^{-1} behavior for wavenumbers smaller than the Batchelor scale and a k^{-4} behavior for wavenumbers much larger than the Batchelor scale.

Influence of kinematical quantities on reacting species

In the continuum model of fluid mechanics, chemical reactions are local phenomena and depend only on the reactant concentrations, and possibly temperature, at each point in space. Molecular diffusion is necessary to mix the reactants together. The rate of change of concentration of reactants, following the fluid motion, has contributions only from the actions of reaction and molecular diffusion. Molecular diffusion is enhanced by the turbulence as the length scales of the concentration field

are reduced. The influence of turbulence on a chemical reaction is, then, that concentration gradients are steepened as isoscalar surfaces are brought together by straining motions.

The equations governing the rate of change of reactant concentrations for an irreversible, single-step, second-order reaction,

$$\frac{\partial A}{\partial t} + \mathbf{u} \cdot \nabla A = D\nabla^2 A - k_R AB, \tag{12.4}$$

can be used to derive equations for the rates of change of the nonlinear terms that appear in this and subsequent equations. For example, Equation (12.4) and a similar equation for species B can be used to derive an expression for the rate of change of the last term on the right-hand side divided by the constant reaction rate coefficient, the normalized reaction rate AB,

$$\frac{\partial (AB)}{\partial t} - \mathbf{u} \cdot \nabla (AB) = D\nabla^2 (AB) - 2D\nabla A \cdot \nabla B - k_R AB(A + B). \tag{12.5}$$

This equation would contain more terms that arise from the rate of change of temperature if the reaction rate coefficient was not assumed to be constant.

In the same manner, expressions for the rate of change of the concentration gradients can be derived by taking the gradient of Equation (12.4),

$$\frac{\partial \nabla A}{\partial t} + \mathbf{u} \cdot \nabla (\nabla A) + \mathbf{e} \cdot \nabla A - \boldsymbol{\omega} \times \nabla A/2 = D\nabla^2 (\nabla A) - k_R \nabla (AB), \tag{12.6}$$

and from this and a similar equation for ∇B, an expression for the pseudo-dissipation term $\nabla A \cdot \nabla B$ in Equation (12.5) can be derived,

$$\frac{\partial (\nabla A \cdot \nabla B)}{\partial t} + \mathbf{u} \cdot \nabla (\nabla A \cdot \nabla B) = D\nabla^2 (\nabla A \cdot \nabla B) - 2D\nabla\nabla A : \nabla\nabla B$$

$$-2\nabla A\cdot\mathbf{e}\cdot\nabla B - k_R(\nabla A+\nabla B)\cdot\nabla(AB). \qquad (12.7)$$

It has been assumed for simplicity that the molecular diffusivities for the two species are equal. The equations for these and other nonlinear terms become more complicated as the order of the terms increase and generate many more nonlinear terms. This, of course, is the root of the closure problem for nonlinear statistical equations.

An important term, for this study, is what we will call the gradient amplification term $\nabla A\cdot\mathbf{e}\cdot\nabla B$, that appears in Equation (12.7) for the pseudo-dissipation term. This term will act to increase the components of the concentration gradients in the direction of compressive straining and decrease the components in extensional directions. The vorticity changes the direction of the concentration gradients by rigid rotation but does not affect their magnitude. Equations (12.4)-(12.7) can be averaged to give the following set of equations for homogeneous turbulence. in which the gradients of mean values are zero:

$$\frac{d\bar{A}}{dt} = -k_R\overline{AB} \qquad (12.8)$$

$$\frac{d\overline{AB}}{dt} = -2D\overline{\nabla A\cdot\nabla B} - k_R\overline{AB(A+B)} \qquad (12.9)$$

$$\frac{d\overline{\nabla A\cdot\nabla B}}{dt} = 2D\overline{\nabla\nabla A:\nabla\nabla B} - 2\overline{\nabla A\cdot\mathbf{e}\cdot\nabla B} - k_R\overline{(\nabla A+\nabla B)\cdot\nabla(AB)}. \qquad (12.10)$$

The rate of strain is the only kinematical quantity appearing in these equations. The mean reactant concentration $\bar{A}$ changes solely from the effect of chemical reaction. The mean reaction rate, $\overline{AB}$, will be increased by the mean pseudo-dissipation $\overline{\nabla A\cdot\nabla B}$, if the directions of the gradients of reactant concentration have opposite signs, as they will in the reaction zones between unmixed reactants, and will be

reduced by the consumption of the reactants. The rate of strain appears in Equation (12.10) for the pseudo-dissipation term. The sign of the mean gradient amplification is determined by the alignment of the scalar gradients with the principal coordinates for the rate of strain. Kerr (1985) and Ashurst et al. (1987) have shown the preferred alignment of inert scalar gradients is in the direction of most compressive strain rate. Therefore, the mean gradient amplification term in the inert case, $\overline{\nabla\phi \cdot \mathbf{e} \cdot \nabla\phi}$, is negative and is the only term that contributes to the growth of the dissipation rate, $\overline{\nabla\phi \cdot \nabla\phi}$.

The mean gradient amplification term, $\overline{\nabla A \cdot \mathbf{e} \cdot \nabla B}$, in the pseudo-dissipation equation will have the opposite sign of the pseudo-dissipation if both of the reactant concentration gradients are aligned with the most compressive strain rate, and will increase the magnitude of the pseudo-dissipation.

CHAPTER 13. PROBLEM DESCRIPTION

Chemical reactions between unmixed reactants in homogeneous turbulent flows are studied in this paper. The velocity, concentration, and temperature fields are calculated by Direct Numerical Simulation (DNS). In this procedure, the detailed, unsteady, three-dimensional equations governing the flows are solved without modeling any of the effects of the turbulence. The Reynolds numbers used in the simulations are low, because all scales of the velocity and scalar fields must be resolved.

The chemical reaction is irreversible and second order in the reactant concentrations, with a reaction rate $-k_R AB$. The reaction rate coefficient k_R is either a constant or has an Arrhenius dependence on the temperature. Both the concentration and temperature fields are passive with respect to the velocity field, and so the density and molecular viscosity can be assumed to be constants. A Newtonian viscosity and a constant effective Fickian diffusivity have also been assumed.

The governing equations used in the simulation are the incompressible Navier-Stokes equations for the conservation of momentum, the global continuity condition for the overall conservation of mass, and conservation equations for the mass of each reactant and for temperature,

$$\frac{\partial u_i}{\partial t} + \tilde{U}_j \frac{\partial u_i}{\partial x_j} = -u_j \frac{\partial \tilde{U}_i}{\partial x_j} - u_j \frac{\partial u_i}{\partial x_j} - \frac{1}{\rho}\frac{\partial p}{\partial x_i} + \nu \nabla^2 u_i, \qquad (13.1)$$

$$\frac{\partial u_j}{\partial x_j} = 0, \tag{13.2}$$

$$\frac{\partial A}{\partial t} + \bar{U}_j \frac{\partial A}{\partial x_j} + u_j \frac{\partial A}{\partial x_j} = D_A \nabla^2 A - k_R AB, \tag{13.3}$$

$$\frac{\partial B}{\partial t} + \bar{U}_j \frac{\partial B}{\partial x_j} + u_j \frac{\partial B}{\partial x_j} = D_B \nabla^2 B - k_R AB, \tag{13.4}$$

$$\frac{\partial \theta}{\partial t} + \bar{U}_j \frac{\partial \theta}{\partial x_j} + u_j \frac{\partial \theta}{\partial x_j} = \alpha \nabla^2 \theta + k_R AB/\bar{A}_0. \tag{13.5}$$

The fluctuating components of the velocity are denoted as u_i, and the mean components as $\bar{U}_i$. The gradient of the mean velocity must be a function only of time for homogeneous turbulence. The fractional approach to the equilibrium temperature (or to the adiabatic flame temperature, in the case of combustion), rather than the temperature itself, is used in Equation (13.5).

Numerical Procedure

Equations (13.1-13.5) are solved with a pseudospectral method (Rogallo, 1981). The code we use was adapted from one originally developed by Rogallo, which is written in Vectoral (Wray, 1989) and is described in some detail by Lee and Reynolds (1985). Homogeneous mean shear and uniform strain are accounted for by a coordinate transformation from a fixed to a deforming grid. Periodic boundary conditions are assumed for the fluctuating components. A truncated Fourier expansion can then be used for each of the velocity, concentrations, and temperature fields. The Fourier expansion for the velocity is

$$u_i(\boldsymbol{\xi}) = \sum v_i(\mathbf{k}) e^{i\mathbf{k}\cdot\boldsymbol{\xi}}, \tag{13.6}$$

where the deforming coordinate $\boldsymbol{\xi}$ is given by the linear transformation

$$\boldsymbol{\xi} = \mathbf{B}(t) \cdot \mathbf{x}. \tag{13.7}$$

The ordinary differential equations for the Fourier coefficients can then be written as

$$\frac{dv_i}{dt} + \nu k_m k_n B_{mj} B_{nj} v_i + S_{ij} v_j + i k_m B_{mj} T\{u_i u_j\} + i k_m B_{mi} T\{p/\rho\} = 0, \tag{13.8}$$

where S_{ij} is the mean velocity gradient and $T\{\,\}$ indicates a Fourier transform. The transformed continuity equation,

$$k_j B_{ji} v_i = 0, \tag{13.9}$$

can be used to eliminate the Fourier transform of the pressure field, $T\{p/\rho\}$. A modified pressure, $(p/\rho)+v_2^2$, is actually used in the calculations to reduce the amount of memory that is needed. The only components of the mean velocity gradient tensor S_{ij} that are allowed to have nonzero values are the diagonal elements and S_{12}, again to reduce memory requirements. The metric tensor B_{ij} evolves as

$$\frac{dB_{ij}}{dt} = -B_{ik} S_{ki}. \tag{13.10}$$

This study used simulations of isotropic turbulence and of homogeneous turbulent shear flow. In the first case, $S_{ij} = 0$ and $B_{ij} = \delta_{ij}$, while in the second case, $S_{12} = S$ and $S_{11} = S_{22} = S_{33} = 0$, where S is a constant value in time.

Equations for the Fourier coefficients of the scalar fields are derived in the same manner as for the coefficients for the velocity field. The terms arising from convection and reaction are nonlinear and are expressed as convolutions in Fourier space. It is more efficient to use Fast Fourier Transforms to evaluate the nonlinear terms

in Equation (13.8) and the corresponding equations for the scalar fields directly in physical space than it is to evaluate the convolutions of the Fourier coefficients.

The evaluation of convolutions in physical space can introduce aliasing errors, which are removed for the quadratic terms in this code by a combination of two methods. The computational domain is shifted randomly on each incremental timestep in the calculation and the coefficients outside a sphere with radius $\sqrt{(8/9)}K$ are truncated. The aliasing errors for the quadratic terms with this procedure are of the order of the square of the timestep (Rogallo, 1981). The errors for the more highly nonlinear terms (i.e., the Arrhenius reaction rate) are not completely removed.

A second-order Runge-Kutta method is used to integrate Equation (13.8) and corresponding equations for the scalar fields. A variable time step is used, based on a Courant (CFL) criterion. We have modified the CFL condition to include the effects of a finite reaction rate, so that the coefficient c,

$$c = \max\left(\sum \frac{u_i}{\Delta x_i} + k_R A\right) \Delta t,$$

is a specified constant (usually set to unity), Δx_i is the grid spacing in the i-direction, and the maximum value is evaluated for the entire domain.

Conditions for the Simulations

Conditions for the four sets of calculations that were made in this study are described in this section and summarized in Table 13.1. Runs W, X, and Z were made with decaying isotropic turbulence, while run U was made with a homogeneous shear flow. Runs U, W, and X used the same initially anisotropic conditions for the concentration fields, whereas run Z used statistically isotropic initial concentration

fields. Runs U, X, and Z used constant reaction rate coefficients, whereas run W used an Arrhenius expression for the kinetics.

A "preconditioning" simulation was made to provide the initial velocity fields for runs W, X, and Z by scaling Fourier coefficients that were chosen from a Gaussian distribution to fit an energy spectrum given by

$$E(k,0) = \frac{8}{\pi}(u')^2 L \frac{(kL)^4}{\left(1+(kL)^2\right)^3}, \tag{13.11}$$

with $u' = 1$ and $L = 0.5$. The simulation with these initial conditions was carried out for 100 steps ($tu'/L = 0.5$), after which the shape of the energy spectrum changed only slowly. The Fourier coefficients were saved at this point to use as the initial conditions of the simulations of decaying turbulence.

The shear flow calculation, run U, did not use a preconditioned initial velocity field. Rather, the initial energy spectrum was chosen to be

$$E(k,0) = \begin{cases} 0.4 & \text{if } 6 < k < 12 \\ 0 & \text{otherwise,} \end{cases} \tag{13.12}$$

which is the same form as used by Rogers et al. (1986). Several shear flow calculations that are not reported here were made, but in these calculations the resolution of the scalar fields was not adequate. In the run reported here, $128 \times 128 \times 64$ coefficients were used, with resolution in the flow and transverse directions twice that in the spanwise direction for a box of size $(2\pi)^3$. A value of 0.01 for the viscosity and 3 for the mean shear (in the intrinsic units of the simulation) were chosen for this calculation. The ratio S/ν is much smaller than Rogers et al. recommend for the resolution of the simulation. The value of the dimensionless parameter $S\Delta^2/\nu$, where

Δ is an average mesh spacing, is 1.15, but is recommended to be in the range 5–10. The higher resolution is required for our simulations because the concentration gradients are steep near the reaction zone. One of the runs not reported here was identical to run U, except that the shear rate was increased by a factor of four. The concentration gradients became too sharp to be resolved by the simulation, which resulted in appreciable negative values of reactant concentration.

We note here that no clipping of concentration values was made in any of the runs. Some negative concentration values are present in all of the runs, but this does not cause any problems with numerical stability. The magnitudes of the negative values are much smaller than the maximum concentrations, and only one of the reactant concentrations is negative at the same point. The rate of change of concentration due to reaction will be small when one value is negative, and will increase the concentrations. Detection of negative concentrations, in fact, is used as one way to evaluate the adequacy of the resolution.

Two different initial conditions are used for the concentration fields. In the first, (runs U, W, and X) the reactants are in parallel slabs that occupy half of the domain. The initial concentration of reactant A is defined as

$$A(\mathbf{x},t) = 1 + \sum_{|k_1|=1}^{K/2} \frac{1}{k_1} \sin\left(\frac{k_1\pi}{2}\right) \cos(k_1 x_1)\, e^{(-Dk^2 t^*)}. \qquad (13.13)$$

Diffusion acts for a small time t^* before the simulation, in order to smooth the Gibb's ringing that results from the sharp concentration gradients between the slabs of reactants. The nominal value of the reactant concentration is 2 in each slab, so that the average value over the entire domain is unity.

The second initial condition for the concentration fields (run Z) is statistically

isotropic. A scalar quantity ϕ with zero mean and an initial scalar energy spectrum of the form

$$E_\phi(k,0) \propto \frac{kL^3}{\left(1+(kL)^2\right)^2} \tag{13.14}$$

was calculated in the preconditioning simulation used to define the initial conditions for the velocity field. At the beginning of run Z, regions of reactants A were defined in the locations where the scalar ϕ from the preconditioning run was positive. Regions of reactant B were defined in the other locations. The values of the concentrations were initially equal to either 2 or 0, but diffusive damping before the beginning of the simulation was used to smooth the concentration gradients. The initial statistics of the concentration fields were not exactly the same because of the finite size of the random number sample. For example, the initial mean concentrations of reactants A and B were 1.03 and 0.97, respectively. The initial concentration gradients were much steeper in run Z than in runs U, W, and X (with the slab geometry), which means a Damköhler number based on a mixing rate ($k_A\lambda_A^2/D$) is smaller.

One run (run W) was made with an Arrhenius expression for the reaction rate. The fraction approach to the adiabatic "flame" temperature θ, or the accomplished temperature rise, was calculated to be the product of the reaction by the proper choice of the stoichiometric coefficient. The local reaction rate coefficient for this simulation was

$$k_0 e^{-\tau_+/(\theta(\tau_\infty-1)+1)},$$

where k_0 was a constant, τ_+ is the ratio of the activation temperature to the initial temperature, and τ_∞ is the ratio of the final temperature to the initial temperature. The values for the parameters in the reaction rate give values of a modified Zel'dovich

Table 13.1: Summary of physical parameters and initial conditions used in each of the runs in this study

Run[a]	ν	Sc [b]	k_R [c]	S	u'	λ_g	$\overline{a^2}$	λ_A
U	0.01	0.7	2	3	1.26	0.245	0.898	1.46
W	0.02	0.7	800, 320000 ($\tau_+ = 6$, 12, $\tau_\infty = 1.2$)	0	1.03	0.381	0.898	1.46
X	0.02	0.7	0, 2, 8	0	1.03	0.381	0.898	1.46
Z	0.02	0.7	0, 2, 8	0	1.03	0.381	0.748	0.332

[a]All runs were made on a Cray 2 supercomputer at the Numerical Aerodynamic Simulation Program. The resolution of runs W, X, and Z was 64^3 coefficients, whereas the resolution of run U was $128 \times 128 \times 64$ coefficients.

[b]Lewis numbers of 1 and 4 were used in run W.

[c]The reaction rate coefficient k_R is a constant in runs U, X, and Z. An Arrhenius form, $k_0 \exp(-\tau_+/(\theta(\tau_\infty - 1) + 1))$ is used in run W, where θ is the accomplished temperature rise, τ_+ is the ratio of the activation temperature to the initial temperature, and τ_∞ is the ratio of the final temperature to the initial temperature. The values reported for run W are for the constant k_0.

number Z', which is defined here as the natural logarithm of the ratio of the reaction rate coefficient at the adiabatic flame temperature to the reaction rate coefficient at the initial temperature, or

$$Z' = \frac{\tau_+}{\tau_\infty}(\tau_\infty - 1),$$

were 1 and 2. It was felt that the thermal and concentration fields could not be resolved numerically for larger values of Z'. The values of k_0 were selected to match the initial reaction rate for the low Damköhler number case of run X.

CHAPTER 14. RESULTS AND DISCUSSION

Results from the simulations were visualized by examining contours lines of quantities, such as the local reaction rate, or projections of vectors, such as the vorticity, in two-dimensional slices of the flow field. (In some cases contour surfaces were also viewed.) It must be remembered that these are samples of a three-dimensional data set when interpreting the data. Statistical information, on the other hand, was obtained by averaging over the entire spatial domain of the simulation at selected times.

Isotropic Decaying Turbulence

In this section we will discuss the results of simulations made with an initially isotropic velocity field (runs W, X, and Z). The results from the cases where the reaction rate was independent of temperature (runs X and Z) are presented first. Data from run X are used to show the structure of the reaction zone in most cases, because only two easily distinguishable reaction zones are present in the domain, and so the results are easier to visualize and interpret. The statistical quantities that are examined in this section are primarily those that appear in Equations (12.8)–(12.10). The time histories of the averages of some of these quantities are shown in Tables 14.1 and 14.2 for runs X and Z. Overlines and angled brackets ($\langle\ \rangle$) are used interchangeably here to denote averages which were taken over all points in the

Table 14.1: Development of selected statistical averages at various times for the large Damköhler number case (Da = 6.4) in run X (slab geometry for the initial concentration values)

	$t = 0.677^a$	$t = 1.10$	$t = 1.60$	$t = 2.18$	$t = 2.89$
$\langle A \rangle$	0.873	0.823	0.765	0.705	0.633
$\langle AB \rangle \times 100$	1.49	1.48	1.39	1.00	1.17
$\langle \nabla A \cdot \nabla B \rangle$	−2.00	−1.79	−1.54	−1.32	−1.08
$\langle \nabla A \cdot \nabla A \rangle$	4.19	4.12	3.96	3.67	3.20
$\langle \nabla A \cdot \mathbf{e} \cdot \nabla B \rangle$	3.18	2.20	1.49	1.03	0.670
$\langle \mathbf{e} : \mathbf{e} \rangle$	8.20	4.89	2.93	1.85	1.17
$\langle \cos\theta_1 \rangle^b$	0.444	0.425	0.409	0.401	0.394
$\langle \cos\theta_2 \rangle$	0.460	0.438	0.428	0.423	0.419
$\langle \cos\theta_3 \rangle$	0.577	0.614	0.636	0.648	0.657
$\langle \nabla\phi \cdot \mathbf{e} \cdot \nabla\phi \rangle$	−4.61	−3.42	−2.48	−1.78	−1.18
$\langle \nabla\phi \cdot \nabla\phi \rangle$	3.11	2.99	2.77	2.50	2.12

[a] All of the quantities reported in this section are dimenional. The values of time can be made dimensionless with the eddy turnover time $t_e = 0.819$.

[b] The symbol θ_i denotes the angle between the concentration gradient for reactant A and the principal eigenvectors of e, where the subscript i refers to the eigenvalues (which are ordered from largest to smallest).

domain.

Reaction zones

The reactants in this study are initially segregated, except for thin regions of overlap. Chemical reactions cannot occur unless the species are mixed at the molecular level, and this mixing only comes about by the action of molecular diffusion. Turbulent motion can enhance molecular mixing by reducing length scales of the concentration field and therefore has an indirect influence on the local chemical reaction rate. Since the rate of reaction is fast, compared to the rate of mixing, for the cases in run X and for the case with the largest Damköhler number in run Z,

Table 14.2: Development of selected statistical averages at various times for the large Damköhler number case (Da = 6.4) in run Z (preconditioned initial concentrations)

	$t = 0.309$	$t = 0.680$	$t = 1.13$	$t = 1.68$	$t = 2.29$
$\langle A \rangle$	0.679	0.512	0.402	0.327	0.272
$\langle AB \rangle \times 100$	7.97	4.05	2.30	1.37	0.855
$\langle \nabla A \cdot \nabla B \rangle$	−8.40	−3.33	−1.45	−0.695	−0.361
$\langle \nabla A \cdot \nabla A \rangle$	13.8	6.69	3.27	1.71	0.951
$\langle \nabla A \cdot \mathbf{e} \cdot \nabla B \rangle$	14.0	4.43	1.44	0.530	0.218
$\langle \mathbf{e} : \mathbf{e} \rangle$	14.2	8.15	4.73	2.78	1.71
$\langle \cos\theta_1 \rangle^a$	0.385	0.385	0.386	0.384	0.383
$\langle \cos\theta_2 \rangle$	0.436	0.425	0.428	0.426	0.425
$\langle \cos\theta_3 \rangle$	0.652	0.664	0.662	0.663	0.663
$\langle \nabla\phi \cdot \mathbf{e} \cdot \nabla\phi \rangle$	−17.6	−6.13	−2.13	−0.841	−0.367
$\langle \nabla\phi \cdot \nabla\phi \rangle$	10.9	4.90	2.30	1.17	0.645

[a]The symbol θ_i denotes the angle between the concentration gradient for reactant A and the principal eigenvectors of $\mathbf{e}$, where the subscript i refers to the eigenvalues (which are ordered from largest to smallest).

the reaction zones remain distinct and the reactants continue to be segregated. The segregation coefficient, defined as $\overline{ab}/\bar{A}\bar{B}$, is a nearly constant value of -0.98 for the large Damköhler number case of run X and is slowly decreasing from -0.83 to -0.88 for the large Damköhler number case of run Z. (A segregation coefficient of -1 corresponds to perfectly segregated reactants.) Figure 14.1 shows contours of the local reaction rate for the high Damköhler number reaction of case X in the plane $x = 0$ at a sequence of times. The two reaction zones are initially planar and centered at $x_2 = \pi/2$ and $x_2 = 3\pi/2$. The locations at subsequent times are determined by the the fluid motion, as the reaction zones are convected with the fluid.

The plane used to show the local reaction rates in Figure 14.1 ($x = 0$) will be used in additional figures for the data from run X in this section. The data in this plane are representative of the entire domain, and any plane of constant x or z (the planes that are perpendicular to the initial reaction fronts) can be used for the visualization of the reaction fronts.

The reaction rate is not uniform along the reaction zone (say, as a contour of the conserved scalar species is followed), since the contours of reaction rate shown in Figure 14.1 are not simply distorted by the fluid motion. Instead, regions of locally intense reaction rate exist and persist throughout the simulation. The reactants would be consumed in these intense regions, causing a reduction in the reaction rate, unless the concentrations of reactants are increased in the reaction zone by diffusion that has been enhanced by increased concentration gradients on either side of the zone. Contours of the pseudo-dissipation term $\nabla A \cdot \nabla B$, which contributes to an increase in the mean levels of AB from Equation (12.9), are shown in Figure 14.2 in the same

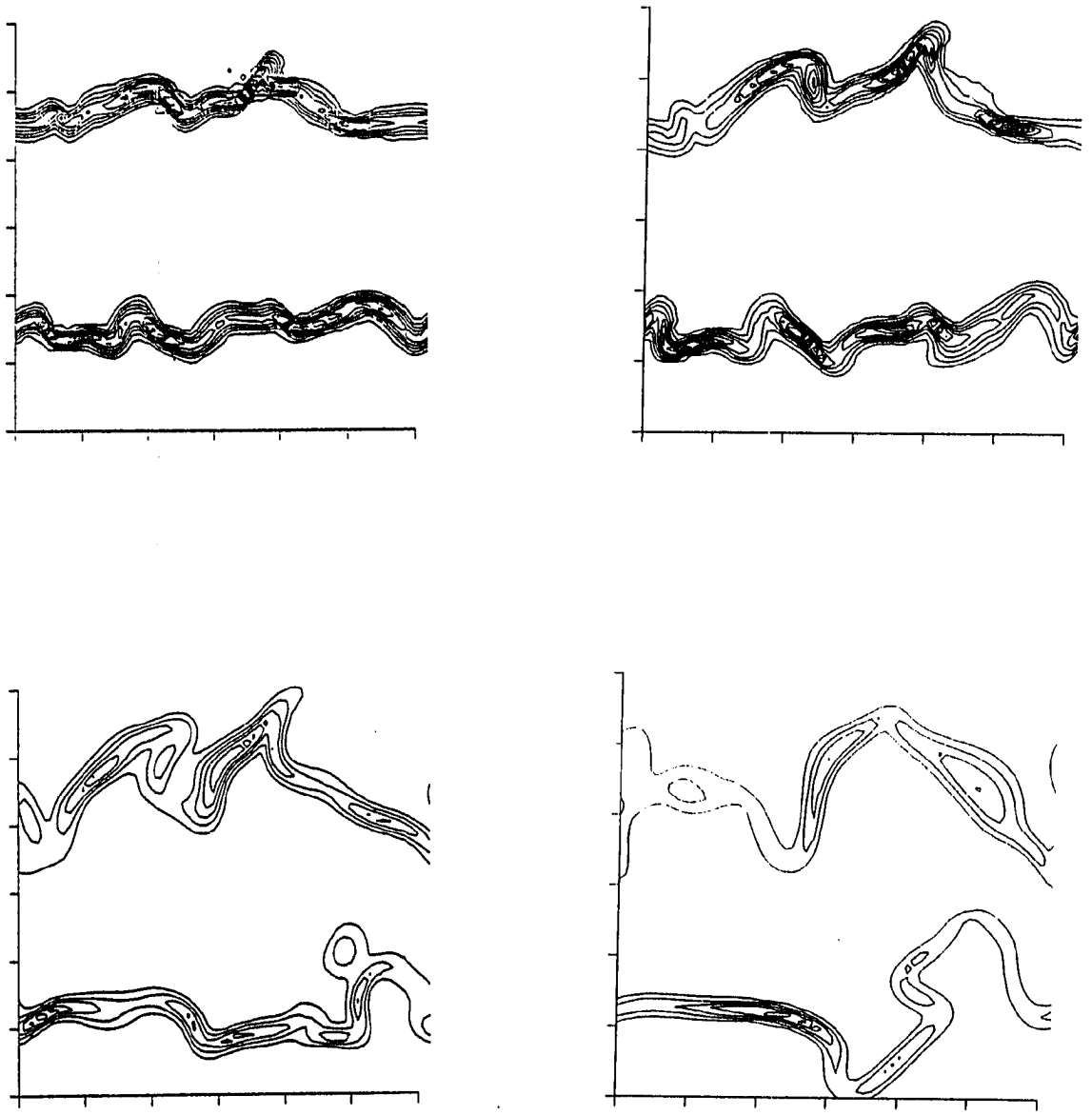

Figure 14.1: Contours of the local reaction rate in the plane $x = 0$ for run X. The contour interval is 0.05. (Da = 6.4)

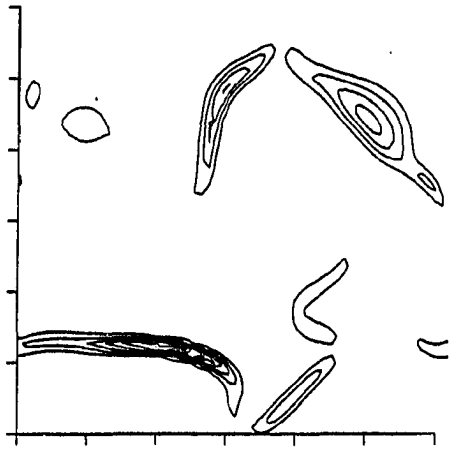

Figure 14.2: Contours of the pseudo-dissipation term $-2D\nabla A \cdot \nabla B$ in the plane $x = 0$ for run X at $t = 2.86$. The contour interval is 0.2. (Da = 6.4)

plane that was used in Figure 14.1. The values are nonzero only in the reaction zones, where the concentration gradients of both reactants are nonzero, and are negative in the reaction zone because the scalar gradients are in opposite directions there. The locations of the largest magnitude of $\nabla A \cdot \nabla B$ correspond to the locations where the reaction rate is highest.

The mean reaction rate, $k_R AB$, is decreased by the consumption of reactants. Contours of the rate of change of the reaction rate due to the reaction itself, $kAB(A+B)$, in Figure 14.3 also show maxima where the reaction rate is largest. The magnitude is less than that for the term $D\nabla A \cdot \nabla B$, and so regions of intense reaction rates tend to persist.

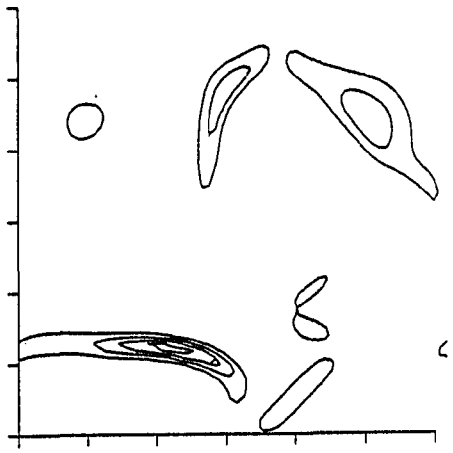

Figure 14.3: Contours of the contribution of the reaction itself to the local reaction rate, $2k_R AB(A+B)$ in the plane $x = 0$ for run X at $t = 2.86$. The contour interval is 0.2. (Da = 6.4)

Local rates of strain and rotation

Gradients of the concentration fields are amplified by the straining motions and turned by rotation. Figure 14.4 shows vorticity vectors superimposed on reaction rate contours from Figure 14.1. As in previous studies (Kerr, 1985; Ashurst et al., 1987) the gradients of the concentration of inert species, which are not shown here, tend to be oriented perpendicular to the vorticity field. Gradients of the concentration of reactants also tend to be oriented perpendicular to vorticity. Vorticity vectors in Figure 14.4, therefore, tend to be parallel to the reaction zone, especially in the regions where the reaction rate is greatest. Since the contribution of vorticity to the rate of change of the concentration gradient depends on the cross product between the two vectors (Equation 12.6), this alignment is the most effective one in changing the

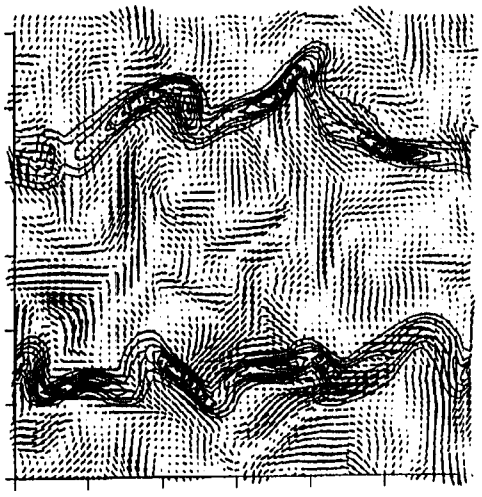

Figure 14.4: Vorticity vectors superimposed on the contour lines of reaction rate from Figure 14.1

direction of the gradient. The contour surfaces of reactant concentration or reaction rate will, therefore, tend to roll up because of vorticity. The vorticity is distributed randomly in space in isotropic turbulence, so there is no particular structure to the reaction zones.

The magnitudes of the concentration gradients and of the term $\nabla A \cdot \nabla B$ do not depend on the vorticity but depend, instead, on the rate of strain. The alignments of the concentration gradients with the principal directions of the rate of strain tensor are important, because the contribution of strain rate to the rate of change of $\nabla A \cdot \nabla B$ is given by $\nabla A \cdot \mathbf{e} \cdot \nabla B$. The strain rate must thus be correlated with the concentration gradients in order to produce any change in their magnitude. If the concentration gradients are aligned with the most compressive direction, then the value of the gradient amplification term is positive and is the most effective at increasing the

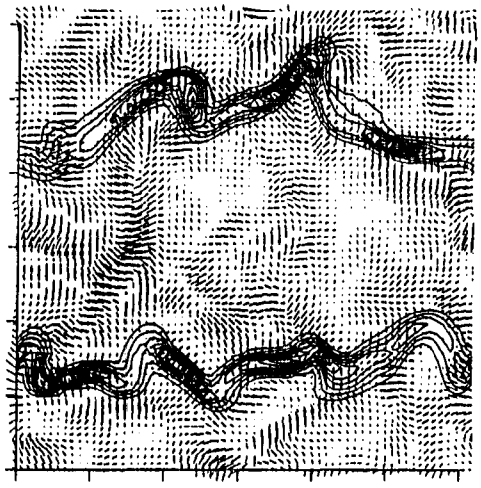

Figure 14.5: Eigenvectors corresponding to the most compressive rate of strain superimposed on the contour lines of reaction rate from Figure 14.1

magnitude of the dot product between gradients of the reactant concentrations, $\nabla A \cdot \nabla B$.

The eigenvectors corresponding to the most negative eigenvalue of e are superimposed on the reaction rate contours in Figure 14.5. The reaction zones tend to be perpendicular to these eigenvectors, and the vectors within the reaction zone are the longest (indicating the greatest magnitude of the strain rate) in the regions where the reaction rate is greatest. This alignment tendency is indicated more clearly by the pdf of the cosine of the angle between each eigenvector and the gradient of reactant A in Figure 14.6. The pdf for the most compressive direction peaks sharply at a value of the cosine equal to one, which corresponds to perfect alignment. Comparison of the pdf for cases with different reaction rates indicates that the gradient alignment with the compressive strain direction is decreased slightly by the reaction. The alignment

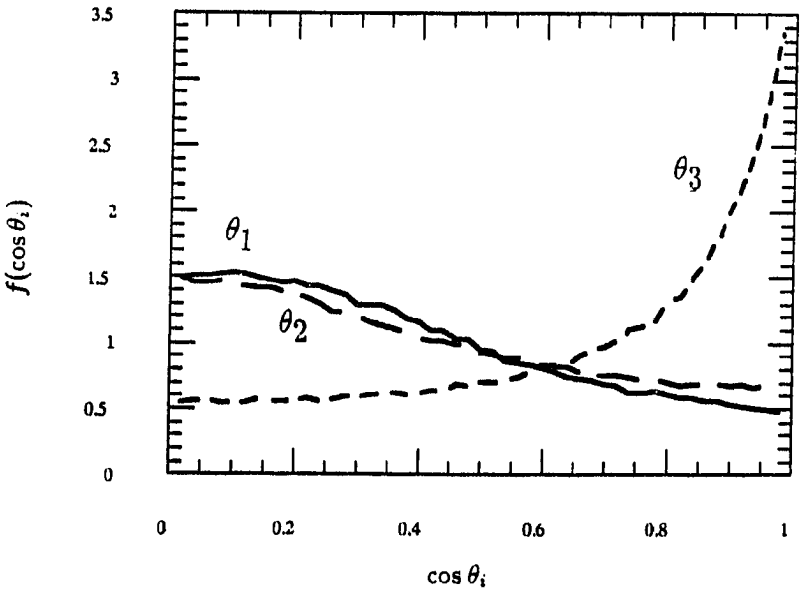

Figure 14.6: Pdf of the cosine of the angle between the gradient of the concentration of reactant A and the principal directions of the rate of strain tensor in run X at time $t = 2.86$

becomes more pronounced as time proceeds in run X, and has reached a steady value in run Z, which has initial concentration fields that have been preconditioned. The average value of the cosine of the angle between the concentration gradients and the principal directions of the rate of strain tensor are reported in Tables 14.1 and 14.2. This is a severe test of the alignment, since it really measures the dispersion of the angle. The average value of the angle will be zero for randomly distributed vectors, since the probability of angles with the opposite sign will be equal.

Contours of the gradient amplification term, $\nabla A \cdot \mathbf{e} \cdot \nabla B$, are shown in Figure 14.7 in the same location and for the same conditions as in Figure 14.2 for the pseudo-dissipation. The value of this term is seldom negative, and the magnitudes of the negative values are small, which confirms the above argument that the orientation

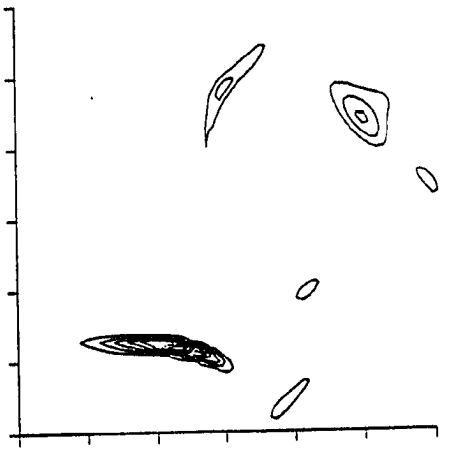

Figure 14.7: Contours of the gradient amplification term $\nabla A \cdot \mathbf{e} \cdot \nabla B$ in the same plane as in Figure 14.1

of the reaction zone is determined by the compressive strain rate. The values of the amplification term are very intermittent, with locations of highest magnitude in the same locations as high reaction rate. At these points the gradients responsible for mixing the two species together are being increased by compressive strain of the fluid in the direction normal to the reaction front. The data in Tables 14.1 and 14.2 show that the correlation between the strain rate and the reactant concentration gradients,

$$\frac{\langle \nabla A \cdot \mathbf{e} \cdot \nabla B \rangle}{\langle \nabla A \cdot \nabla A \rangle^{1/2} \langle \nabla B \cdot \nabla B \rangle^{1/2} \langle \mathbf{e} : \mathbf{e} \rangle^{1/2}},$$

decreases with time, even though the concentration gradients are becoming more closely aligned with the direction of compressive straining, because the correlation between the two concentration gradients is decreasing as a result of the consumption of the reactants.

The alignment of the reactant concentration gradients with the principal direc-

tions of the strain rate tensor and the correlations between the strain rate and the concentration gradients are very similar for the two cases with different initial conditions for the concentration field. As a result of the tendency for the reaction fronts to align with the strain-rate field, the locations of peak reaction rates do not seem to be very sensitive to the initial conditions used for the concentration fields in some cases. Contours of reaction rate for runs X and Z are shown in Figure 14.8 in the same plane, which was the center of one of the initial reaction zones in run X. Even though the initial conditions were different for the two runs, the regions of the most intense reaction rate tend to coincide.

Mixing mechanisms for inert flows

Since the chemical reaction studied in this paper is dominated by mixing, we examine here the two mixing mechanisms proposed by Gibson (1968a) and Gibson et al. (1988) for nonreacting scalars. The concentration fields of an inert species with isotropic initial conditions in run Z are used to examine these mixing mechanisms. Figure 14.9 shows contours of the values of the conserved scalar variable, $Z \equiv A - B$, at the time $t = 2.29$. Regions where the magnitude of the scalar gradient is small are shaded. The plot is only a cross section of the domain, so points that appear to be extrema, but are not shaded, have a nonzero component of the gradient in the normal direction.

The local values of the gradient amplification term $\nabla Z \cdot \mathbf{e} \cdot \nabla Z$ in the equation

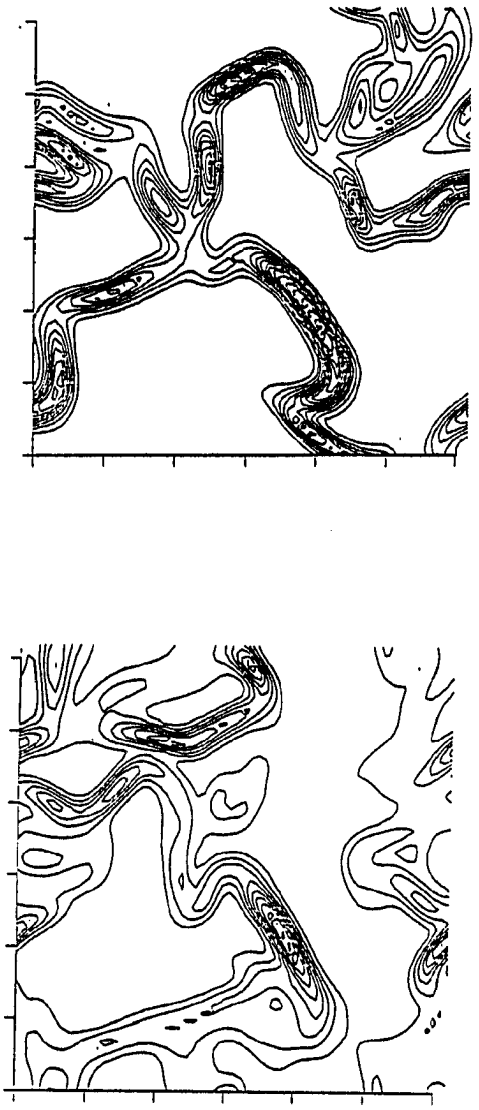

Figure 14.8: Contours of local reaction rate from runs X and Z in a plane that was one of the initial reaction zones in run X. (Run Z has isotropic concentration fields.) Note that intense reaction rates tend to occur in the same places, even though the initial conditions for the two runs were different

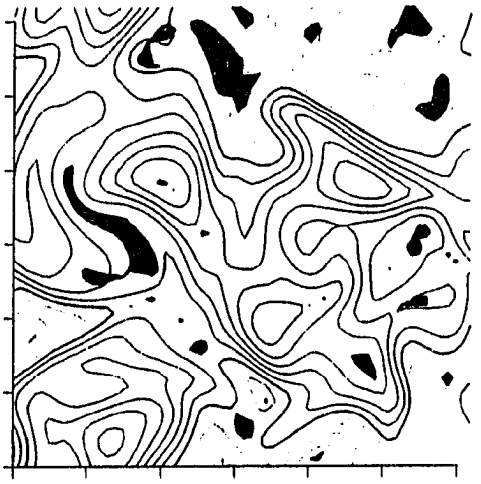

Figure 14.9: Contours of the values of the conserved scalar $Z \equiv A - B$ from run Z at $t = 1.06$

for the dissipation rate for the conserved scalar,

$$\frac{\partial(\nabla Z \cdot \nabla Z)}{\partial t} + \mathbf{u} \cdot \nabla(\nabla Z \cdot \nabla Z) = D\nabla^2(\nabla Z \cdot \nabla Z) - 2D\nabla\nabla Z : \nabla\nabla Z - 2\nabla Z \cdot \mathbf{e} \cdot \nabla Z, \tag{14.1}$$

are shown in Figure 14.10. This is the only term that contributes to the mean production of scalar dissipation. The values of the correlation between the strain rate and the conserved scalar gradient,

$$\frac{-\langle \nabla Z \cdot \mathbf{e} \cdot \nabla Z \rangle}{\langle \nabla Z \cdot \nabla Z \rangle \langle \mathbf{e} : \mathbf{e} \rangle^{1/2}},$$

are in the range 0.4–0.5 for runs X and Z, which is consistent with Kerr's (1985) results for forced isotropic turbulence. The values of the correlation are not changing with time, although the cases with different initial concentration distributions have different values.

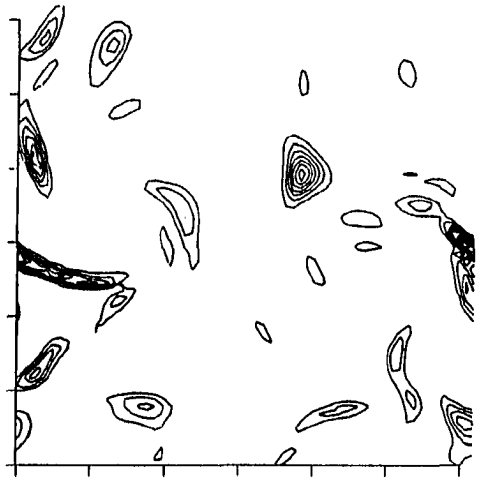

Figure 14.10: Contours of the gradient amplification of the conserved scalar dissipation rate in the same plane as Figure 14.9

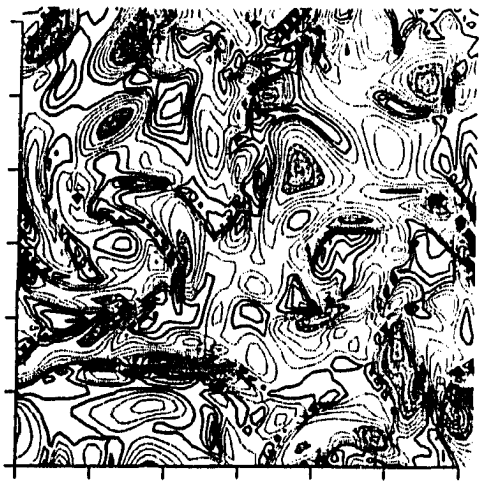

Figure 14.11: Contours of the normalized gradient amplification of the conserved scalar dissipation, or the effective local strain rate, in the same plane as Figure 14.9

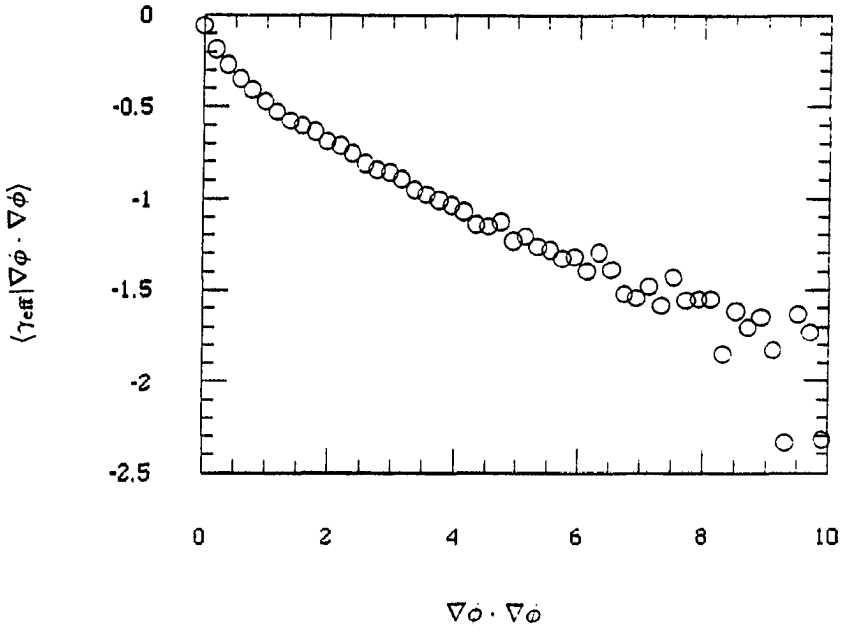

Figure 14.12: Conditional expectation of the local effective strain rate, given the local dissipation rate of the conserved scalar. This statistic is calculated by averaging over the entire domain for the same time as used in Figure 14.11

The contributions of the gradient amplification term to the rate of change of the local dissipation rate shown in Figure 14.10 are greatest where the gradients are largest. This is direct evidence of the mixing mechanism proposed by Gibson et al. (1988). which is supposedly applicable for all values of the magnitude of the scalar gradient. The mechanism proposed by Gibson (1968a) for mixing should be the most effective if the local gradient amplification term, when normalized with the local scalar dissipation rate to give an effective local strain rate,

$$\gamma_{\text{eff}} = \frac{\nabla Z \cdot \mathbf{e} \cdot \nabla Z}{\nabla Z \cdot \nabla Z}, \tag{14.2}$$

is large for small values of $|\nabla Z|$. The values of the effective strain rate shown in Figure 14.11 with the largest magnitudes are almost always at the points where the gradients are large. This is also shown in Figure 14.12 by the conditional expectation of the effective strain rate, given the value of the scalar dissipation rate. which increases in magnitude for larger values of the conserved scalar gradient. The magnitude of the relative amplification is largest for the largest values of the dissipation rate. These two figures suggest that the mechanism proposed by Gibson et al. (1988) dominates the mechanism proposed by Gibson (1968a) for the conditions used here. It may be that the Reynolds numbers used in the simulation are too small for the zero-gradient pinching mechanism to be effective.

The importance of the mixing mechanism on reaction can be seen by examining the contours of reaction rate in the same plane as in Figures 14.9–14.11 for the values of the conserved scalar and of the amplification of the conserved scalar gradients (Figure 14.13). The conserved scalar dissipation rate is used as a parameter in the flamelet models that were discussed earlier. Locations where the gradient amplifica-

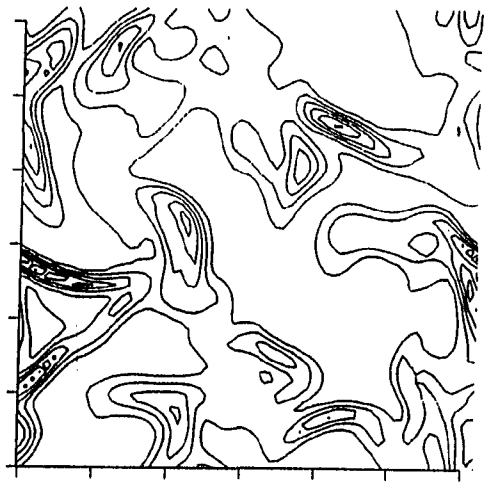

Figure 14.13: Contours of the reaction rate ($Da = 6.4$) in run Z in the same plane as Figure 14.9

tion is high are also regions where the reaction rate, for both values of Damköhler number, is high.

Kinematic structures

Since the reactant concentrations are passive scalars in this study, the alignment of concentration contours with features of the flow must be a response to the fluid motion. It may then be possible to include the kinematics of the flow field in modeling the progress of the reaction.

For fast reactions, it has been conjectured (Hunt et al., 1988) that reactions will tend to occur in the convergence zones defined by the Hunt-Wray-Moin criteria, and slow reactions will tend to occur in the eddy regions. The convergence zones can only be important to the reaction if they are near the reaction front for a fast reaction.

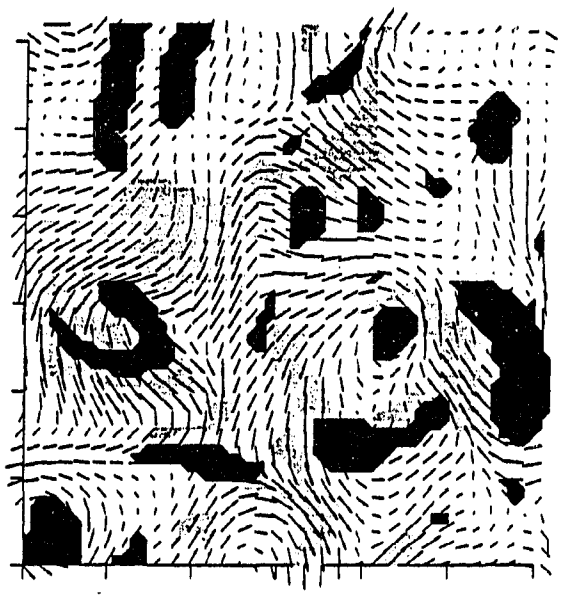

Figure 14.14: Velocity vectors superimposed on the kinematic structures defined by Hunt et al. (1988) for run X. The eddies are denoted by the darkest gray, the streams by the lightest gray, and the convergence zones by the intermediate gray level

Any convergence zones far from reaction fronts can only steepen gradients of one of the reactants, which does not help increase the local reaction rate.

Figure 14.14 shows velocity vectors superimposed on the Hunt-Wray-Moin structures from run X, for same location and time that were used in Figures 14.1–14.7. The convergence zones, which are expected to be locations of high local values of the reaction rate, occupy only about 5% of the domain. The eddy regions appear to occupy a larger fraction of the domain (about 15% in this study) than in the results of Hunt et al. (1988), and the streaming regions appear to occupy a smaller fraction (about 20% here). Reaction rate contours superimposed on the structures in plots such as Figure 14.15 do not show any obvious correlation between the locations of the the reaction zones and any of the structures. There are regions of high reaction

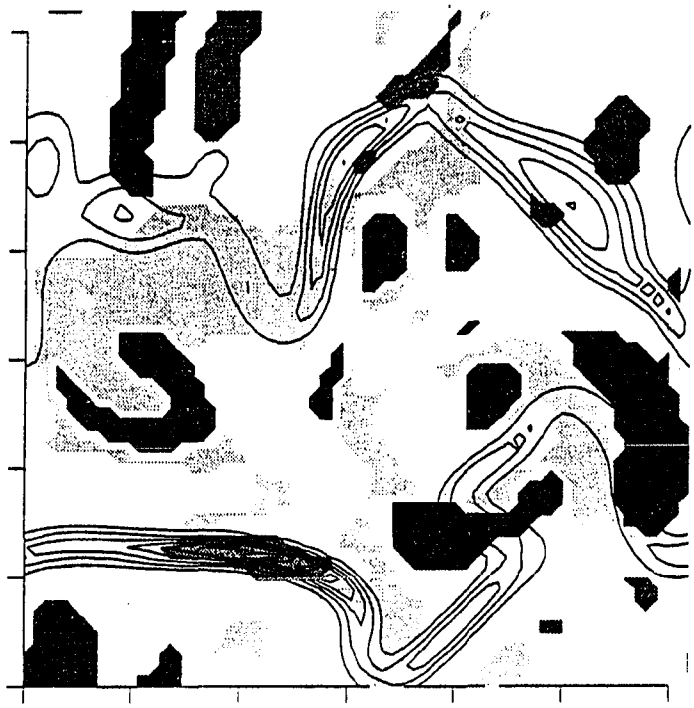

Figure 14.15: Contours of reaction rate (Da = 6.4) superimposed on the kinematic structures defined by Hunt et al. (1988) for run X. The eddies are denoted by the darkest gray, the streams by the lightest gray, and the convergence zones by the intermediate gray level

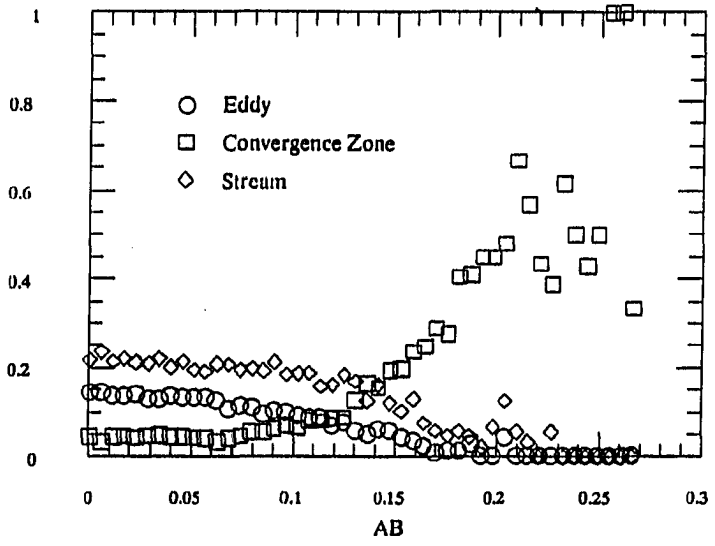

Figure 14.16: Fraction of points in the domain that are defined to be a kinematic structure, given the local value of the reaction rate for run X at t=1.95

rate in or near convergence zones, but not all of the most intense regions occur in convergence zones.

In order to gain more insight into the application of the kinematic structures for a reacting system, the characteristics of the reaction zone are examined in a more quantitative manner by considering conditional averages of kinematical quantities, such as those used to define the HWM structures, given values of the reaction rate.

In support of Hunt's hypothesis, the average reaction rate in the convergence zones is almost twice the volume average, and the fraction of sample points for each value of the reaction rate that are in the convergence zones increases for the very highest reaction rates (Figure 14.16). On the other hand, and contrary to the hypothesis, there is more likelihood for a region of high reaction rate to be at a point which does not meet any of the criteria for the kinematic structures than to be in a

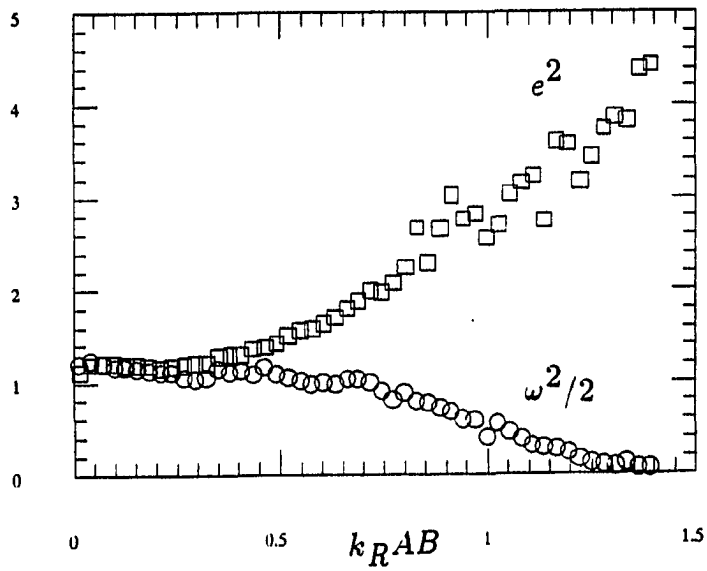

Figure 14.17: Conditional expectations of $e_{ij}e_{ji}$ and $\omega_i\omega_i$, given the local value of the reaction rate for run X at t=1.95

convergence zone. Figure 14.17 shows the conditional averages of $e_{ij}e_{ji}$ and $\omega_i\omega_i$, given values of the reaction rate. The conditional averages of both of these quantities are nearly the same as the volume averages, both in the regions outside of the reaction zone ($k_R AB = 0$) and for most of the points within the reaction zone ($k_R AB < 0.4$). It is only for the few points with the most intense reaction rate that the conditional averages are appreciably different than the volume averages. At these points, the straining rate is much more pronounced and the vorticity is significantly less than the average values. The conditional average of the pressure, which is not shown here, is also larger than the volume average for large values of the reaction rate. The conditional structure of the highest reaction rate regions, then, is similar to the definition of a convergence zone. The failure to see an obvious correspondence between reaction zones and convergence zones in Figure 14.15 may suggest that one problem with the

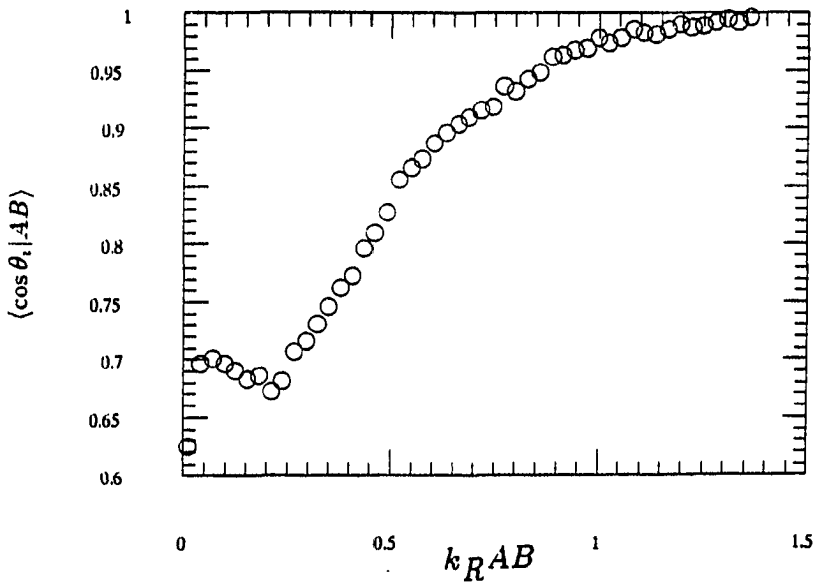

Figure 14.18: Conditional expectation of the cosine of the angle between the gradient of the concentration of reactant A and the principal direction for the most compressive strain rate at $t = 2.86$ in run X

classification scheme may be a question of cutoff values for each region. Changing the parameters used to define each region could ensure that locations of intense reaction rates are more likely to occur at or near convergence zones, but this would also define more regions as convergence zones where the reaction rate is not high. Since there are parameters that can be adjusted in the definition of each region, some subjectivity is included in the classification method. The criteria in Table 12.1 should perhaps be considered more as guidelines than as fixed rules.

The nature of the reaction zones can be studied more fully by considering other conditional averages. In the regions of the most intense reaction, the concentration gradients are more closely aligned with the compressive straining direction and the gradient amplification is much larger than in the rest of the domain, as seen from the

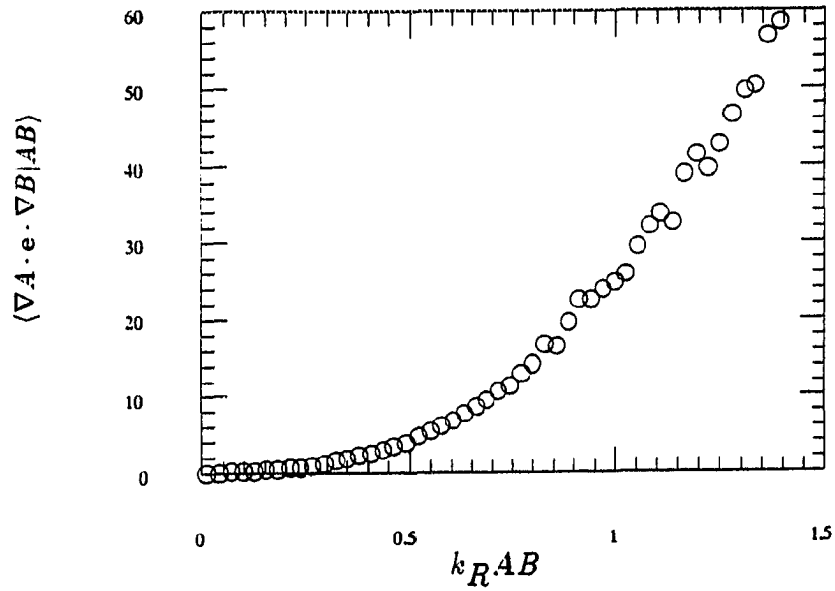

Figure 14.19: Conditional expectation of the gradient amplification term for the pseudo-dissipation at $t = 2.86$ in run X

conditional averages in Figures 14.18 and 14.19. In addition, the magnitudes of the principal values of the rate of strain are larger in the intense reaction rate regions than in regions outside the reaction zone. This supports the observations we made earlier in the discussion of the local structure of the reaction zone (Figure 14.5).

Arrhenius kinetics

Up to this point we have discussed simulations in which the reaction rate is independent of the temperature. Studies of the conditional averages of kinematical quantities, given reaction rate values, show that the regions of intense reaction rates are regions which are highly strained and oriented so that the reaction front is perpendicular to the direction of the most compressive strain rate. The local rate of strain amplifies the gradients of reactant concentration at these points, which increases the

mass transport of reactants to the reaction zones. These are the points at which one would expect to see extinction in a combustion process as heat is transported away from the reaction zone, since in such cases the reaction rate has an exponential dependence on temperature.

Run W used an Arrhenius expression for the reaction rate coefficient in order to determine if a reduction in reaction rate would be seen for regions with high strain rates. Figure 14.20 shows contours of the local reaction rate for two cases with a Zel'dovich number of 2 and Lewis numbers of 1 and 4, and an isothermal case. There is not much difference in the structure of the reaction zone for the temperature-dependent and isothermal cases. The regions of most intense reaction rate are in the same location, but the reaction rates have sharper peaks for the temperature-dependent cases than for the isothermal case, which one would expect from the exponential dependence of the reaction rate on temperature. The peak values of the Arrhenius reaction rate, however, do not correspond to the peak values in temperature, plotted in Figure 14.21. The temperature rise is a result of the heat produced by the reaction. An earlier study (Leonard and Hill, 1988) showed that the regions of high concentration of products were not the same as the regions of high local reaction rate. The amount of product, or the value of the temperature, depends on the history of the reaction. In addition, if the regions where the local reaction rate is high are stagnation points in the flow, with the most compressive principal direction of the straining normal to the reaction front, then the continuity condition requires extensional straining motion in at least one direction tangent to the reaction front. Products or temperature will, therefore, be convected away from regions where

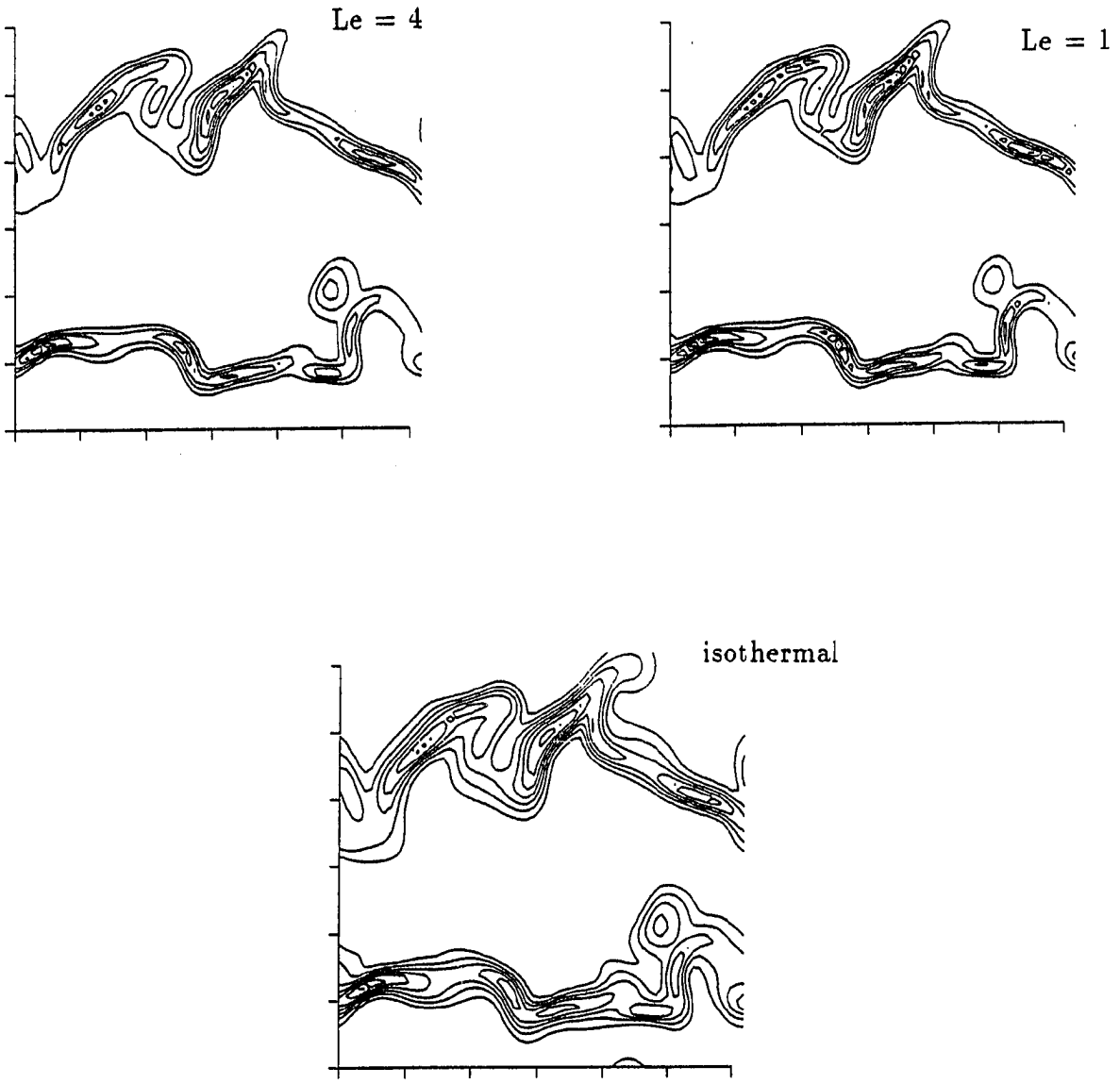

Figure 14.20: Contours of the local reaction rate for the Arrhenius kinetics in run W

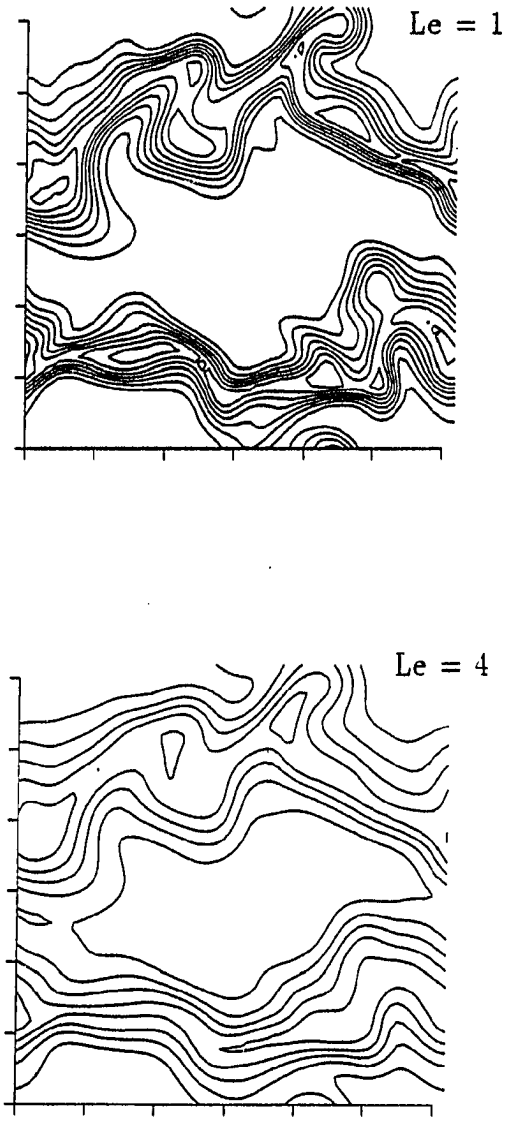

Figure 14.21: Contours of the local temperature values for the Arrhenius kinetics in run W

the reaction rate is highest.

The values of temperature are much more sharply peaked for the case with Le = 1 than for the case with Le = 4, but the peak reaction rates are only slightly higher. Enhanced transport of heat away from the reaction zone reduces the reaction rate slightly but does not extinguish the reaction for this value of the Zel'dovich number. For comparison, Anand and Pope (1987) use a value of 250 for Z' in the pdf calculations for a turbulent premixed flame. For our conditions the reactions cannot be extinguished by fluid straining because the reaction rate is nonzero at the initial temperature, and an ignition condition is not needed for the reaction to occur.

Homogeneous Turbulent Shear Flow

In the isotropic turbulent flows studied here, the reaction zones became aligned with features of the turbulence (i.e., the principal coordinates of the rate of strain), but the turbulence itself had no apparent organization. Rogers and Moin (1987) have shown that a mean shear causes alignment of the vorticity fields and is responsible for the development of hairpin vortices in homogeneous turbulence. The existence of coherent structures was used to explain the transport of a passive scalar. We have included a chemical reaction in a simulation of a homogeneous shear flow to study the effects of any organized motions such as hairpins on the local reaction rate. The conditions for this calculation (run U) are given in Table 13.1. The velocity field was still developing in this simulation. The rate of production of kinetic energy by the mean shear was less than the dissipation rate until the end of the simulation. The simulation was not carried further because of concerns about resolving the small-scale

structure of the concentration fields and the large-scale structure of the velocity field.

Contour plots of reaction rate in the plane $z = 0$ are shown in Figure 14.22 for the dimensionless times St = 1, 2, 3, and 4. The mean flow is in the x direction and the mean velocity gradient is in the y direction. Only half of the domain is shown, in order to focus on a single reaction zone. The most intense reaction rate occurs in thin regions which have approximately the same inclination to the mean flow direction and are stretched by the mean flow, since the parts of the reaction zone that are displaced by the turbulent motion in the positive y direction have a positive mean velocity relative to the parts of the reaction zone that are displaced in the negative y direction. The inclination of the regions of intense reaction rate is approximately the same as that for the contours of a passive scalar shown by Rogers et al. (1986). The regions of high reaction rate are in the same locations as regions of large magnitudes of scalar dissipation and gradient amplification, which are shown in the same plane in Figure 14.23 at time $St = 4$. The amplification of concentration gradients is much greater in the shear flow than in the isotropic flow, in part because of the different initial velocity field, but also due to the mean strain. The maximum value of the magnitude of the gradient of reactant concentration at $St = 1$ is 25, and the maximum value of $\nabla A \cdot \mathbf{e} \cdot \nabla B$ is 13,500. The values of the statistics given in Tables 14.1 and 14.2 for the isotropic turbulent flow are given in Table 14.3 for the homogeneous turbulent shear flow.

The alignment of the concentration gradients with the direction of compressive straining that was observed in the isotropic flow is seen in the shear flow, but the degree of the alignment is less than for than the isotropic flow. (The total rate of

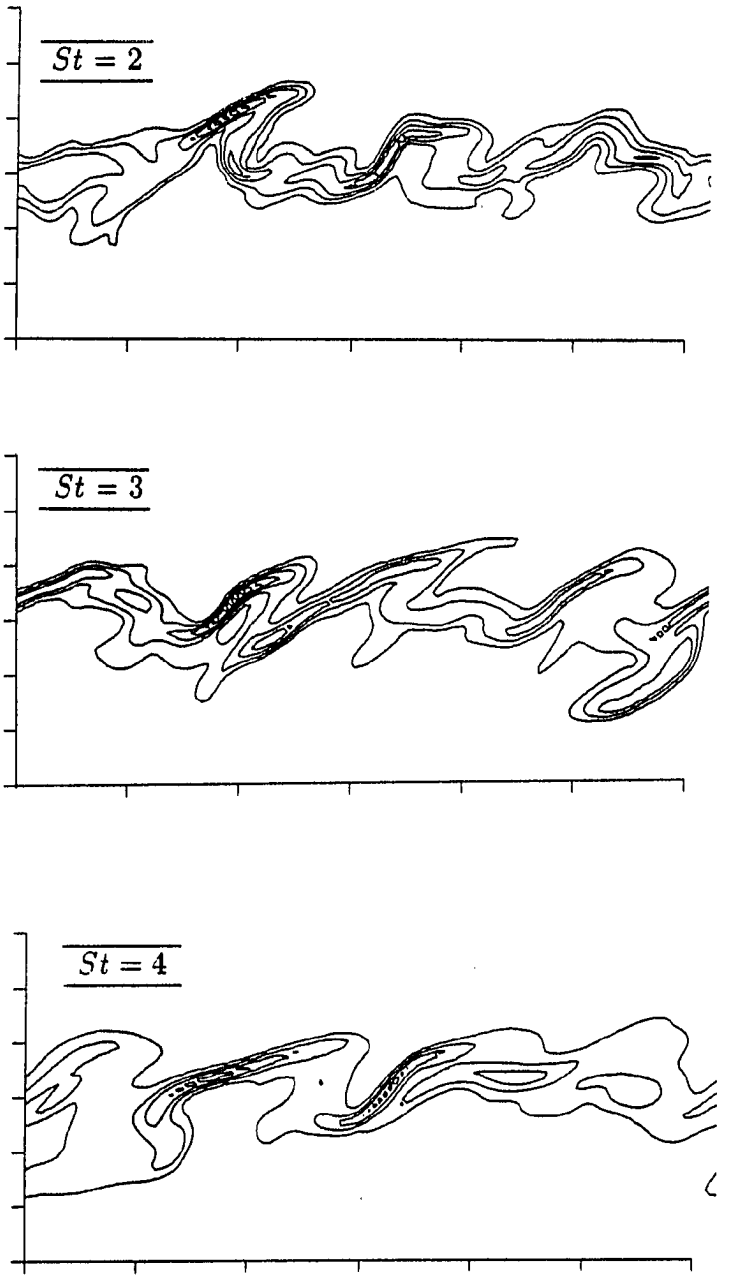

Figure 14.22: Contours of local reaction rate in the plane $z = 0$ for the homogeneous shear flow (run U) at times $St = 2$, 3, and 4. Only the portion of the domain $0 \leq y < \pi$ is shown

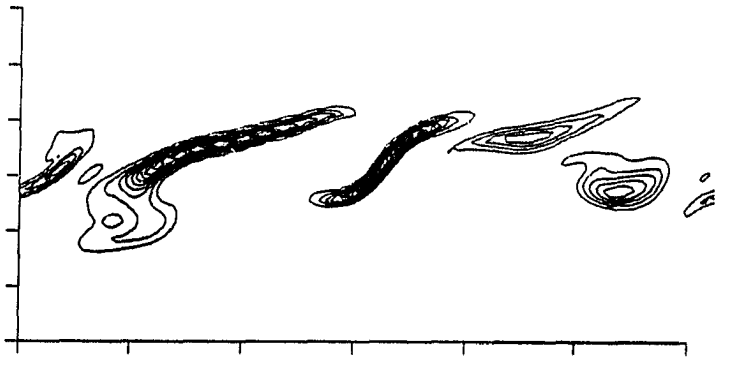

(a)

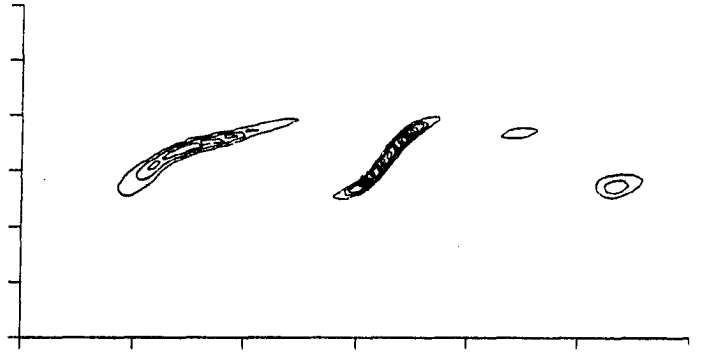

(b)

Figure 14.23: Contours of the local values of (a) the pseudo-dissipation term $\nabla A \cdot \nabla B$ and (b) the gradient amplification term $\nabla A \cdot \mathrm{e} \cdot \nabla B$ in the same plane as the data in Figure 14.22

Table 14.3: Development of selected statistical averages at various times for the homogeneous shear flow (run U)

	$St = 1$	$St = 2$	$St = 3$	$St = 4$
$\langle A \rangle$	0.951	0.908	0.868	0.835
$\langle AB \rangle \times 100$	6.54	6.25	5.48	4.64
$\langle \nabla A \cdot \nabla B \rangle$	−7.18	−5.30	−3.93	−2.89
$\langle \nabla A \cdot \nabla A \rangle$	8.33	6.99	5.87	4.92
$\langle \nabla A \cdot \mathbf{e} \cdot \nabla B \rangle$	33.3	16.9	10.3	6.03
$\langle \mathbf{e} : \mathbf{e} \rangle$	86.5	43.5	28.9	23.2
$\langle \cos\theta_1 \rangle^a$	0.469	0.456	0.453	0.471
$\langle \cos\theta_2 \rangle$	0.457	0.443	0.429	0.409
$\langle \cos\theta_3 \rangle$	0.566	0.591	0.608	0.613

[a]The symbol θ_i denotes the angle between the concentration gradient for reactant A and the principal eigenvectors of $\mathbf{e}$, where the subscript i refers to the eigenvalues (which are ordered from largest to smallest).

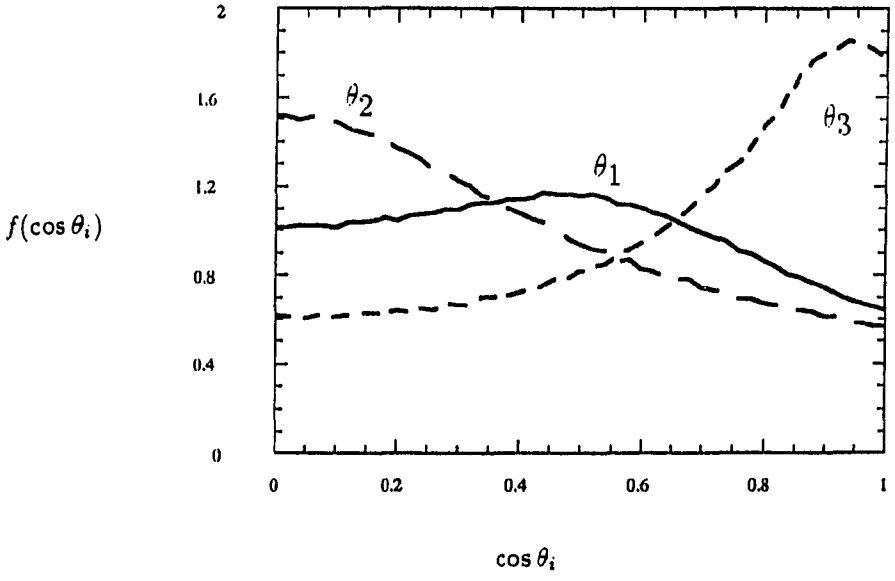

Figure 14.24: Probability density function of the cosine of the angle between the gradient of the concentration of reactant A and each of the principal directions of the rate of strain tensor for the homogeneous shear flow. ($St = 4$)

strain, including the mean shear, was used to evaluate the eigenvalues and eigenvectors of e.) The mean value of the cosine of the angle between the gradient of concentration and the most compressive direction is about 0.6 for the shear flow and 0.67 for the isotropic flow. The pdf of the cosine of the angle between the gradient of reactant concentration and each principal direction of the rate of strain tensor is shown in Figure 14.24 at times $St = 3$ and 4. The pdf of the alignment with the most compressive strain rate is less sharply peaked than in the isotropic case. This is consistent with the findings of Ashurst et al. (1987). The alignment of the reactant concentration gradient with the intermediate strain rate was nearly identical to that in the isotropic flows. The alignment with the most extensional strain rate, however, differed considerably from that in the isotropic flows. The pdf of the cosine of the angle between the reactant concentration and the principal direction of most extensional strain develops a peak at intermediate values of the cosine and remains relatively flat. The reason for this is not clear, but it is consistent with the findings of Ashurst et al. (1987).

Three-dimensional contour surfaces of a high value of the reaction rate show that the reaction zones are organized by the mean shear. In isotropic turbulence the vorticity creates bulges in the reaction zone by rotating concentration gradients. Rogers and Moin (1987) have shown that in the homogeneous shear flow the vorticity vectors tend to be aligned. This causes bulges in the the contour surfaces of the reactant concentration or of the reaction rate that are longer in the streamwise direction than in the spanwise direction. The most intense reaction occurs in regions that tend to be either flat sheets or thin tubes. The tubes resemble the reaction rate contours occur-

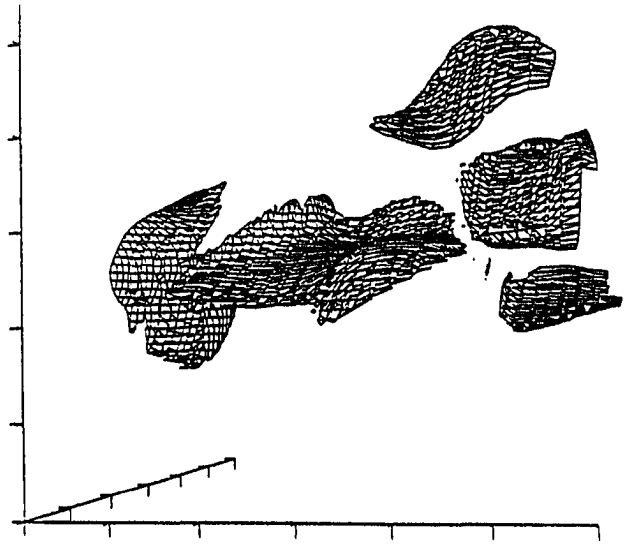

Figure 14.25: Contour surface of the local reaction rate at the level $k_R AB = 1$ for run U at time $St = 4$. Only a portion of the domain is shown, and the flow direction is normal to the page

ring in the braids between the large structures in the numerically simulated mixing layer of Metcalfe and Hussain (1989). The flat sheets of most intense reaction rate shown in Figure 14.25 are more prevalent at the end of the simulation, presumably because the level of vorticity fluctuations is decreasing.

Rogers et al. (1986) observed an abundance of horseshoe vortices inclined at angles to the mean flow direction between 22° and 45°. We have projected vorticity vectors and reaction rate contours on a plane inclined at 26.6° from the mean flow direction in Figure 14.26. This plane was chosen because it is computationally convenient and because vorticity vectors and the reaction structures are inclined from the direction of the mean flow. The vorticity vectors show some organization that might be interpreted as being horseshoe vortices. These structures do not appear to be as

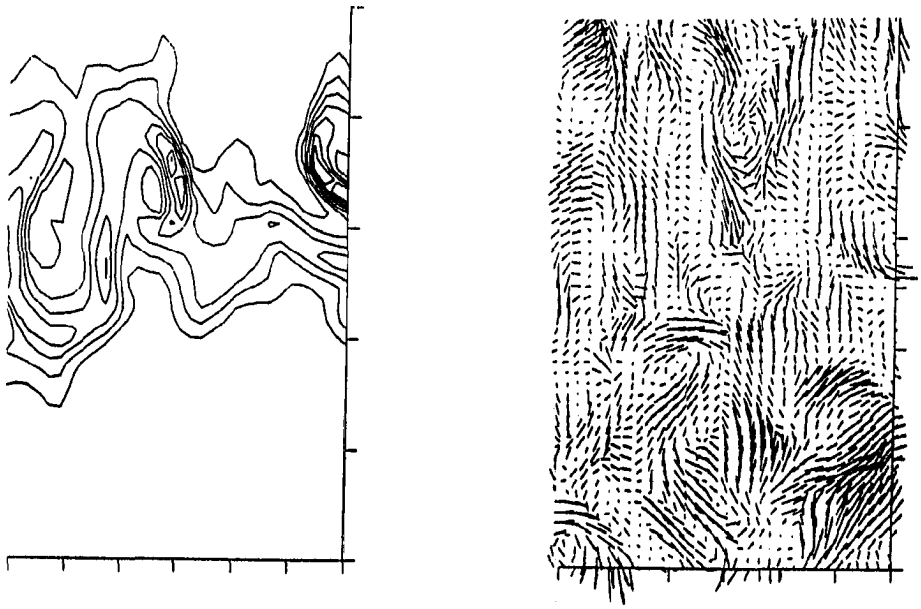

Figure 14.26: Contours of local reaction rate and projections of the vorticity vectors in a plane inclined at an angle of 26.6° to the mean flow direction in the homogeneous shear flow. ($St = 4$)

organized as those found by Rogers et al. (1986), but this flow is still developing. The vorticity structures are located near regions of the reaction zones showing strong curvature and large reaction rates. Contour lines for the reaction rate tend be parallel to the vorticity vectors where the reaction rates are highest.

CHAPTER 15. SUMMARY AND CONCLUSIONS

Direct numerical simulations have been used to examine the local structure of the reaction zone for a fast reaction between unmixed species in homogeneous turbulence. Both decaying isotropic turbulence and a homogeneous shear flow were calculated in this study. An Arrhenius reaction rate and a second-order reaction rate with a constant reaction rate coefficient were used in the calculations of reactant concentrations.

Locally intense reaction rates occurred within the reaction zones, and these intense regions tended to persist throughout the simulation. The regions of intense reaction rate occurred in locations where the gradients of both reactant concentrations were large and were being amplified by the local rate of strain. The gradients of reactant concentration tended to align with the direction of the most compressive principal strain rate. The reaction rate was high where the alignment of the strain rate and the reactant concentration gradients was strongest, and also where the local strain rate was high.

The role of the rate of strain in the mixing of reactants supports the mixing mechanism proposed by Gibson et al. (1988), that the scalar gradients with large magnitudes become aligned with and are amplified by the rate of strain. The locally intense regions of reaction rate did not show a high degree of correlation with regions

defined by Hunt et al. (1988) as convergence zones, or highly strained regions.

The tendency for the concentration gradients to align with the strain rate causes the reaction zoned to be distorted, and reaction zones for cases with different initial concentration fields become aligned such that the regions of most intense reaction rate are in the same locations.

Large local strain rates did not cause quenching of the reaction rate when an Arrhenius expression was used, although the dependence of the reaction rate on temperature was not strong. The high local values of reaction rate were due to the mixing of reactants and not to high temperature values, since the peaks in temperature and the reaction rate were at different location.

The reaction zones were more organized for the case with a uniform mean shear than for the cases with isotropic turbulence, since the vorticity vectors that rotate the concentration gradients become aligned. The concentration gradients were much steeper in the shear flow, as a result of amplification by a much larger rate of strain. The concentration gradients tend to align with the direction of the most compressive principal rate of strain, although to a slightly lesser degree than in the isotropic turbulence.

In summary, the regions of the most intense reaction rates in these simulations have been rotated so that the direction of most compressive straining sn normal to the reaction front. The concentration gradients are amplified by the straining motion, which results in an increased rate of mixing of the reactants, and a corresponding increase in the reaction rate.

Models which incorporate some information about the structure of the velocity

and scalar fields would seem to be appropriate to use in a statistical treatment. This does not necessarily mean that the reaction front can be expressed as a laminar diffusion flame or as a lamellar structure, but the influence of kinematic quantities (in particular, the rate of strain) is important in the local structure of the reaction zone.

SUMMARY

This dissertation considered, in three parts, problems concerning mixing and chemical reactions in homogeneous turbulent flows. Direct numerical simulations of finite-rate chemical reactions occurring in moderate Reynolds number turbulence were used in this study. In the first two parts, models for two phenomena contributing to unknown terms in statistical treatments of reacting flow were considered. In Part I models that are used in the solution of probability density function (pdf) equations were examined, whereas in Part II models used in moment methods for the mean reaction rate were evaluated. In Part III, results of the simulations were used to examine the structure of the reaction zone. In all three parts the simulations provided data that are difficult to measure experimentally.

In Part I, coalescence-dispersion (C/D) models for pdf equations were tested by assuming that the time scale for mixing is known. All of the models examined in this study predicted the means and variances of the concentrations of reactant and inert species well. However, the shapes of the pdf's did not agree with the data. The modifications of Curl's model made by Pope (1982) and by Janicka et al. (1979) are fairly easy to implement as part of a Monte Carlo solution, and produce more acceptable pdf's than does Curl's model. Details of the models were examined by directly evaluating the unknown mixing term in Janicka's model from the simulation

data. The actual values of the conditional expectations contained in the terms were also evaluated.

In Part II, several moment closures for the reaction term were evaluated. Of the models tested, the one by Toor (1969) produced the best agreement with the simulation data. In these tests the decay rate for the conserved scalar variance was assumed to be known, so the tests would reflect the effects of reaction and not problems in estimating the rate of scalar dissipation.

Finally, in Part III, examination of the local structure of the reaction zone, which becomes quite distorted by the turbulence, showed that the reaction zone becomes oriented perpendicular to the most compressive rate of strain. Concentration gradients were amplified by the rate of strain tensor, and this increased the rate of mixing of the reactants and, therefore, the local reaction rates. The reaction rates are highest at regions in the reaction zone where the rate of strain is high and where the concentration gradient is aligned with the most compressive rate of strain. Locations of intense reaction rate seem to be somewhat insensitive to the initial conditions used for the concentration fields.

ACKNOWLEDGEMENTS

.I would like to thank my major professor, Dr. James C. Hill, for sparking my interest in the subject, and for providing guidance and advice during my studies. I would also like to thank the members of my program of study committee, Dr. John M. Eggebrecht, Dr. Kenneth R. Jolls, Dr. Richard H. Pletcher, and Dr. Eugene S. Takle.

The compuational resources used for the simulations were made available by the National Center for Supercomputer Applications in Urbana, Illinois (in part under grant ECS 8515047 from the National Science Foundation) and the Numerical Aerodynamic Simulation Program at the NASA-Ames Research Center in Moffett Field, California. Additional computer resources were provided by the ISU Compuation Center and Dr. Kenneth R. Jolls.

I would like to thank the Department of Chemical Engineering and the Engineering Research Institute for their financial support.

The computer programs used in this study were developed from codes written by Dr. Robert M. Kerr, National Center for Atmosheric Research, Boulder, Colorado and by Dr. Robert S. Rogallo, NASA-Ames Research Center, Moffett Field California. A post-processing program was developed from a code written by Dr. Alan A. Wray, NASA-Ames Research Center. I would like to express my thanks to them for their

assistance and for the access to their codes.

I would like to thank the organizers of the 1987 Summer School on Geophysical and Astrophysical Turbulence at the National Center for Atmospheric Research for allowing me to participate. I would also like to thank officials of the Center for Turbulence Research for letting me participate in the 1987 and 1988 Summer Programs and to thank Dr. Shankar Mahalingham for his assistance during the 1988 Summer Program. In addition, I would like to thank the following participants of the CTR programs for helpful discussions: Dr. W. T. Ashurst, Dr. J. H. Ferziger, Dr. J. C. R. Hunt, Dr. P. Moin, Mr. Kyle Squires, Dr. J. J. Riley, Dr. W. C. Reynolds, Dr. M. M. Rogers, and Dr. C. Rutland. I would also like to thank my fellow graduate students R. C. Sanderson and R. C. Hamlen for their help at Iowa State University.

Finally, I would like to thank my family for their love and support, and especially my mother, Shirley Leonard, and my wife, Julie Hardwick, for her patience.

REFERENCES

Adrian, R. J. (1979). Conditional eddies in isotropic turbulence. *Phys. Fluids* **22**, 2065–2070.

Anand, M. S. and Pope, S. B. (1987). Calculations of premixed turbulent flames by pdf methods. *Combust. Flame* **67**, 127–142.

Ajmera, P. V., Singh, M. and Toor, H. L. (1976). Reactive mixing in turbulent gases. *Chem. Eng. Commun.* **2**, 115–120.

Ashurst, W. T., Kerstein, A. R., Kerr, R. M. and Gibson, C. H. (1987). Alignment of vorticity and scalar gradient with strain rate in simulated Navier-Stokes turbulence. *Phys. Fluids* **30**, 2343-2353.

Batchelor, G. K. (1952). The effect of homogeneous turbulence on material lines and surfaces. *Proc. R. Soc. London A* **213**, 349–366.

Batchelor, G. K. (1959). Small-scale variations of convected quantities like temperature in turbulent fluid. Part 1. General discussion and the case of small conductivity. *J. Fluid Mech.* **5**, 113–133.

Batchelor, G. K., Howells, I. D. and Townsend, A. A. (1959). Small-scale variations of convected quantities like temperature in turbulent fluid. Part 2. The case of large conductivity. *J. Fluid Mech.* **5**, 134-139.

Bennani, A., Gence, J. N. and Mathieu, J. (1985). The influence of a grid-generated turbulence on the development of chemical reactions. *AIChE J.* **31**, 1157–1166.

Bilger, R. W. (1980). Turbulent flows with nonpremixed reactants. Pp. 65–113. In Libby, P. A. and Williams, F. A. (eds.), *Turbulent Reacting Flows, Topics in Applied Physics* **44**. Springer-Verlag, Heidelberg.

Bird, R. B., Stewart, W. E. and Lightfoot, E. N. (1960). *Transport Phenomena.* Wiley, New York.

Bonniot, C. and Borghi, R. (1979). Joint probability density function in turbulent combustion. *Acta Astronaut.* **6**, 309–327.

Borghi, R. (1988). Turbulent combustion modeling. *Prog. Energy Combust. Sci.* **14**, 245–292.

Borghi, R., Picart, A., and Gonzalez, M. (1989). On the problem of modelling time or length scales in turbulent combustion. Pp. 564–588. In Borghi, R. and Murthy, S. N. B. (eds.), *Turbulent Reactive Flows.* Springer-Verlag, New-York.

Cantwell, B. J. (1981). Organized motion in turbulent flow. *Ann. Rev. Fluid Mech.* **13**, 457–515.

Coles, D. (1981). Prospects for useful research on coherent structure in turbulent shear flow. *Proc. Indian Acad. Sci. Eng. Sci.* **4**, 111–127.

Comte-Bellot, G. and Corrsin, S. (1966). The use of a contraction to improve the isotropy of grid-generated turbulence. *J. Fluid Mech.* **25**, 657–682.

Corrsin, S. (1951a). On the spectrum of isotropic temperature fluctuations in an isotropic turbulence. *J. Appl. Phys.* **22**, 469–473.

Corrsin, S. (1951b). The decay of isotropic temperature fluctuations in an isotropic turbulence. *J. Aero. Sci.* **18**, 417–433.

Corrsin, S. (1957). Simple theory of an idealized turbulent mixer. *AIChE J.* **3**, 329–330.

Corrsin, S. (1964). The isotropic turbulent mixer: Part II. Arbitrary Schmidt number. *AIChE J.* **10**, 870–877.

Curl, R. I. (1963). Dispersed phase mixing theory and effects in simple reactors. *AIChE J.* **9**, 175–181.

Donaldson, C. duP. (1975). On the modeling of the scalar-correlations necessary to construct a second-order closure description of a turbulent flow. Pp. 131–162. In Murthy, S. N. B. (ed.), *Turbulent Mixing in Nonreactive and Reactive Flows.* Plenum, New York.

Donaldson, C. duP. and Varma, A. K. (1976). Remarks on the construction of a second order closure description of turbulent reacting flows. *Combust. Sci. Technol.* **13**, 55–78.

Dopazo, C. (1979). Relaxation of initial probability density functions in the turbulent convection of scalar fields. *Phys. Fluids* **22**, 20–30.

Dopazo, C. and O'Brien, E. E. (1974). An approach to the autoignition of a turbulent mixture. *Acta Astronaut.* **1**, 1239–1266.

Durbin, P. A. (1982). Analysis of the decay of temperature fluctuations in isotropic turbulence. *Phys. Fluids* **25**, 1328–1332.

Dutta, A. and Tarbell, J. M. (1989). A closure model for turbulent reacting flows. To appear in *AIChE J.*

Eswaran, V., O'Brien, E. E. and Decker, A. (1989). The modeling of the two-point probability density function of a reacting scalar in isotropic turbulence. *Combust. Sci. Technol.* **65**, 1–18.

Eswaran, V. and Pope, S. B. (1988). Direct numerical simulations of the turbulent mixing of a passive scalar. *Phys. Fluids* **31**, 506–520.

Favre, A. (1965). Équations des gaz turbulents compressibles. I. Formes générals. *J. Mecanique* **4**, 361–390.

Gibson, C. H. (1968a). Fine structure of scalar fields mixed by turbulence. I. Zero-gradient points and minimal gradient surfaces. *Phys. Fluids* **11**, 2305–2315.

Gibson, C. H. (1969b). Fine structure of scalar fields mixed by turbulence. II. Spectral theory. *Phys. Fluids* **11**, 2316–2327.

Gibson, C. H., Ashurst, W. T. and Kerstein, A. R. (1988). Mixing of strongly diffusive passive scalars like temperature by turbulence. *J. Fluid Mech.* **194**, 261–293.

Givi, P. (1989). Model-free simulations of turbulent reactive flows. *Prog. Energy Combust. Sci.* **15**, 1–107.

Givi, P. and Jou, W.-H. (1988). Direct numerical simulations of a two dimensional

reacting spatially developing mixing layer by a spectral element method. *Twenty-second Symp. (Int.) Combust.*, 635–643.

Givi, P., Jou, W.-H. and Metcalfe, R. W. (1986). Flame extinction in a temporally developing mixing layer. Twenty-first Symp. (Int.) Combust., 1251–1261.

Givi, P. and McMurtry, P. A. (1988). Non-premixed reaction in homogeneous turbulence: Direct numerical simulations. *AIChE J.* **34**, 1039–1042.

Hamlen, R. C. (1984). Computer simulation of turbulent scalar transport with applications to chemical reaction. M.S. Thesis. Iowa State University. 183 pp.

Haworth, D. C. and Pope, S. B. (1987). A pdf modeling study of self-similar turbulent free shear flows. *Phys. Fluids* **30**, 1026–1044.

Hill, J. C. (1970). Zero diffusivity invariance for turbulent chemical reaction. *Phys. Fluids* **13**, 1394–1396.

Hill, J. C. (1976). Homogeneous turbulent mixing with chemical reaction. *Ann. Rev. Fluid Mech.* **8**, 135–161.

Hinze, J. O. (1975). *Turbulence.* McGraw-Hill, New York.

Hsieh, T.-H. J. and O'Brien, E. E. (1986). Prediction of single point concentration statistics in a chemically-reactive, turbulent, grid flow. *Combust. Sci. Technol.* **46**, 267–287.

Hunt, J. C. R., Wray, A. A. and Moin, P. (1988). Eddies, streams, and convergence zones in turbulent flows. *Studying Turbulence Using Numerical Simulation Databases—II. Proceedings of the 1988 Summer Program.* Center for Turbulence Research Report CTR-S88, 193–208.

Hussain, A. K. M. F. (1986). Coherent Structures and Turbulence. *J. Fluid Mech.* **173**, 303–356.

Ievlev, V. M. (1973). Equations for the finite-dimensional probability distributions of pulsating variables in a turbulent flow. *Sov. Phys. Dokl.* **18**, 117–119.

Janicka, J., Kolbe, W. and Kollmann, W. (1978). The solution of a pdf-transport equation for turbulent diffusion flames. Pp. 296–312. In Crowe, C. T. and Grosshandler, W. L. (eds.), *Proc. Heat Transf. Fluid Mech. Inst.* Stanford

University, Stanford, California.

Janicka, J., Kolbe, W. and Kollmann, W. (1979). Closure of the transport equation for the probability density function of turbulent scalar fields. *J. Non-Equilib. Thermodyn.* **4**, 47–66.

Jones, W. P. and Whitelaw, J. H. (1982). Calculation methods for reacting turbulent flows: A review. *Combust. Flame* **48**, 1–26.

Jou, W.-H. and Riley, J. J. (1987). On direct numerical simulations of turbulent reacting flows. AIAA Paper 87-1324.

Kerr, R.M. (1985). Higher-order derivative correlations and the alignment of small-scale structures in isotropic numerical turbulence. *J. Fluid Mech.* **153**, 31–58.

Kim, J. and Moin, P. (1986). The structure of the vorticity field in turbulent channel flow. Part 2. Study of ensemble-averaged fields. *J. Fluid Mech.* **162**, 339–363.

Kosàly, G. (1986). Theoretical remarks on a phenomenological model of turbulent mixing. *Combust. Sci. Technol.* **49**, 227–234.

Kosàly, G. (1987). Non-premixed simple reaction in homogeneous turbulence. *AIChE J.* **33**, 1998–2002.

Kosàly, G. and Givi, P. (1987). Modeling of turbulent molecular mixing. *Combust. Flame* **70**, 101–118.

Kuo, Y.-Y. and O'Brien, E. E. (1981). Two-point probability density function closure applied to a diffusive-reactive system. *Phys. Fluids* **24**, 194–201.

Launder, B. E. (1978). Heat and mass transport. Pp. 231–287. In Bradshaw, P. (ed.) *Turbulence, Topics in Applied Physics* **12**. Springer-Verlag, Berlin.

Lee, M. J. and Reynolds, W. C. (1985). Numerical experiments on the structure of homogeneous turbulence. *Dept. Mech. Engng. Rep. TF-24*. Stanford University, Stanford, California.

Leonard, A. D. (1988). Numerical studies of turbulent reacting flows. M.S. Thesis. Iowa State University. 70 pp.

Leonard, A. D. and Hill, J. C. (1986). Direct simulation of turbulent mixing with

irreversible chemical reaction. *Proc. World Congress III Chem. Eng.* **4**, 177–180.

Leonard, A. D. and Hill, J. C. (1988). Direct numerical simulation of turbulent flows with chemical reaction. *J. Sci. Comput.* **3**, 25–43.

Leonard, A. D. and Hill, J. C. (1989). Direct numerical simulation and simple closure theory for a chemical reaction in homogeneous turbulence. Pp. 515–540. In Borghi, R. and Murthy, S. N. B. (eds.), *Turbulent Reactive Flows.* Springer-Verlag, New-York.

Liew, S. K., Bray, K. N. C. and Moss, J. B. (1984). A stretched laminar flamelet model of turbulent nonpremixed combustion. *Combust. Flame* **56**, 199–213.

Lin, C.-H. and O'Brien, E. E. (1972). Two species isothermal reaction in homogeneous turbulence. *Astronaut. Acta* **17**, 771–781.

Lumley, J. L. (1967). The structure of inhomogeous turbulent flows. Pp. 166–178 In Yaglom, A. M. and Tatarsky, V. I. (eds.) *Atmospheric Turbulence and Radio Wave Propagation.* NAUKA, Moscow.

Lumley, J. L. (1981). Coherent structures in turbulence. Pp. 215–242. In Meyer, R. E. (ed.), *Transition and Turbulence.* Academic, New York.

Lumley, J. L. (1980). Second-order modeling of turbulent flows. Pp. 1–32. In Kollmann, W. (ed.) *Prediction Methods for Turbulent Flows.* Hemisphere, Washington.

Lundgren, T. S. (1967). Distribution functions in the statistical theory of turbulence. *Phys. Fluids* **10**, 969–975.

Lundgren, T. S. (1972). A closure hypothesis for the hierarchy of equations for turbulent probability distribution functions. Pp. 70–100. In Rosenblatt, M. and Van Atta, C. (eds.), *Statistical Models and Turbulence, Lecture Notes in Physics* **12.** Springer-Verlag, New York.

Lundgren, T. S. (1982). Strained spiral vortex model for turbulent fine structure. *Phys. Fluids* **25**, 2193–2203.

Lundgren, T. S. (1985). The concentration spectrum of the product of a fast bimolecular reaction. *Chem. Engng. Sci.* **40**, 1641–1652.

Mao, K. W. and Toor, H. L. (1970). Second-order chemical reactions with turbulent mixing. *Ind. Eng. Chem. Fundam.* **10**, 192–197.

McKelvey, K. N., Yieh, H.-N., Zakanycz, S. and Brodkey, R. S. (1975). Turbulent motion, mixing, and kinetics in a chemical reactor configuration. *AIChE J.* **21**, 1165–1176.

McMurtry, P. A. and Givi, P. (1989). Direct numerical simulations of mixing and reaction in a nonpremixed homogeneous turbulent flow. *Combust. Flame* **77**, 171–185.

McMurtry, P. A., Jou, W.-H., Riley, J. J. and Metcalfe, R. W. (1986). Direct numerical simulations of a reacting mixing layer with chemical heat release. *AIAA J.* **24**, 962-970.

Metcalfe, R. W. and Hussain, F. (1989). Topology of coherent structures and flame sheets in reacting mixing layers. To appear in *Topological Fluid Mechanics*. Cambridge Press, Cambridge.

Meyers, R. E. and O'Brien, E. E. (1981). The joint pdf of a scalar and its gradient at a point in a turbulent fluid. *Combust. Sci. Technol.* **26**, 123–134.

Miyawaki, O., Tsujikawa, H and Uraguchi, Y. (1974). Turbulent mixing in multi-nozzle injection tubular mixer. *J. Chem. Eng. Jpn.* **7**, 52–56.

Moffatt, H. K. (1985). Magnetostatic equilibria and analogous Euler flows of arbitrarily complex topology. Part 1. Fundamentals. *J. Fluid Mech.* **159**, 359–378.

Monin, A. S. (1967). Equations of turbulent motion. *J. Appl. Math. Mech.* **31**, 1057–1068.

Mudford, N. R. and Bilger, R. W. (1984). Examination of closure models for mean chemical reaction rate using experimental results for an isothermal turbulent reacting flow. *Twentieth Symp. (Int.) on Combust.*, 387–394.

Newman, G. R. and Herring, J. R. (1979). A test field model study of a passive scalar in isotropic turbulence. *J. Fluid Mech.* **94**, 163–194.

Newman, G. R., Launder, B. E. and Lumley, J. L. (1979). Modelling the behavior of homogeneous scalar turbulence. *J. Fluid Mech.* **111**, 217–232.

O'Brien, E. E. (1986). Recent contributions to the statistical theory of chemical reactants in turbulent flows. *Physicochem. Hydrodyn.* **7**, 1–15.

Oran, E. S. and Boris, J. P. (1987). *Numerical Simulation of Reactive Flow.* Elsevier, New York.

Orszag, S. A. (1971). Numerical simulation of incompressible flows within simple boundaries. I. Galerkin (spectral) representations. *Studies Appl. Math.* **50**, 293–327.

Orszag, S. A. (1972). Comparison of pseudospectral and spectral approximations. *Studies Appl. Math.* **51**, 253–259.

Ottino, J. M. (1980). Lamellar mixing model for structured chemical reactions and their relationship to statistical models, macro- and microo-mixing and the problem of averages. *Chem. Engng. Sci.* **35**, 1377–1391.

Ottino, J. M., Ranz, W. E. and Macosko, C. W. (1979). A lamellar model for analysis of liquid-liquid mixing. *Chem. Engng. Sci.* **34**, 877-890.

Patterson, G. K. (1981). Application of turbulence fundamentals to reactor modelling and scaleup. *Chem. Eng. Commun.* **8**, 25–52.

Peters, N. (1984). Laminar diffusion flamelet models in non-premixed turbulent combustion. *Prog. Energy Combust. Sci.* **10**, 319–339.

Peters, N. (1986). Laminar flamelet concepts in turbulent combustion. *Twenty-first Symp. (Int.) on Combust.*, 1231–1250.

Pope, S. B. (1976). The probability approach to the modelling of turbulent reacting flows. *Combust. Flame* **27**, 299–312.

Pope, S. B. (1981). Monte Carlo calculations of premixed turbulent flames. *Eighteenth Symp. (Int.) Combust.*, 1001–1010.

Pope, S. B. (1982). An improved turbulent mixing model. *Combust. Sci. Technol.* **28**, 131–135.

Pope, S. B. (1985). Pdf methods for turbulent reactive flows. *Prog. Energy Combust. Sci.* **11**, 119–192.

Ranz, W. E. (1979). Applications of a stretch model to mixing, diffusion, and

reaction in laminar and turbulent flows. *AIChe J.* **25**, 41–47.

Reynolds, O. (1883). An experimental investigation of the circumstances which determine whether the motion of water shall be direct of sinuous, and of the law of resistance in parallel channels. *Philos. Trans. R. Soc. London A* **174**, 935–982.

Reynolds, W. C. (1976). Computation of turbulent flows. *Ann. Rev. Fluid Mech.* **8**, 183–208.

Reynolds, W. C. and Cebeci, T. (1978). Calculations of turbulent flows. Pp. 193–229. In Bradshaw, P. (ed.) *Turbulence, Topics in Applied Physics* **12**. Springer, Berlin.

Riley, J. J. and McMurtry, P. A. (1989). The use of direct numerical simulation in the study of turbulent, chemically-reacting flows. Pp. 486–514. In Borghi, R. and Murthy, S. N. B. (eds.), *Turbulent Reactive Flows*. Springer-Verlag, New-York.

Riley, J. J., Metcalfe, R. W. and Orszag, S. A. (1986). Direct numerical simulations of chemically reacting turbulent mixing layers. *Phys. Fluids* **29**, 406–422.

Rogers, M. M. and Moin, P. (1987). The structure of the vorticity field in homogeneous turbulent flows. *J. Fluid Mech.* **176**, 33–66.

Rogers, M. M., Moin, P. and Reynolds, W. C. (1986). The structure and modeling of the hydrodynamic and passive scalar fields in homogeneous turbulent shear flow. *Dept. Mech. Engng. Rep. TF-25*. Stanford University, Stanford, California.

Rogallo, R. S. (1981). Numerical experiments in homogeneous turbulence. *NASA TM 81315*.

Sinai, Y. G. and Yakhot, V. (1989). Limiting probability distributions of a passive scalar in a random velocity field. *Phys. Rev. Let.* **63**, 1962–1964.

Sreenivasan, K. R., Tavoularis, S., Henry, R. and Corrsin, S. (1980). Temperature fluctuations and scales in grid- generated turbulence. *J. Fluid Mech.* **100**, 597–621.

Tarbell, J. M. and Mehta, R. V. (1986). Mechanistic models of mixing and chemical reaction with a turbulence analogy. *Physicochem. Hydrodyn.* **7**, 17–32.

Toor, H. L. (1962). Mass transfer in dilute turbulent and nonturbulent systems with rapid irreversible reactions and equal diffusivities. *AIChE J.* **8**, 70–78.

Toor, H. L. (1969). Turbulent mixing of two species with and without chemical reactions. *Ind. Eng. Chem. Fundam.* **8**, 655–659.

Vassilatos, G. and Toor, H. L. (1965). Second-order chemical reactions in a nonhomogeneous turbulent fluid. *AIChE J.* **11**, 666–673.

Vieillefosse, P. (1984). Internal motion of a small element of fluid in an inviscid flow. *Physica A* **125**, 150–162.

Warhaft, Z. and Lumley, J. L. (1978). An experimental study of the decay of temperature fluctuations in grid-generated turbulence. *J. Fluid Mech.* **88**, 659–684.

Williams, F. A. (1975). Recent advances in theoretical descriptions of turbulent diffusion flames. Pp. 189-208. In Murthy, S. N. B. (ed.), *Turbulent Mixing in Nonreactive and Reactive Flows*. Plenum, New York.

Wray, A. A. (1989). A manual of the Vectoral language, including comparisons to FORTRAN. NASA-Ames Research Center. Unpublished.